R-1096
CU-326
NEVIS-220

Nevis Laboratories
Columbia University
Physics Department
Irvington-on-Hudson
New York

Photoproduction of New Hadronic Resonances

PATRICK SHAU-PARK LEUNG

Reproduction in whole or in part
is permitted for any purpose of the
United States Government

Submitted in partial fulfillment of
the requirements for the degree
of Doctor of Philosophy in the Faculty
of Pure Science, Columbia University

1977

National Science Foundation
NSF PHY 75-06955

Photoproduction of New Hadronic Resonances *

PATRICK SHAU-PARK LEUNG †

Columbia University, New York, N.Y. 10027

---

* Research supported by the National Science Foundation.

† Submitted in partial fulfillment of the requirements for the degree of Doctor of Philosophy in the Faculty of Pure Science, Columbia University.

ABSTRACT

Several narrow resonances associated with strange particles are observed in the reaction:

$$\gamma + \mathrm{Be} \rightarrow \mathrm{hadrons} \quad .$$

We present evidence for the production of a new antibaryon state ($\sim$ 2.26 GeV/c^2), which decays into $\bar{\Lambda}\pi^+\pi^-\pi^-$. Combining the above state with an additional π^+ gives an indication of the cascade process:

$$\bar{\Lambda}\pi^+\pi^-\pi^+\pi^- \ (\sim 2.45) \rightarrow \bar{\Lambda}\pi^+\pi^-\pi^- \ (\sim 2.26) + \pi^+ \quad .$$

In the same experiment, we also observe a narrow peak near 1.86 GeV/c^2 decaying into $K_S^{\,o}\pi^+\pi^-\pi^+\pi^-$. The above observations strongly suggest these states are the predicted charmed hadrons.

TABLE OF CONTENTS

	Page
I. INTRODUCTION	1
II. REVIEW	
A. Fermi and Yang Model	4
B. Quark Model	4
C. Charm Model	6
III. CURRENT EXPERIMENTAL STATUS OF CHARM	
A. ψ/J, ψ' and Others	11
B. Dilepton and $\mu^- e^+ K_S^o$ Neutrino-Induced Events	11
C. K_S^o-e Coincidence in e^+e^- Annihilations	12
D. $\nu p \rightarrow \mu^- \Lambda \pi^+ \pi^+ \pi^+ \pi^-$	12
E. $e^+e^- \rightarrow K^\mp \pi^\pm$, $K^\mp \pi^\pm \pi^+ \pi^-$, $K_S^o \pi^+ \pi^-$ and $K^\mp \pi^+ \pi^\pm$	13
F. Other Indications	14
IV. BROAD BAND PHOTON BEAM	15
V. APPARATUS AND ELECTRONICS	16
A. Proportional Chambers	16
B. Particle Identifiers and Calorimeters	16
C. Target Counters	17
D. Analyzing Magnet	17
E. Trigger Logic	18
F. Selective Trigger Logic	18
VI. ANALYSIS OF DATA	
A. V^o Identification	20
B. Other Searches	24
C. $\bar{\Lambda} \pi^+ \pi^- \pi^-$	25
D. $\bar{\Lambda} \pi^+ \pi^- \pi^+ \pi^-$	37
E. $K_S^o \pi^+ \pi^- \pi^+ \pi^-$	38

VII. CONCLUSIONS 42

ACKNOWLEDGMENTS 43

APPENDICES 45

TABLES 63

REFERENCES 67

FIGURE CAPTIONS AND FIGURES 76

I. INTRODUCTION

Since the dramatic discoveries of ψ/J[1] and ψ',[2] there have been speculations whether these resonances are manifestations of a new quantum number called charm.[3] The suggestion that ψ/J and ψ' are charm-anticharm bound states[4] further implies the existence of a rich spectrum of mesons and baryons explicitly possessing the conjectured quantum number.

From our earlier experimental data,[5] it was obvious that ψ/J is readily photoproduced diffractively. It is likely that the photon beam will be an ideal tool to probe the new physics. The apparent rise in the cross section for ($\gamma N \rightarrow \psi/J$ N + anything) from 11 GeV to approximately 100 GeV,[5,6] together with the fact that diffraction is a reflection of inelastic (non-diffractive) processes, indicates that charmed particles are being photoproduced at Fermilab.

The inclusive cross section, $\sigma(\gamma + N \rightarrow C + \text{anything})$, where C denotes a charmed hadron, has been estimated to be around 1 microbarn (see Appendix I). Therefore, unlike the case of hadron-hadron collisions, there exists a firm estimate of the charmed particles produced via photoproduction. The cross section is rather large, being of the order of 1% of the total hadronic photoproduction cross section. The charm production cross section in pp collisions is estimated, though much less accurately, to be around 1-10 microbarns.[7] This represents only 1/300 - 1/30% of the total pp cross section.

Furthermore, in a photon beam, the charm pair carries all of the momentum of the beam, unlike the valence quarks of a hadron beam which carry only a fraction of the momentum. The $x(= p/p_{max}$ in the center of mass of the nucleon-nucleon system) dependence of the ψ/J production in the hadron-hadron interactions[8] is consistent with this hypothesis. The search for charmed particles is, experimentally, more difficult in the low x region. The signal will be buried by the ordinary hadronic background. This has become painfully obvious in the charm-searching experiments using the hadron beams.[9]

The other problems facing experimentalists engaging in charm searches have been the predicted high multiplicities in the decay of the charmed particles. The hadron-hadron experiments are notoriously handicapped in this aspect. Our detectors are designed to cope with this problem. The counting rates are reasonable and the background is relatively small. Taken together, our experiment is ideally suited for charmed particle searches in the proton accelerators.

The experiment was carried out in the broad-band photon beam at Fermi National Accelerator Laboratory. About 15 million events were recorded in the last three months of 1975. Our analysis of the search for charmed particles was based on the study of the multihadron final states, with emphasis on events associated with V^o, namely $K_S{}^o$, lambda and anti-lambda.

The results are presented in the first section in Chapter VI. The more detailed study of several new resonances is given in the ensuing sections. The main conclusion is that both charmed mesons and charmed baryons are observed via photoproduction.

II. REVIEW

A. Fermi and Yang Model

One of the first attempts to classify the strong interacting particles, as combinations of a "fundamental" set of particles, was made by Fermi and Yang in 1949.[10] According to this model, pions are conjectured as bound states of nucleon-antinucleon pairs. Written out specifically in terms of isospin components:

Mesons

$L = 0$

	$I = 1$		$I = 0$
$I_3 = +1$	$I_3 = 0$	$I_3 = -1$	
π^+	π^o	π^-	η

Baryons

$J = 1/2$

$I = 1/2,\ I_3 = +1/2$	$I = 1/2,\ I_3 = -1/2$
p	n

B. Quark Model

When the quantum number strangeness was postulated, several problems of the Fermi-Yang model emerged. One of the serious defects of the model was that it did not incorporate the strange particles. Several models were proposed to remedy this shortcoming. Among the more successful ones are the Sakata (1956) model[11] and later the eightfold way introduced by Gell-Mann and Ne'eman in 1964.[12]

In the quark model, three quarks, u, d, s, are taken as fundamental components from which all hadrons are to be constructed. Each quark has spin 1/2. The quantum numbers of the quarks are tabulated as follows:

Quarks	I	I_3	Q	S	B	Y
u	1/2	+1/2	+2/3	0	1/3	+1/3
d	1/2	-1/2	-1/3	0	1/3	+1/3
s	0	0	-1/3	-1	1/3	-2/3

For antiquarks, all entries in the table have the opposite sign.

In this scheme, mesons are made out of bound states of quark-antiquark ($q\bar{q}$) pairs and baryons are constructed by using three quarks (qqq).

We turn next to a detailed classification of low-lying meson and baryon states, according to the rules of the so-called L-excited quark model, in which one assumes that the quark interaction is a potential well with orbital energies increasing with orbital angular momentum. Particles and resonances are formed as composites of quarks and antiquarks with different excitation energies. The lowest lying mesons and baryons are given in Appendix II.A.

No resonances were found before 1974 that could not be accommodated within the framework of the simple quark model. In particular, the non-observation of the "exotic"

meson substantiated the model considerably. The prediction of the existence of the Ω^-, among other things, was a spectacular success of the SU(3) model.[13]

In this model, the electromagnetic current is:

$$i[\frac{2}{3}\bar{u}\gamma_\lambda u - \frac{1}{3}\bar{d}\gamma_\lambda d - \frac{1}{3}\bar{s}\gamma_\lambda s] \ .$$

For the weak current, the expression is given by:

$$i\bar{u}(1-\gamma_5)(d\cos\theta + s\sin\theta)$$

($\cos\theta$ is the Cabibbo angle)

which is in obvious parallel with

$$i\bar{\nu}_e\gamma_\lambda(1-\gamma_5)e \quad \text{and} \quad i\bar{\nu}_\mu\gamma_\lambda(1-\gamma_5)u \ .$$

Features of Cabibbo's picture of the weak current have surfaced: namely, the selection rules of $|\Delta I| = 1$, $\Delta Y = 0$ or $|\Delta I| = 1/2$, $\Delta Y = \Delta Q$, and the conserved $\Delta Y = 0$ current with coefficient $\cos\theta$.

One of the reasons to modify the quark model comes from the study of the strangeness-changing second order processes, such as $K_L \to \mu^+\mu^-$, $K^+ \to \pi^+\nu\bar{\nu}$ and K_L-K_S mass difference. Experimentally, these processes have been found to be relatively suppressed.[14] As shown in Appendix III.A, the hadronic neutral current contains an undesirable $|\Delta S| = 1$ term, which would be contradictory to the experimental area.

C. Charm Model

In the following, we shall interpret "charm quark" in the narrow sense -- this is the fourth quark postulated by

Bjorken, Glashow, Iliopoulos and Maiani,[3] and incorporated into the Weinberg-Salam model[15], to suppress strangeness-changing neutral currents. The model is based on the principle of lepton-hadron symmetry:

$$q = \begin{pmatrix} c \\ u \\ d \\ s \end{pmatrix} \qquad l = \begin{pmatrix} \nu_e \\ \nu_u \\ e^- \\ u^- \end{pmatrix}$$

The weak hadronic current is constructed in precise analogy with the weak lepton current, thereby revealing suggestive lepton-quark symmetry.

The quantum numbers of the four quarks are:

Quarks	I	I_3	Q	S	B	Y	C
c	0	0	+2/3	0	1/3	+1/3	1
u	1/2	+1/2	+2/3	0	1/3	+1/3	0
d	1/2	-1/2	-1/3	0	1/3	+1/3	0
s	0	0	-1/3	-1	1/3	-2/3	0

With the additional quark, we can show that the $\Delta S = 1$ amplitude of the neutral current vanished completely if the SU(4) were exact (see Appendix III.B). Now if the quark masses are introduced, possibly via the Higgs mechanism, the $|\Delta S| = 1$ couplings of the neutral current are of the order $G(GM^2)$, where G is the Fermi coupling constant and M is the cutoff momentum. Since the observed amplitudes are very small, M cannot

exceed several GeV: charmed hadrons, if they exist, cannot have masses more than several GeV.

$|\Delta S| = 2$ nonleptonic amplitudes (e.g., K_L-K_S mass difference), which appear in higher orders of perturbation theory, are similarly suppressed.

The charm model is compatible with the observed hadron spectroscopy (pre-1974), as the Gell-Mann quark model is unmodified. Hence, all the essential features of the quark model are preserved. However, the strangeness-changing neutral current is banished and many new hadronic states associated with the charm quark are predicted. The charmed states, filling out SU(4) representations, are expected to appear in a higher mass region, with the lowest mass meson, ~ 1.8 GeV/c^2.

The hadrons, then, will group themselves into multiplets of SU(3), each multiplet containing particles of varying charm, C. This new quantum number, C, if it exists, should behave similarly to strangeness -- it is conserved in strong and electromagnetic interactions, but is violated in weak interactions.

Those states containing only uncharmed quarks, u, d, and s, form the familiar multiplets of mesons and baryons. The low-lying mesons and baryons are listed in Appendix II.B.

In order to clarify some of the issues in the experimental searches for charm, we find it instructive to list some of

the properties of the charmed particles in the Glashow-Iliopoulos-Maiani scheme. They include: masses, lifetimes, decay modes and production mechanism.

To set a mass scale for the charmed mesons, we interpret ψ/J as ϕ_c, a $^3S_1$ $c\bar{c}$ state and ψ' as ϕ_c', a radially excited $^3S_1$ $c\bar{c}$ state. In order to explain their narrow widths, a mechanism by the name of Zweig's rule is invoked.[16] According to this rule, the preferential ψ/J decays would be to charmed particles. However, if they lie below the charm-anticharm threshold, the decay would be energetically forbidden and the width would be narrow. The existence of the narrow ψ', at 3.7 GeV/c^2, implies the lowest charmed particle must be above 1850 MeV/c^2 in mass. Absence of another narrow peak, above 3.7 GeV/c^2, as well as the considerable width of the enhancement observed at 4.15 GeV, may indicate the charmed particle production threshold lies below 4.15 GeV. These have led to the speculation that the lightest charmed meson lies between 1.85 and 2.1 GeV/c^2. The charmed baryons are assumed to have masses not much higher than those of charmed mesons as the charm quark is much heavier than the ordinary quarks. The lowest lying charmed baryons are estimated to have masses between 2.1 and 2.3 GeV/c^2.

Since charm is conserved in strong and electromagnetic interactions, the ground state charmed particles are all stable against strong decays and are expected to have relatively long lifetimes ($\sim 10^{-13}$ sec). Thus, the most direct and convincing way of observing unhidden charm is to observe a narrow peak

in the effective mass spectrum of several hadrons. The expected long lifetimes of charmed particles have stimulated, for example, charm search experiments using an emulsion technique.

Charmed particles are predicted to decay preferentially to strange particles. The charm quark decays predominantly to a strange quark because this decay is a Cabibbo-favored weak transition. One of the manifestations of charmed particle decays is the observation of strange particles in the final state. Consequently, looking for sharp spikes in the invariant mass distributions with strange particles participating may produce the best signal for charm production.

III. CURRENT EXPERIMENTAL STATUS OF CHARM

A. ψ/J, ψ' and Others

The observed spectrum of the charmonium states now involves ψ/J (3.1), ψ' (3.7), ψ'' (4.1), ψ''' (4.4), η_c (2.8), χ (3.41), χ (3.45), P_c (3.51), and χ (3.55).[17,18,19] Both η_c (2.8) and χ (3.45) may need further confirmation. ψ'' (4.1) probably consists of several resonances and/or threshold. The overall situation in the charmonium spectroscopy is quite satisfactory and the idea of the new heavy particles being fermion-antifermion bound states is established.

B. Dilepton and $\mu^- e^+ K_S^o$ Neutrino-Induced Events

The observations of neutrino- or antineutrino-induced dimuons,[20] as well as ue events,[21] have been reported. The phenomenum is compatible with the production of a new hadron and its subsequent semileptonic decay. Charged currents of the weak interactions do not conserve charm. Thus, the process, $\nu p \rightarrow \mu^- C \ldots$, followed by leptonic or semileptonic decay of the charmed particle, $C \rightarrow \mu^+ + x$, is a possible source of prompt dileptons. Notice the opposite signs of the two leptons, a consequence of the $\Delta C = \Delta Q$ rule obeyed by the weak current. The observed $(E(\mu^+))/(E(\mu^-))$ has ruled out the heavy lepton as the sole source of dileptons.

The $\mu^- e K_S^o$ events, reported by the bubble chamber neutrino experiments, are consistent with the charm model. In the model, charmed particles have Cabibbo-favored decays into states with one unit of strangeness. Thus, one expects large neutral kaon yields in the μ-e events.

C. K_S^o-e Coincidence in e^+e^- Annihilations

The data[22] are compatible with a charm interpretation and apparently not with a heavy lepton hypothesis: the overall multiplicity is high and the lepton spectrum soft.

D. $\nu p \to \mu^- \Lambda \pi^+ \pi^+ \pi^+ \pi^-$

One event,

$$\nu p \to \mu^- \Lambda \pi^+ \pi^+ \pi^+ \pi^- ,$$

with a $\Delta S = -\Delta Q$ signature has been reported by a Brookhaven neutrino experiment.[23] This event represents either a violation of the $\Delta S = \Delta Q$ rule or the production and decay of a charmed baryon state.

The event can be interpreted in the charm scheme as the chain:

$$\nu p \to \Sigma_c^{++} \mu^-$$
$$\hookrightarrow \Lambda_c^+ \pi^+ \text{ (strong decay)}$$
$$\hookrightarrow \Lambda \pi^+ \pi^+ \pi^- \text{ (weak decay)} ,$$

then the observed masses are:

$$M_{\Sigma_c^{++}}(\Lambda' \pi^+ \pi^+ \pi^+ \pi^-) = 2426 \pm 12 \text{ MeV}/c^2 ,$$

and the three possible mass assignments for $\Lambda \pi^+ \pi^+ \pi^-$ are:

$$M_{\Lambda_c^+}(\Lambda \pi^+ \pi^+ \pi^-) = 2260 \pm 9 \text{ MeV}/c^2$$

or

$$M_{\Lambda_c^+}(\Lambda \pi^+ \pi^+ \pi^-) = 2099 \pm 4 \text{ MeV}/c^2$$

or

$$M_{\Lambda_c^+}(\Lambda \pi^+ \pi^+ \pi^-) = 2088 \pm 3 \text{ MeV}/c^2 .$$

The observed mass of the $\Lambda \pi^+ \pi^+ \pi^+ \pi^-$ and the highest possible mass assignment of $\Lambda \pi^+ \pi^+ \pi^-$ are in excellent agreement with the predicted values.

E. $e^+e^- \rightarrow K^{\mp}\pi^{\pm}$, $K^{\mp}\pi^{\pm}\pi^+\pi^-$, $K_S{}^o\pi^+\pi^-$ and $K^{\mp}\pi^{\pm}\pi^{\pm}$

The first direct evidence for particles with non-zero charm came in mid-1976, when SPEAR reported the observation of a narrow state decaying into $K^{\mp}\pi^{\pm}$, $K^{\mp}\pi^+\pi^+\pi^-$ and $K_S{}^o\pi^+\pi^-$ and its charged partner decaying into $K^{\mp}\pi^{\pm}\pi^{\pm}$.[24] The experimental observations agree beautifully with what has been expected of the charm model. Let us just briefly mention some of the features:

(a) The new resonance's width is consistent with the experimental resolution for a zero-width state.

(b) The neutral particle and its charged partner have masses of 1.865 ± 0.015 GeV/c^2 and 1.876 ± 0.015 GeV/c^2, respectively.

(c) The recoil mass spectra indicate the associated production mechanism and the existence of the predicted charm vector mesons, D_o^* and D_+^*.

(d) Both particles decay to states of strangeness $S = \pm 1$. The charged particle decays only to $K^{\mp}\pi^{\pm}\pi^{\pm}$ (an exotic state) and not to $K^{\pm}\pi^{\pm}\pi^{\mp}$.

(e) There exists some evidence for parity violation in the decays indicating the weak interaction mechanism is involved.

(f) The production of these new particles has shown a threshold behavior, the threshold energy being near 4 GeV, but above the narrow ψ' resonance (3.7 GeV).

The new particles are beautiful candidates for D_o ($\sim$ 1865 MeV/c^2) and D_+ ($\sim$ 1876 MeV/c^2), the charmed pseudoscalar isodoublet. The recoil mass structures may have to do with D_o^* ($\sim$ 2.01 GeV/c^2) and D_+^* ($\sim$ 2.01 GeV/c^2), the charmed isovector doublet.

F. Other Indications

1. Rise in R

Below 2.5 GeV, $R = \sigma(e^+e^- \to \text{hadrons})/\sigma(e^+e^- \to \mu^+\mu^-)$ is approximately constant with a value around 2.5.[25] Above 5 GeV, R is found to be in the neighborhood of 5. It is tempting to speculate that the rise in R is associated with the onset of the charm and particle production threshold. The coincidence of the calculated charmed mesons and baryons threshold, with the two jumps in R, substantiates this conjecture. Incidentally, the first jump has been found to be connected to the production of the new particles mentioned in Section E of this chapter.

2. Emulsion Event

An emulsion event reported last year is consistent (on the basis of lifetimes and effective masses) with the production of $\Lambda_c^+\bar{\Lambda}_c^-$ and subsequent decay into π^o + charged Σ or $\bar{\Sigma}$ and η + charged Σ or $\bar{\Sigma}$.[26]

IV. BROAD BAND PHOTON BEAM

The photons are obtained from 0-mrad neutral secondaries produced by the interactions of 400 GeV protons in a 12 in. long beryllium target (Fig. 1). The photon-to-neutron ratio is improved by a factor of roughly 200 above the initial photon-to-neutron ratio by passing the beam through two cryostats, 35 feet and 70 feet long, respectively, filled with liquid deuterium. To monitor the hadronic components of the beam, a device is installed between the two cryostats for remotely inserting up to six radiation lengths of lead into the beam. For photon running, the lead flippers are, of course, withdrawn; for background running, all six lead sheets are inserted to attenuate the electromagnetic component of the beam. We shall label this mode of running, the K_L runs, for the obvious reason that the K_L^o component is enhanced relative to the other components in the beam. To study the background introduced by neutrons, interactions were recorded for a brief period with the lead absorbers in the beam with only one-third of the deuterium . We refer to such running configuration as neutron runs. The essential features of these runs are summarized in Table I.

The photon flux available at the experimental target, about 200 feet beyond the proton target, is shown in Fig. 2.

V. APPARATUS AND ELECTRONICS

The detector consists of a multiwire proportional chamber magnetic spectrometer, particle identifiers, scintillation detectors and a Wilson-type quantameter. The detector layout is shown in Fig. 3. A very brief description of the apparatus will be given here. More detailed expositions can be found in References 27, 28 and 29.

A. Proportional Chambers

There are five multiwire proportional chambers, P0, P1, P2, P3 and P4. Each chamber has three signal planes, x, u, v. The u and v planes subtend an angle θ ($\tan\theta = 1/5$) with respect to the horizontal; the x plane is parallel to the vertical.

P0 and P1 each have an active area of 10 in. x 15 in., P2 and P3, 20 in. x 28 in. The largest chamber, P4, has an active area of 40 in. x 60 in. All planes have 2 mm wire spacing, except the x-plane in P4, where the spacing is 3 mm.

B. Particle Identifiers and Calorimeters

The electromagnetic shower detectors consist of lead scintillator sandwiches, and serve to detect electromagnetically showering particles, such as electrons and photons. The hadron calorimeter is made up of twenty-four 1.75 in. thick steel plates interspersed with 0.25 in. thick plastic scintillators.

It identifies hadrons and measures their energy to about 25%.

A copper plate electromagnetic shower device, known as the Wilson-type quantameter, was used in the experiment to monitor the photon beam intensity.

The muon identifier consists of vertical and horizontal scintillation counter hodoscopes embedded in a 72 in. steel absorber.

C. Target Counters

The target is surrounded by eight T counters that detect wide angle secondaries. The two counters AB, each with 0.25 in. lead converter between them and the target, and the four AW counters behind the P1 frame, cover forward angles outside the spectrometer aperture.

D. Analyzing Magnet

The dipole magnet, M2, with apertures of 16 in. horizontally by 24 in. vertically and a field integral of 20 kG-meter, bends particle trajectories in the vertical plane. The polarity is reversible and approximately the same amount of data were accumulated for each polarity in order to cancel out the effects of minor asymmetries.

The spectrometer was found to give a resolution of $\Delta P/P = \pm 3.5\%$ (P/100 GeV/c).

E. Trigger Logic

In this experiment, the trigger logic is divided into two levels: a master gate (MG) and a selective trigger. A detailed description of the trigger logic, used in the present data sample, can be found in Reference 29.

1. Master Gate (MG)

The master gate, generated by fast logic, defines the minimum requirement an event must have before being considered. The master gate is:

$$MG = (B3 + (LXR) + HC)_{2/3}$$

where:

B3 = the counter just downstream of the target,

(LXR) = at least one hit (two overlapping counters) on either side of the trigger array (H,V),

HC = a preset (4 GeV) energy deposit in the hadron calorimeter,

( )2/3 = at least two of the three conditions (i.e., B3, (LXR) and HC are satisfied.

F. Selective Trigger Logic

The selective trigger is more restrictive than the master gate, but sufficiently loose to allow the collection of events from a variety of interesting processes.

MG is sent to the input trigger generator which sorts the event into the coincidence registers. DC logic is used to make all logical operations from information stored in the coincidence registers. Up to sixteen logical definitions are derived and distributed to a data bus, to which many logic

modules (pin logic) can be connected. The sixteen bus lines are described in Table II. Each pin logic module defines an event classification according to internal preset switch connections corresponding to either "True", "False", or "Ignore" for each of the sixteen bus lines. Up to twelve different pin logic were employed during the runs. The requirements of the ten major pin logic are given in Table III.

Each pin logic has associated with it a prescale module, which can be set to generate one output pulse for every 1, 2, 4, 8, 16 ... 65336 input pulses. The use of the pin logic , with and without prescale, provides the ability to minimize system deadtime and the versatility in acquisition or suppression of different types of events. The content of each data run was determined by the master gate, the choice of pin logic , and the prescale requirements attached to the pin logic .

VI. ANALYSIS OF DATA

A. V^o Identification

All events were reconstructed by a computer program which identified and fitted individual tracks. These tracks were extrapolated upstream and a search was made for neutral vertices consistent with K_S^o, lambda and antilambda decays. A decay length of 165 in. in length was available, extending from 27 in. downstream of the production target to P2, the last proportional chamber before the analyzing magnet. All pairs of oppositely charged tracks, which resulted in vertices inside this regions, were potential candidates for $K_S^o \rightarrow \pi^+\pi^-$, $\Lambda \rightarrow p\pi^-$, $\bar{\Lambda} \rightarrow \bar{p}\pi^+$, or new long-lived objects. Furthermore, we required that the V^o intersect with at least one charged track within the production target (Fig. 5a). For the remaining V^o, the masses of the two tracks were calculated assuming both of them were pions. The mass distribution is shown in Fig. 6. We observe a clear signal at the K_S^o mass.

If we then exclude the V^o's with pion pair mass within 15 MeV/c^2 of the K_S^o (498 MeV/c^2) and recalculate the invariant mass, we assume the more energetic particle to be a proton or an antiproton. A distinct lambda (antilambda) was observed in Fig. 7. (Fig. 8)

The mass resolutions for K_S^o, lambda, and antilambda are 10 MeV/c^2 (fwhm), 5 MeV/c^2, and 5 MeV/c^2, respectively,

and grow with energy. This was demonstrated in Figs. 9a-c. The background of K_S^o is less than 1%, while the background for lambda (antilambda) is roughly 2% (4%).

For K_S^o, lambda (or antilambda) considered in this thesis, mass cuts of 498 $\pm$ 5 MeV/c^2 and 1116 $\pm$ 2 MeV/c^2, respectively, were imposed. A small number of events which fit both the K_S^o (498 $\pm$ 15 MeV/c^2) and Λ or $\bar{\Lambda}$ (1116 $\pm$ 6 MeV/c^2) were removed.

To further illustrate the spatial resolution of this experiment, as well as the cleanliness of the lambda (antilambda) identification, we considered events in which a V^o, identified as a lambda or antilambda, appeared to intersect another charged particle downstream from the interaction vertex (Fig. 5b). The invariant mass distribution of the $\Lambda\pi^+$, $\Lambda\pi^-$, $\bar{\Lambda}\pi^+$, and $\bar{\Lambda}\pi^-$ is shown in Figs. 13 and 14. We observe a clear peak near 1320 MeV/c^2 in the $\Lambda\pi^-$ and $\bar{\Lambda}\pi^+$ but not in the $\Lambda\pi^+$ or $\bar{\Lambda}\pi^-$ states. The peak corresponds to the hyperon, Ξ^-, and its antiparticle, $\bar{\Xi}^+$, decaying weakly into $\Lambda\pi^-$ and $\bar{\Lambda}\pi^+$, respectively.

$$\Xi^- \underset{\text{weak}}{\rightarrow} \Lambda + \pi^-$$

$$\bar{\Xi}^+ \underset{\text{weak}}{\rightarrow} \bar{\Lambda} + \pi^+ \quad .$$

The energy and the transverse momentum distributions of the inclusive K_S^o, Λ and $\bar{\Lambda}$ are given in Figs. 10 and 11. The energy of the V^o extends from $\sim$ 10 GeV to $\sim$ 100 GeV and the transverse momentum cutoff is approximately 1.5 GeV/c.

The total energy of the charged tracks of an event, which has a K_S^o, Λ or $\bar{\Lambda}$, is shown in Fig. 12. The cut at 200 GeV did not lose too many events but it reduced combinatorial problems for our analysis.

Just about the only distinguishing property of an unknown particle is its mass, so making invariant mass plots is a natural first attempt. We have used our multihadron data to search for mass peaks in these channels: (a) $K_S^o + n\pi^{\pm}$, where K_S^o is identified through $K_S^o \rightarrow \pi^+\pi^-$, (b) $\Lambda + n\pi^{\pm}$, where Λ is identified through $\Lambda \rightarrow p\pi^-$, and (c) $\bar{\Lambda} + n\pi^{\pm}$, where $\bar{\Lambda}$ is identified through $\bar{\Lambda} \rightarrow \bar{p}\pi^-$. In all cases, n = 1 ... 4. These channels are expected to be some of the dominant decay modes of the conjectured charmed mesons, D^+, D^o, charmed baryons, Λ_c, Σ_c, and their antiparticles.

We have made the following cuts in order to reduce the hadron-induced events:

(1) The total energy of the charged tracks of an event is less than 200 GeV.

(2) The total number of reconstructed tracks is less than nine.

With a resolution of $\Delta m/m \sim 2\%$, we plotted the invariant masses for all charged track combinations with a K_S^o, Λ or $\bar{\Lambda}$, assigning tentatively the rest mass of the pion to all tracks whose charges and momenta were measured.

This method, in cases of high multiplicity and absence of particle identification, will clearly suffer from

combinatorial backgrounds. With good statistics, they will however, be smoothly varying functions of the invariant mass.

The mass plots are shown in Figs. 15 to 18 for $K_S^o + n\pi^{\pm}$, Figs. 19 to 28 for $\Lambda(\bar{\Lambda}) + n\pi^{\pm}$. We should remark here that more than 30% of the events here are induced by hadrons, mostly K_L^o. In Figs. 39-43, we show some of the $K_S^o + n\pi^{\pm}$, $\Lambda + n\pi^{\pm}$, $\bar{\Lambda} + n\pi^{\pm}$ mass distributions, where we inserted Pb (lead) in the beam to attenuate photons. The solid curve represents events from the K_L and neutron runs. The shaded areas are events from the K_L runs only. For the $\Lambda(\bar{\Lambda}) + n\pi^{\pm}$ mass distributions (Figs. 40 to 43), we use both the K_L and neutron runs.

A test of this procedure: In the mass plots of $K_S^o\pi^{\pm}$, $\Lambda\pi^{\pm}$ and $\bar{\Lambda}\pi^{\pm}$ (Figs. 15, 19-22), we look for the well known resonances, K^* (mass = 892 MeV/c^2, width $\sim$ 50 MeV/c^2) and Y^* (mass = 1385 MeV/c^2, width $\sim$ 40 MeV/c^2). Enhancements are clearly seen at the proper mass values and the widths are consistent with the full width of these states.

A striking feature in the data is the peak in the $\bar{\Lambda}\pi^+\pi^-\pi^-$ mass plot near 2.26 GeV/c^2. This is the first indication that the charmed antibaryon is produced. A more detailed discussion is found in Section C. The slight enhancement in the region of 2.45 GeV/c^2 in the $\bar{\Lambda}\pi^+\pi^-\pi^+\pi^-$ mass plot turns out to be related to the peak in the $\bar{\Lambda}\pi^+\pi^-\pi^-$. This feature will be discussed in Section D .

A slight signal was seen in the $K_S^o\pi^+\pi^-\pi^+\pi^-$ channel that had a mass close to that of D^o, reported by the SLAC-LBL group's experiment. Section E will be devoted to further studies on this observation.

We found no convincing narrow peak in the remaining invariant mass distributions. The particles for which we are searching were assumed to have narrow width in mass. Our sensitivity reaches 10 to 500 nanobarns/Be nucleus level, depending on the particular channel and the degree of contribution from the background.

B. Other Searches

Besides the $K_S^o + n\pi^\pm$, $\Lambda + n\pi^\pm$ and $\bar{\Lambda} + n\pi^\pm$ mass plots shown, similar combinations were made of $K_S^oK^\pm$, K_S^op, $K_S^o\bar{p}$, $K_S^oK^\pm\pi^\pm\pi^\pm$ and $K_S^oK_S^o\pi^\pm$, where rest masses of m_π, m_K, or m_p were assigned to appropriate tracks. We did not observe any narrow peak, but the background and/or combinatorial problems were too prohibitive to provide any sensitive search.

Since charm is conserved in strong and electromagnetic interactions, charmed particles must be produced in pairs in the photon-induced reactions. The leptonic branching ratio for the weak decaying charmed particles is assumed to be of the order of 10%. Correspondingly, we seek evidence for the following reactions:

$$\gamma + Be \rightarrow C + \bar{C}'$$

where,

$$c + \bar{c}' \qquad \bar{c}' \to K_S^{o} + n\pi^{\pm} \qquad n = 1, \ldots 4$$
$$c \to \mu^{\pm} + X$$

or

$$c + \bar{c}' \qquad \bar{c}' \to K_S^{o} + n\pi^{\pm} \qquad n = 1, \ldots 4$$
$$c \to K_S^{o} + X$$

or

$$c + \bar{c}' \qquad \bar{c}' \to \mu^{\pm} + X, \text{ or } K_S^{o} + X$$
$$c \to K_S^{o} u^{\pm} + X$$

The statistics are too low to draw any meaningful conclusion.

C. $\bar{\Lambda}\pi^{+}\pi^{-}\pi^{-}$

1. Properties

We have examined, in some detail, the properties of the $\bar{\Lambda}\pi^{+}\pi^{-}\pi^{-}$ peak. We shall discuss some of the features:

a. Statistical significance, mass and width. The number of combinations in the peak, defined as three 25 MeV/c^2 bins, is 136 with a background of approximately 75 obtained from a smooth polynomial fit. This gives 7 standard deviations in excess of the smooth background. Multiple counting might affect the statistical significance to some extent, although not seriously.

We have fit the peak to a Breit-Wigner distribution with a polynomial background. The mass is found to be

2.26 ± 0.02 GeV/c^2 and the measured width is 40 ± 20 MeV/c^2.

It is interesting to note that the measured mass coincides with the following two values: (a) As mentioned earlier in Chapter III, one of the three possible mass assignments for $\Lambda\pi^+\pi^-\pi^+$ in the $\Delta S = -\Delta Q$ neutrino event is 2.26 ± 0.02 GeV/c^2. (b) Glashow, De Rujula and Georgi have predicted the lowest mass charmed baryon (Λ_c^+) to be of the mass 2.25 ± 0.05 GeV/c^2. The observed mass of the $\bar{\Lambda}\pi^+\pi^-\pi^-$ in our experiment is in astonishing agreement with the value predicted in (a) and the observed in (b).

The measured width is consistent with our experimental mass resolution ($\sim$ 30 MeV/c^2) for a zero-width state.

b. <u>No charge + 1 partner</u>. We observe the peak only in $\bar{\Lambda}\pi^+\pi^-\pi^-$ near 2.26 GeV/c^2 but not in the $\bar{\Lambda}\pi^+\pi^-\pi^+$ states. The slightly enhanced broad bump around this mass region in the graph could be understood as follows: In most cases, as can be seen from the multiplicity distribution shown in Fig. 29, the peak in $\bar{\Lambda}\pi^+\pi^-\pi^-$ appears to be associated with extra charged particles. Then there are many kinematical reflections for these mass plots. For example, one of the pions in the signal is replaced with another pion belonging to the recoil system. Depending on the details of the recoil system, such a $\bar{\Lambda}3\pi$ system can have a mass fairly close to 2.26 GeV/c^2, say within 100 to 200 MeV/c^2. This will generate a broad bump near 2.26 GeV/c^2 in $\bar{\Lambda}\pi^+\pi^-\pi^+$.

This hypothesis has been checked by a simple Monte Carlo , where we assume $\bar{\Lambda}\pi^+\pi^-\pi^+\pi^-$ is produced in a fashion as described in Appendix V, and decays to $\bar{\Lambda}\pi^+\pi^-\pi^-$ (2.26) + π^+. We then calculated the invariant mass of $\bar{\Lambda}\pi^+\pi^-\pi^+$ and observed a broad bump near 2.26 GeV/c^2, which agrees quite well with the data.

Incidentally, the absence of the charge +1 state for the antibaryon case is one of the most oft-mentioned characteristics of the hypothetical charmed antibaryon $\bar{\Lambda}_{\bar{c}}$.

c. Parity violation test. One of the attractive features of the antilambda final state is that, by establishing a non-zero longitudinal polarization of the final antilambda, we can infer that parity is violated and subsequently, the 2.26 GeV/c^2 state must have decayed weakly. This would be the case if the resonance were identified as the $\bar{\Lambda}_{\bar{c}}$, the lowest mass charmed antibaryon.

We studied, in the $\bar{\Lambda}3\pi$ rest system, the forward/backward asymmetry in the angular distribution of the $\bar{p}$ with respect to the antilambda direction. The angular distribution is shown in Fig. 30. The dashed line is for the angular distribution for the events just outside the $\bar{\Lambda}\pi^+\pi^-\pi^-$ peak. Although we do not observe a statistically significant asymmetry ($\sim 2\sigma$), we do find that $\bar{p}$ favors the forward direction.

The spectrometer acceptance has undoubtedly played an important role in shaping the angular distribution. In order

to minimize this effect, we have attempted the following technique: For every event, in the antilambda rest system, we interchange the $\bar{p}$ and the π^+ (from the antilambda decay) and then Lorentz-transform them to the laboratory frame. By use of a simple Monte Carlo program, we can determine whether these new states would have been accepted by our spectrometer. For those events that would have fitted our spectrometer aperture, we studied again the same forward/backward asymmetry. The result shows the same insignificant asymmetry ($\sim 1.5\sigma$), and $\bar{p}$ was still found to favor the forward direction.

It should be pointed out that our limited statistics would not, in any case, give us unmistakable proof of parity violation. Assuming the most favorable conditions, i.e., maximum longitudinal polarization of the final antilambda and no background, the large statistical error would have yielded a mere 3 standard deviations effect (see Appendix IV).

In short, our present data are not statistically conclusive to establish the parity violation in the $\bar{\Lambda}\pi^+\pi^-\pi^-$ decay. With more data, presumably from our next run, we should be in a position to improve our knowledge of the observed effect.

d. <u>Other properties</u>. We have looked at the momentum distribution of the π^+ and that of the π^- in the $\bar{\Lambda}\pi^+\pi^-\pi^-$ state. The distribution is presented in Fig. 31. On the

average, the energy of π^+ is higher than that of π^-. It is interesting to note that the soft pion theorem forbids emission of a soft π^+: In the absence of pole terms, the emission of soft pions is calculated by attaching them in all possible ways to the quarks in the non-leptonic weak Hamiltonian. It is possible to join an outgoing π^- or π^0 to the quarks in $\bar{c} \to \bar{s}\ \bar{u}\ \bar{d}$, whereas π^+ cannot be attached. Our data are consistent with the soft pion theorem requirement.

The energy and the transverse momentum distributions for the events inside the $\bar{\Lambda}\pi^+\pi^-\pi^-$ peak are shown in Fig. 33. The peak seems to have moderate transverse momentum ($\sim$ 700 MeV/c). The energy distribution agrees quite well with the Monte Carlo result (see Appendix II).

We have plotted the mass distributions of the $\bar{\Lambda}\pi$ and $\bar{\Lambda}\pi\pi$ from the $\bar{\Lambda}\pi^+\pi^-\pi^-$ state (Fig. 32). We observe no resonance-like structure in any of the combinations. In particular, we do not see any enhancement in the Y*(1385) region in the $\bar{\Lambda}\pi^{\pm}$ plots. A similar study is also made for the $\bar{\Lambda}\pi^+\pi^-\pi^-$ combinations just outside the peak. The mass distributions of the $\bar{\Lambda}\pi$ and $\bar{\Lambda}\pi\pi$ show similar shape although some enhancement is observed in the Y*(1385) region. These comparisons might be quite misleading because of the nature of the high multiplicities of these events. For example, a replacement of one of the π's in the $\bar{\Lambda}\pi^+\pi^-\pi^-$ signal with a spectator π

might appear as an event in the $\bar{\Lambda}\pi^+\pi^-\pi^-$ background. Hence, two of the $\bar{\Lambda}\pi$ mass combinations and one of the $\Lambda\pi\pi$ mass combinations will appear both in the signal and background samples. A comparison between these two sample will, undoubtedly, show some degree of similarity.

The next question is: "Is the peak produced in association with leptons?" Of all events inside the peak, we found 7 events which have a muon (5 positive, 2 negative) accompanying the $\bar{\Lambda}\pi^+\pi^-\pi^-$. With a χ^2 cut to eliminate those events, which are obviously from pion or kaon decays, three (all positive) events were left. All of them have low energy muons. Since the contributions from the hadron decays are calculated to be in the order of a few events, we do not have strong evidence that the $\bar{\Lambda}\pi^+\pi^-\pi^-$ peak is accompanied by extra muons. It is, however, noted that our acceptance for the extra muon is quite small, especially for the low energy ones, hence, 15-20% of $\bar{\Lambda}\pi^+\pi^-\pi^-$ muon coincidence cannot be ruled out.

The multiplicity of the event, associated with the peak, is shown in Fig. 29. From the graph, we can conclude that the $\bar{\Lambda}\pi^+\pi^-\pi^-$ peak is produced in association with other charged particles. Upon closer study, we found the events, where we observed at least one positive charged spectator track, outnumber those with at least one negative spectator charged track by 5 to 1. Many of the positive charged tracks have

momentum higher than 30 GeV, an indication that these might be protons. Some events have neutrals detected in the shower counters. However, the limited acceptance of the spectrometer, together with the poor neutrals detection efficiency, forbids us to reconstruct and study the complete event.

e. Cross section. To determine the cross section, we have to know the detection efficiency for the resonance. For a complicated system, such as $\bar{\Lambda}\pi^+\pi^-\pi^-$, it is extremely difficult to accurately determine the detection efficiency. This is mainly due to our ignorance of the production and decay mechanism. The situation becomes even worse when we have to include the experimental bias caused by the trigger requirements.

Nevertheless, we have made our most educated estimate on the cross section (see Appendix Vb): The product of the production cross section times the branching ratio to $\bar{\Lambda}\pi^+\pi^-\pi^-$ final state,

$$\sigma(\gamma+\mathrm{Be} \rightarrow \bar{\Lambda}_{\bar{c}}+X) \times BR(\bar{\Lambda}_c \rightarrow \bar{\Lambda}\pi^+\pi^-\pi^-) ,$$

is 34 → 340 nanobarns/Be nucleus, where the lower number is obtained by assuming perfect triggering efficiency and the higher one is obtained by 10% triggering efficiency.

2. Background

The first question is whether the peak is simply an ordinary hadronic resonance. There exists in the literature a particle, Σ (2.25 GeV/c^2), with a full width of 100-230 MeV/c^2.[30] The upper limit of our measured width is substantially smaller than the quoted width. We also believe if this were an ordinary hadron, we should have observed a peak in $\bar{\Lambda}\pi^+\pi^-\pi^+$.

In our experiment, charged hadrons were not differentiated. However, it is well known that the correct choice of the particles' masses would give the best signal for a narrow resonance. We made use of this fact by studying the following combinations: $\bar{\Lambda}p\pi^-\pi^-$, $\bar{\Lambda}K^+\pi^-\pi^-$ and $\bar{\Lambda}K^-\pi^+\pi^-$. For the $\bar{\Lambda}p\pi^-\pi^-$ and $\bar{\Lambda}K^+\pi^-\pi^-$ combinations, the positive particle was assumed to have the mass of a charged pion or a charged kaon. For $\bar{\Lambda}K^-\pi^+\pi^-$, the combination was entered twice in the mass histogram -- once for each of the two possible particle mass assignments. As can be seen from Figs. 35a-c, no narrow peak is observed in any of the three mass combinations. Accordingly, our choices of particle mass assignments are likely to be correct.

To ensure that the magnet polarities have no effect on the mass enhancement in $\bar{\Lambda}\pi^+\pi^-\pi^-$, we have divided the data into two separate samples: one obtained from runs with positive polarity and the other from negative polarity. The $\bar{\Lambda}\pi^+\pi^-\pi^+$ and the $\bar{\Lambda}\pi^+\pi^-\pi^-$ mass plots from the two samples are shown in Figs. 36 and 37. The mass spectra are similar

in both samples and the peak in $\bar{\Lambda}\pi^+\pi^-\pi^-$ appears in both magnet settings. This absence of asymmetry argues against gross effects caused by the magnet polarities.

We have also studied the background due to other particles other than the photon. We can investigate the contributions from K_L, neutrons and antineutrons in the neutral beam by suppressing the photon component. In Fig. 41, we plot the mass spectra from the K_L and neutron runs. Within the limitation of statistics, we have observed no enhancement in $\bar{\Lambda}\pi^+\pi^-\pi^-$ or $\bar{\Lambda}\pi^+\pi^-\pi^+$. It is clear from the histograms that the shapes of the mass spectra are far from smooth, obviously contributed from various kinds of kinematic reflections. This behavior might have a harmful effect on the photon-induced data.

We believe the antilambda data present spectacular confirmation of the theoretical prediction of charmed antibaryon structure. One would, in any conventional sense, expect to see similar structure in $\Lambda\pi^+\pi^-\pi^+$, its charge conjugate state. Disappointingly, the $\Lambda\pi^+\pi^-\pi^+$ mass plot (Fig.25a) shows no similar enhancement in the 2.26 GeV/c^2 region. The number of combinations of $\Lambda\pi^+\pi^-\pi^+$ is about three times larger than the one for $\bar{\Lambda}\pi^+\pi^-\pi^-$. This is because the $\bar{K}^0$'s and neutrons in the neutral beam could produce lambda quite copiously, while final states involving an antilambda have a much lower cross section. If we

assume the peak contains 50 events, then we expect a similar number of $\Lambda\pi^+\pi^-\pi^+$ signals above the background. The lambda data show about 3 standard deviations of not observing the signal.

In the following, we discuss some of the possible origins of the non-observation of the $\Lambda\pi^+\pi^+\pi^-$ signal in the data:

1. The magnitude of the $\bar{\Lambda}\pi^+\pi^-\pi^-$ signal has been inflated by a statistical fluctuation and/or the signal in $\Lambda\pi^+\pi^-\pi^+$ has been thrusted downward statistically. It is, however, quite inconceivable that the $\bar{\Lambda}\pi^+\pi^-\pi^-$ peak is nothing but a statistical fluke.

2. There might have been some asymmetry in the detectors which would have favored particles of one charge but not the other. These could include the positions of the counters and chambers, the non-uniformity of the magnetic field and the possible slight difference in the magnet current for the two magnet polarities. To cancel out most of the asymmetries, we have reversed the polarity of the magnet regularly during data-taking and the amount of quanta accumulated is roughly equal in each setting. However, minor differences can still be expected.

3. The possibility that the peak is produced by other neutral particles, such as antineutrons in our beam, is extremely small, although it is still not completely ruled out by our insufficient background data. Even with this mechanism

in mind, the problem remains unsolved. Suppose, for a moment, that the peak is antineutron-induced. By conventional methods, we would expect $\bar{\Lambda}\pi^+\pi^-\pi^+$ produced in equal number. In addition, we would also expect similar signals in $\Lambda\pi^+\pi^-\pi^+$, as well as $\Lambda\pi^+\pi^-\pi^-$ produced by neutrons. The signal might even be larger in the later cases as the number of neutrons (or particles) in our beam is much larger than that of antineutrons (or antiparticles). The absence of a peak in all of the three states does not support the idea that the $\bar{\Lambda}\pi^+\pi^-\pi^-$ peak is produced by antineutrons (Figs. 25, 26, 40 and 41).

4. Naturally, there is always a "conspiracy" explanation. The mass resolution difference, together with the possibility that the $\Lambda\pi^+\pi^-\pi^+$ background has a minimum at 2.26 GeV/c^2, might conspire to obscure the signal in the photon-induced lambda data.

5. We might have observed an apparent difference in either production or decay of the particle and its antiparticle. Our acceptance for many-body decay of a particle depends strongly on the mechanisms of production and decay. For example, the acceptance is relatively poor for the event which has the lambda decaying in the forward direction in the center of the mass frame of $\bar{\Lambda}\pi^+\pi^-\pi^-$ (or $\Lambda\pi^+\pi^-\pi^+$). This implies, for example, that some degree of CP violation in the decay, if it existed, might have prevented us from seeing the $\Lambda\pi^+\pi^-\pi^+$ signal. If the transition $\Lambda_c^+ \rightarrow \Lambda\pi^+$ is a weak decay, we will expect the process to be analogous to $\Lambda \rightarrow p\pi^-$. Observing

the Λ helicity by its decay, the Λ has the angular distribution:

$$P(\theta) = 1 + \alpha P_{\Lambda_C} \cos\theta ,$$

where θ is the polar angle of the Λ momentum in the helicity frame of the Λ_{C_Λ} and P_{Λ_C} is the polarization of Λ_C. If CP invariance were not valid, then we would have:

$$P(\theta) = 1 + \alpha P_{\Lambda_C} \cos\theta ,$$

$$\bar{P}(\theta) = 1 - \bar{\alpha} P_{\bar{\Lambda}_C} \cos\theta ,$$

with α and $\bar{\alpha}$ generally quite different numbers. If this were the case, it is clear that the Λ_C and $\bar{\Lambda}_C$ decay distributions would be different and correspondingly, the acceptance for Λ_C and $\bar{\Lambda}_C$ would not be identical. Obviously $\Lambda_C^+ \rightarrow \Lambda\pi^+\pi^-\pi^+$ would have a much more complicated decay but similar arguments would have produced the same result. Since the acceptance also depends strongly on the longitudinal momentum of the resonance, the $\Lambda\pi^+\pi^-\pi^+$ and the $\bar{\Lambda}\pi^+\pi^-\pi^-$ data would be different if Λ_C and $\bar{\Lambda}_C$ were produced with different energies.

Another remark we would like to add is the effect due to the presence of other particles produced in association with the $\bar{\Lambda}\pi^+\pi^-\pi^-$. Our trigger efficiency depends on the details of those particles. Any anomaly would make a difference in the labmda and antilambda data.

So far, we have not found an aesthetically satisfying way out of the perplexing asymmetry. It is possible, but

unlikely, that one of the five aforementioned factors could account for the absence of the $\Lambda\pi^+\pi^-\pi^+$ signal. It is more probable that more than one of them would combine to produce such a discrepancy in our data.

D. $\bar{\Lambda}\pi^+\pi^-\pi^+\pi^-$

In Fig. 28, we see the mass spectra for $\bar{\Lambda}(4\pi)$ combinations of charge 0 and -2. The statistics are clearly too limited for immediate conclusions. Upon further investigation, the suggestion of a peak in the vicinity of 2.45 GeV/c^2 in the $\bar{\Lambda}\pi^+\pi^-\pi^+\pi^-$ mode appears to be associated with the 2.26 GeV/c^2 peak in the $\bar{\Lambda}\pi^+\pi^-\pi^-$. We can observe this effect in Fig. 34, which shows the mass difference between $\bar{\Lambda}\pi^+\pi^-\pi^+\pi^-$ and $\bar{\Lambda}\pi^+\pi^-\pi^-$ combinations for $\bar{\Lambda}\pi^+\pi^-\pi^-$ combinations within the 2.26 GeV/c^2 peak, and separately (dashed line) for $\bar{\Lambda}\pi^+\pi^-\pi^-$ combinations just outside the peak. For events inside the peak, we include only those with a $\bar{\Lambda}\pi^+\pi^-\pi^-$ mass between 2.250 GeV/c^2 and 2.275 GeV/c^2 in order to reduce the background. The mass difference shows an enhancement around 200 MeV/c^2 with a width of 75 MeV/c^2.

We consider this to be evidence for a cascade process,

$$\underset{2.45\ \mathrm{GeV}/c^2}{\bar{\Lambda}\pi^+\pi^-\pi^+\pi^-} \rightarrow \underset{2.26\ \mathrm{GeV}/c^2}{\bar{\Lambda}\pi^+\pi^-\pi^-} + \pi^+$$

very close to threshold.

From the graph, we can see the peak contains approximately 13 events in excess of the background. This implies at least 25% of the $\bar{\Lambda}\pi^+\pi^-\pi^-$ signal comes from this $\bar{\Lambda}\pi^+\pi^-\pi^+\pi^-$ peak.

After putting in the detection efficiency, we believe the $\bar{\Lambda}\pi^+\pi^-\pi^+\pi^-$ peak contributes more than half the $\bar{\Lambda}\pi^+\pi^-\pi^-$ signal.

This observed state can be identified with the predicted $\Sigma_C(C_1{}^o)$ and/or $\Sigma_C{}^*(C_1{}^{o*})$, the charmed analogues of the Σ and Y*(1385), respectively. With the $\Sigma_C(C_1{}^o)$ and/or $\Sigma_C{}^*(C_1{}^{o*})$ heavier than the $\Lambda_C{}^+(C_o{}^+)$ by more than a pion mass (the mass difference is predicted $\sim$ 160 MeV/c^2), $\Sigma_C(C_1{}^o)$ and/or $\Sigma_C{}^*(C_1{}^{o*})$ should decay strongly via pion emission to $\Lambda_C{}^+(C_o{}^+)$. All these predictions have been confirmed by the data.

The coincidence in masses with the BNL neutrino event is remarkable: a $\Lambda\pi^+\pi^-\pi^+\pi^+$ mass of 2.426 GeV/c^2 and a similar cascade process to $\Lambda\pi^+\pi^-\pi^+$ (2.244 GeV/c^2).

E. $K_S{}^o\pi^+\pi^-\pi^+\pi^-$

A small signal was observed in the $K_S{}^o\pi^+\pi^-\pi^+\pi^-$ mass combinations near the region 1.86 GeV/c^2. This signal might correspond to a five-body decay of the D^o, the charmed particle reported by the SLAC-LBL group. The channel, $K_S{}^o\pi^+\pi^-\pi^+\pi^-$, is not totally unexpected as $K_S{}^o\pi^+\pi^-$ is one of the decay modes of D^o being observed. Furthermore, D^o is predicted to decay into states of high multiplicity with kaons.

To eliminate the combinatorial problems and to reduce the hadron-induced events, we have considered only 6-prong events, that is, those with six completely reconstructed tracks. The invariant mass plot is shown in Fig. 38a. We observe a clear peak centered at 1860 MeV/c^2. The single 25 MeV/c^2 bin from 1850 to 1875 MeV/c^2 contains an excess of

events with a statistical significance of about 4 standard deviations. With the present statistics, the signal might have been overlooked with a different binning or if D^o had been unknown.

To assure that there are no charged particles accompanying the peak, we further required that the anticounters AW and AB not detect any particles and the number of unused hits in the proportional chambers be less than 10. The mass plot is given in Fig. 38b. It is clear from the figure that the magnitude of the peak has remained unchanged and the background has reduced somewhat.

Our photon spectrum falls rapidly with energy and the number of photons above 250 GeV is relatively small and the hadron contamination in the beam dominates above this energy region. Assuming D^o is produced via associated production, the D^o will be unlikely to have more than 150 GeV in energy. In Fig. 38c, we have plotted the invariant mass of the K_S^o with the total energy of the five particles less than 150 GeV. The peak is quite prominent with a statistical significance exceeding 5 standard deviations. This observation strengthens our claim that D^o's have been produced in this experiment.

The total measured width ($\sim$ 25 MeV/c^2) of the $K_S^o\pi^+\pi^-\pi^+\pi^-$ signal is smaller than that of the $\bar{\Lambda}\pi^+\pi^-\pi^-$ ($\sim$ 75 MeV/c^2) because the $K_S^o\pi^+\pi^-\pi^+\pi^-$ events contain all the charged tracks in the event and the numbers of unused hits in the proportional chambers are much smaller.

Multiple counting problems are completely eliminated and the track fitting works much more efficiently. Our

mass resolution improves if the tracks share evenly the energy of the total system. This is the case for the $K_S^o\pi^+\pi^-\pi^+\pi^-$ and not for the $\bar{\Lambda}\pi^+\pi^-\pi^-$.

Although our π^o (or γ) detection efficiency is relatively poor, we do observe that about half of the events in the peak have neutrals detected in the shower counters. The K_L^o's, if they are present, are difficult to detect. The high multiplicity of the event makes the unambiguous identification of K_L^o almost impossible.

To show that the signal is indeed photoproduced, we have studied the $K_S^o\pi^+\pi^-\pi^+\pi^-$ final states with the photons attenuated (i.e., from K_L and neutrons runs). In Fig. 39a-c, we have plotted the $K_S^o\pi^+\pi^-\pi^+\pi^-$ mass distributions with the same cuts as employed in Figs. 38a-c. The graphs include events from both K_L^o and neutron runs. The shaded ones include the K_L^o runs only. A striking feature of those background events is the broad bump below 1.8 GeV/c^2 persists, but the D^o region is now a local minimum.

We conclude that the $K_S^o\pi^+\pi^-\pi^+\pi^-$ data highly suggest D^o's are photoproduced and decay at least occasionally to $K_S^o\pi^+\pi^-\pi^+\pi^-$.

We do not observe a similar signal in the $K_S^o\pi^+\pi^-$ channel. However, in this mode, the background is much larger due to the K_L^o induced events and the mass resolution would not be as good as in the case of $K_S^o\pi^+\pi^-\pi^+\pi^-$.

With the assumption that the $K_S^o\pi^+\pi^-\pi^+\pi^-$ signal corresponds to the D^o observed at SLAC, we derive a limit (see Appendix VI),

$$BR(D^o \to K_S^o\pi^+\pi^-)/BR(D^o \to K_S^o\pi^+\pi^-\pi^+\pi^-) < 2 .$$

The production cross section times branching ratio for the $K_S^o\pi^+\pi^-\pi^+\pi^-$ has been estimated in Appendix Vc. We obtain,

$$(\gamma \to D^o + \text{all neutrals}) \times BR(D^o \to K_S^o\pi^+\pi^-\pi^+\pi^-)$$

to be around 12 → 120 nb/Be nucleus.

VII. CONCLUSIONS

In conclusion, we have observed a clean peak near 2.26 GeV/c^2 in the $\bar{\Lambda}\pi^+\pi^-\pi^-$ final state, though not in the $\bar{\Lambda}\pi^+\pi^-\pi^+$ final state. The above signature, the measured width and the evidence for a higher mass state, $\bar{\Lambda}\pi^+\pi^-\pi^+\pi^-$, cascading to $\bar{\Lambda}\pi^+\pi^-\pi^-$ are consistent with charmed (anti) baryon production. The 1.86 GeV/c^2 signal in the $K_S^o\pi^+\pi^-\pi^+\pi^-$ mass is interpreted as the evidence for the charmed meson, D^o, being photoproduced.

Taken together, our findings point to the existence of a new family of hadrons, carrying a new quantum number, charm.

ACKNOWLEDGMENTS

I owe a great debt to Professor Bruce Knapp who has helped me in every imaginable way throughout the experiment.

In the past three years, Dr. Tony Wijangco exposed me to different phases of the experiment. My fellow graduate student, David Smith, provided many ideas embedded in this thesis, and Dr. Steve Holmes, William Wisniewski, as well as Maged Atiya, assisted in processing the data. I wish to express my appreciation to all of them.

I would like to thank my colleagues Morris Binkley, John Bronstein, Rick Coleman, Larry Cormell, Irwin Gaines, Gary Gladding, Maury Goodman, Mike Gormley, Jim Knauer, Bob Messner, David Nease, Tom O'Halloran, Rich Orr, John Peoples, A. Lincoln Read, John Sarracino, Albert Wattenberg, Dean Wheeler, and Dave Yount. The experiment would not have been possible without their hard work and dedication.

I am grateful to Ken Gray for his excellent technical expertise, Al Teho and Andre Vermeulen for their enormous help with the figures and Jean Therrien for her photography. For other technical support, I wish to acknowledge the Nevis Electronics Shop, the FNAL Proton Laboratory and both the Computing Departments at Nevis and at FNAL.

My appreciation to Dr. Benjamin Lee of Fermilab for his helpful remarks.

Thanks go to my friends for their unfailing support and encouragement.

I wish to dedicate this thesis to my parents, my brother S, and my sister W, whose love and understanding have contributed immensely to the realization of my goal in physics.

I am profoundly thankful to Ann Therrien for her arduous effort in typing this thesis. Furthermore, she has helped me in countless ways when I was doing my research at Nevis, and I must thank her once again.

Finally, I would like to express my gratitude to my sponsor, Professor Wonyong Lee. His insight and creativity have initiated the experiment and his energy and dedication are largely responsible for it success. His guidance and encouragement have made this thesis possible.

APPENDIX I

Complete vector dominance implies that the photon cannot interact with a hadron except as it first becomes a vector meson (ρ, ω, ϕ, etc.) and then this V interacts with the hadrons. We would expect:

$$A(\gamma + N \to B + X) = \sqrt{4\pi e^2} \sum_V \frac{1}{\gamma_V} (V + N \to B + X)$$

($\gamma_V^2/4\pi$ is the V-photon coupling constant)

assuming that off-shell and on-shell VN scattering are equal at all invariant momentum transfer t.

If we neglect possible off-diagonal terms, $V'N \to VN$, then

$$A(\gamma + N \to \psi + N) = \sqrt{4\pi e^2} \frac{1}{\gamma_\psi} (\psi N \to \psi N) \quad .$$

To extract the ψN total cross section, further assumption is made: The forward scattering amplitude is purely imaginary. Using the optical theorem:

$$\sigma_{total} = \frac{4\pi}{K} \operatorname{Im} A(\theta=0)$$

$$\left.\frac{d\sigma}{dt}\right|_{t=0} = \left.\left(\frac{d\sigma}{d\Omega}\frac{d\Omega}{dt}\right)\right|_{t=0}$$

$$= |A|^2 \frac{K^2}{\pi}$$

$$\left.\frac{d\sigma}{dt}(\psi N \to \psi N)\right|_{t=0} = \frac{1}{16\pi} \sigma^2_{total}(\psi N) \quad .$$

We now have:

$$\left.\frac{d\sigma}{dt}(\gamma N \to \psi N)\right|_{t=0} = \frac{4\pi e^2}{\gamma_\psi^2} \frac{1}{16\pi} \sigma^2_{total}(\psi N) \quad .$$

From the e^+e^- experiment,[31]

$$BR\left(\frac{\psi \to \mu^+\mu^-}{\psi \to \text{all}}\right) = 0.069 \quad .$$

Assuming $\gamma_\psi^2/4\pi$, the photon-ψ coupling constant, is the same value for real and virtual photons,

$$\Gamma(\psi \to \mu^+\mu^-) = \frac{\alpha^2}{3}\left(\frac{4\pi}{\gamma_\psi^2}\right)M_\psi = 4.8 \text{ keV} \ ,$$

where,

$$\alpha = e^2 \approx 1/137 \ ,$$

$$M_\psi = 3095 \text{ MeV}/c^2 \quad .$$

Then,

$$\frac{\gamma_\psi^2}{4\pi} = \frac{\alpha^2}{3} \ \frac{M_\psi}{\Gamma(\psi \to \mu^+\mu^-)} = 11.45 \ .$$

In our photoproduction experiment,[29] we measured

$$BR\left(\frac{\psi \to \mu^+\mu^-}{\psi \to \text{all}}\right) \times \sigma(\gamma A \to \psi A) \quad .$$

Assuming[27]

$$\frac{d\sigma}{dt}(\gamma A \to \psi A) = \frac{d\sigma}{dt}(\gamma N \to \psi N)\Big|_{t=0} \times [A^2 e^{42t} + A e^{4t}] \ ,$$

where A = atomic number .

We have,

$$\sigma(\gamma A \to \psi A) = \left[\frac{A^2}{42} + \frac{A}{4}\right] \frac{d\sigma}{dt}(\gamma N \to \psi N)\Big|_{t=0} \ ,$$

using $\sigma(\gamma A \to \psi A) = 25$ nb , A = 9 for the beryllium target and

$$\hookrightarrow \mu^+\mu^-$$

$$BR\left(\frac{\psi \to \mu^+\mu^-}{\psi \to \text{all}}\right) \quad \text{from the } e^+e^- \text{ experiment,}$$

we obtain,

$$\frac{d\sigma}{dt}\,(\gamma N \to \psi N)\Big|_{t=0} = 8.7\ \mathrm{nb}/(\mathrm{GeV}/c)^2 \quad .$$

Then,

$$\sigma_{\mathrm{total}}(\psi N) = \sqrt{16\pi\,\frac{\gamma_\psi^{\,2}}{4\pi e^2}\,\frac{d\sigma}{dt}\,(\gamma N \to \psi N)\Big|_{t=0}} = 1.6\ \mathrm{mb}.$$

We can estimate $\sigma(\gamma p \to \mathrm{charm}\ \ldots)$, if we assume the part of the electromagnetic current which couples to charmed quarks is dominated by the ψ.

$$A(\gamma+N \to \mathrm{charm}) = \sqrt{4\pi e^2}\ \frac{1}{\gamma_\psi}\,A(\psi N \to \mathrm{charm})$$

$$\approx \sqrt{4\pi e^2}\ \frac{1}{\gamma_\psi}\,A(\psi N \to \mathrm{all}) \quad .$$

We then have,

$$\sigma(\gamma+N \to \mathrm{charm}\ \ldots) \cong \frac{4\pi e^2}{\gamma_\psi^{\,2}}\,\sigma_{\mathrm{total}}\ (\psi N) \cong 1\ \mu\mathrm{b}\ .$$

APPENDIX II

A. Classification of Mesons and Baryons in the Quark Model

Mesons

$L = 0, \quad J = 0, 1 \qquad \text{parity} = (-1)^{L+1} = -1$

J^P	$I = 1, Y = 0$	$I = 1/2, Y = 1$	$I = 0, Y = 0$	$I = 0, Y = 0$
0^-	π	K	η	η'
1	ρ	K^*	ω	ϕ

The mixing of the isosinglet states is neglected.

Baryons

$L = 0$

J^P	$I = 1/2, Y = 1$	$I = 0, Y = 0$	$I = 1, Y = 0$	$I = 1/2, Y = -1$
$1/2$	$N(935)$	$\Lambda(1116)$	$\Sigma(1192)$	$\Xi(1315)$
	$J = 3/2, Y = 1$	$I = 1, Y = 0$	$J = 1/2, Y = -1$	$I = 0, Y = -2$
$3/2$	$\Delta(1236)$	$Y^*(1385)$	$\Xi^*(1530)$	$\Omega(1652)$

B. Classification of Mesons and Baryons in the Charmed Model

Charmed Mesons

$L = 0$

Label	Quark Content
$C = +1$	
D^+	$c\bar{d}$
D^0	$c\bar{u}$
F^+	$c\bar{s}$
$C = 0$	
η	$(u\bar{u} + d\bar{d} - 2s\bar{s})/\sqrt{6}$
η'	$(u\bar{u} + d\bar{d} + s\bar{s} + c\bar{c})/\sqrt{2}$
η_c'	$(u\bar{u} + d\bar{d} + s\bar{s} - 3c\bar{c})/\sqrt{12}$

C = -1

D^0	$\bar{c}u$
D^-	$\bar{c}d$
F^-	$\bar{c}s$

<u>Charmed Baryons</u>

J = 1/2

C = 1

C_1^{++} (Σ_c^{++})	cuu
C_1^{+} (Σ_c^{+})	$c(ud)_{sym}$
C_1^{0} (Σ_c^{0})	cdd
C_0^{+} (Λ_c^{+})	$c(ud)_{anti}$
S^+	$c(su)_{sym}$
S^0	$c(sd)_{sym}$
A^+	$c(su)_{anti}$
A^0	$c(sd)_{anti}$
T^0	css

C = 2

X_u^{++}	ccu
X_d^{+}	ccd
X_s^{+}	ccs

C = 3

X_c^{++}	ccc

APPENDIX III

A. Strangeness Changing Neutral Current in the Quark Model

In the following, we shall show how the quark model runs into trouble with the strangeness changing neutral current:

$$J_+ = \bar{u}\cos\theta\, d + u \sin\theta\, s$$

$$(\bar{u}\ \bar{d}\ \bar{s}) \begin{pmatrix} 0 & \cos\theta & \sin\theta \\ 0 & 0 & 0 \\ 0 & 0 & 0 \end{pmatrix} \begin{pmatrix} u \\ d \\ s \end{pmatrix}$$

$$= \bar{q}\, C_+\, q$$

where

$$q = \begin{pmatrix} u \\ d \\ s \end{pmatrix}$$

$$C_+ = \begin{pmatrix} 0 & \cos\theta & \sin\theta \\ 0 & 0 & 0 \\ 0 & 0 & 0 \end{pmatrix}$$

θ = Cabibbo angle .

Similarly, the negative charged current is:

$$J_- = \bar{d}\cos\theta\, u + \bar{s}\sin\theta\, u$$

$$= \bar{q}\, C_-\, q$$

where $C_- = \begin{pmatrix} 0 & 0 & 0 \\ \cos\theta & 0 & 0 \\ \sin\theta & 0 & 0 \end{pmatrix}$

The neutral hadronic current is then given by:

$$2\,J_0 = \bar{q}\,[C_+,\ C_-]\,q$$

$$= (\ \bar{u}\ \bar{d}\ \bar{s}\ )\begin{pmatrix} 1 & 0 & 0 \\ 0 & -\cos\theta\cos\theta & -\cos\theta\sin\theta \\ 0 & -\cos\theta\sin\theta & -\sin\theta\sin\theta \end{pmatrix}\begin{pmatrix} u \\ d \\ s \end{pmatrix}$$

$$= (\ \bar{u}u - \cos^2\theta\bar{d}d - \sin^2\theta\bar{s}s\ ) \rightarrow \Delta S = 0$$

$$- \sin\theta\cos\theta\ (\bar{d}s + \bar{s}d) \qquad \rightarrow \Delta S = 1$$

The hadronic current, therefore, contains a $\Delta S = 1$ term as well as a $\Delta S = 0$ term .

B. Strangeness Changing Neutral Current in the Charmed Model

In this section, we shall show how the introduction of the charm quark can cancel the strangeness changing neutral current.

With the additional quark, the weak charged currents are:

$$J_+ = \bar{u}(\cos\theta\ d + \sin\theta\ s) + \bar{c}(-\sin\theta\ d + \cos\theta\ s)$$

$$(\bar{c}\ \bar{u}\ \bar{d}\ \bar{s})\begin{pmatrix} 0 & 0 & -\sin\theta & \cos\theta \\ 0 & 0 & \cos\theta & \sin\theta \\ 0 & 0 & 0 & 0 \\ 0 & 0 & 0 & 0 \end{pmatrix}\begin{pmatrix} c \\ u \\ d \\ s \end{pmatrix}$$

$$= \bar{q}\ C_+ q$$

where

$$q = \begin{pmatrix} c \\ u \\ d \\ s \end{pmatrix}$$

and

$$C_+ = \begin{pmatrix} 0 & 0 & -\sin\theta & \cos\theta \\ 0 & 0 & \cos\theta & \sin\theta \\ 0 & 0 & 0 & 0 \\ 0 & 0 & 0 & 0 \end{pmatrix}$$

$$J_- = (\cos\theta\, \bar{d} + \sin\theta\, \bar{s})u + (-\sin\theta\, \bar{d} + \cos\theta\, \bar{s})\, c$$

$$= \bar{q}\, C_-\, q$$

where

$$C_- = \begin{pmatrix} 0 & 0 & 0 & 0 \\ 0 & 0 & 0 & 0 \\ -\sin\theta & \cos\theta & 0 & 0 \\ \cos\theta & \sin\theta & 0 & 0 \end{pmatrix}$$

$$[C_+, C_-] = \begin{pmatrix} 1 & 0 & 0 & 0 \\ 0 & 1 & 0 & 0 \\ 0 & 0 & -1 & 0 \\ 0 & 0 & 0 & 0 \end{pmatrix}$$

$$2J_0 = \bar{q}\, [C_+, C_-]\, q$$

$$= \bar{c}c + \bar{u}u - \bar{d}d - \bar{s}s$$

which contains no strangeness or charm changing neutral currents.

APPENDIX IV

Define $R = (F-B)/(F+B)$ where $F(B)$ is the number of events in the forward (backward) direction of the $\bar{p}$ with respect to the antilambda direction.

The error, δR, of the measured R is given by:

$$\delta R = \frac{(F+B)(\delta F-\delta B)-(F-B)(\delta F+\delta B)}{(F+B)^2} .$$

$\delta F(\delta B)$ is the error of the measured $F(B)$.

$$\delta R^2 = 4(F^2(\delta B)^2+B^2(\delta F)^2-2FB\delta F\delta B)/(F+B)^4 .$$

Using the standard procedure:

$$<(\delta B^2)> = B$$

$$<(\delta F^2)> = F$$

$$<(\delta F\delta B> = 0 .$$

We have

$$\sqrt{<\delta R^2>} = 2\sqrt{\frac{FB}{(F+B)^3}}$$

$$= \sqrt{\frac{(1-R^2)}{N}}$$

where N is the total number of events.

$$\frac{d\sigma}{d\cos\theta} = 1 + \alpha P_z \cos$$

where P_z is the longitudinal polarization, θ is the angle between the $\bar{p}$ and $\bar{\Lambda}$.

$$R = \frac{\int_0^1 (1+\alpha\cos\theta)\,d\cos\theta - \int_{-1}^0 (1+\chi\cos\theta)\,d\cos\theta}{\int_0^1 (1+\alpha\cos\theta)\,d\cos\theta + \int_{-1}^0 (1+\chi\cos\theta)\,d\cos\theta} .$$

Assuming maximum longitudinal polarization of antilambda, ($\alpha \approx 2/3$),

$$R = \frac{(\cos\theta+(2/3)(\cos^2\theta/2)\Big|_{\cos\theta=0}^{\cos\theta=1} - (\cos\theta+(2/3)(\cos^2\theta/2)\Big|_{\cos\theta=-1}^{\cos\theta=0}}{(\cos\theta+(2/3)(\cos^2\theta/2)\Big|_{\cos\theta=0}^{\cos\theta=1} \quad (\cos\theta+(2/3)(\cos^2\theta/2)\Big|_{\cos\theta=-1}^{\cos\theta=0}}$$

$$\simeq \frac{(4/3)+(-2/3)}{(4/3)-(-2/3)}$$

$$= 1/3$$

$$\simeq 0.33 \quad .$$

With the total number of events ~ 120,

$$\sqrt{<\delta R^2>} = \sqrt{(1-0.33^2)/120} = 0.09 \ .$$

Therefore, assuming a maximum longitudinal polarization of the final antilambda and zero background subtraction, we expect a 3 1/2 standard deviations effect in our present parity non-conservation test.

APPENDIX V

The cross section is given by

$$\sigma = \frac{N}{A \times B \times C \times ER(E_k) \times F \times L}$$

where

N = number of events observed

A = acceptance

B = effective number of atoms in the target per unit volume

C = all efficiency corrections

$ER(E_k)$ = ratio of number of photons with energy above E_k to the total number of photons with all energies

F = total photon flux

L = target length .

To get the photon flux F, we have used the quantameter reading and the measured photon spectrum.

F = Q/("e" x QC x (EK))

where:

Q = quantameter accumulated

= 3108×10^{-6} coulombs

"e"= 1.6022×10^{-19} coulombs/ion

QC = quantameter constant[27,28]

= 416.1 ions/GeV

(EK) = mean photon energy

= 42 GeV .

Therefore,

$F = 3108 \times 10^{-6}/1.6022 \times 10^{-19} \times 416.1 \times 42$

$= 1.1 \times 10^{12}$.

In this experiment, we have

$B = N_0(\text{atoms/mole}) \times D(\text{gm/cc})/A(\text{gm/mole})$

where,

N_0 = Avagadro's number = 6.02×10^{23}

D = density of Be = 1.848 gm/cc

A = atomic number of Be = 9 .

Therefore,

$B = 6.02 \times 10^{23} \times 1.848 \times 1/9$

$= 1.236 \times 10^{23}\text{nuclei/cm}^3$.

L = target length

= 2.46 cm of Be.

To illustrate our procedure, we have performed three cross section calculations for:

(a) $\gamma + \text{Be} \rightarrow \psi/J + X$

$\hookrightarrow \mu^+\mu^-$

(b) $\gamma + \text{Be} \rightarrow R_1 + X$

$\hookrightarrow \bar{\Lambda}\pi^+\pi^-\pi^-$ (2.26 GeV/c^2)

$\hookrightarrow \bar{p}\pi^+$

(c) $\gamma + \text{Be} \rightarrow R_2 + X$

$\hookrightarrow K_S^0\pi^+\pi^-\pi^+\pi^-$ (1.86 GeV/c^2)

$\hookrightarrow \pi^+\pi^-$

These calculations are used to illustrate the orders of magnitude for the cross sections. As a result, no error estimates are made.

(a) $\gamma + Be \rightarrow \psi/J + X$

$\hookrightarrow \mu^+\mu^-$

(i) N = number of $\mu^+\mu^-$ from mass 2.9 GeV/c^2 to 3.3 GeV/c^2.

(ii) A = acceptance

= 0.2.

The acceptance was calculated using a Monte Carlo program. The program assumed a photon spectrum $\alpha e^{-k/40}$, a production cross section for the ψe^{40t} and the angular distribution of the $\mu^+\mu^-$ from at rest following $1 + \cos^2$. The acceptance is found to be 20% for $\psi(\rightarrow \mu^+\mu^-)$ photoproduction.

(iii) C = correction factor

= 0.9 .

The correction factor comes largely from the deadtime correction.

(iv) $ER(E_k > 80) = 0.141$.

We require the energy of the photon to be above 80 GeV as the acceptance below that is negligible. From the measured photon spectrum, we found the above value. Therefore, we have

$= (\gamma + Be \rightarrow \psi/J + X)$

$\hookrightarrow \mu^+\mu^-$

$$= \frac{N}{A \times B \times C \times ER(E_k) \times F \times L}$$

$$= \frac{194}{0.2 \times 1.236 \times 10^{23} \times 0.9 \times 1.1 \times 10^{12} \times 0.141 \times 2.46}$$

$= 23 \times 10^{-33}$ cm^2/Be nucleus.

(b) $\gamma + Be \rightarrow R_1 + X$

$\hookrightarrow \bar{\Lambda}\pi^+\pi^-\pi^-$ (2.26)

$\hookrightarrow \bar{p}\pi^+$

(i) N = 50

(ii) A = 0.052 .

The acceptance was calculated using a Monte Carlo program. The program assumed: (a) a photon spectrum, $e^{-k/40}$, (b) a uniform energy distribution (from 0 to k GeV) for the energy of R_1, (c) zero transverse momentum of R_1 (an $e^{-6\ P}$ distribution reduces the acceptance by 20%), and (d) a phase space decay distribution. The data do not agree with the phase space distribution. However, any reasonable decay distribution will not critically modify the result. The lambda is then allowed to decay uniformly in its rest frame. The decay point is determined by using the distribution $e^{-z/c\,(E/m)}$ where:

z = distance downstream of the target (the allowed range for acceptance is 35 in. to 190 in., exactly the same as the cut imposed in the analysis)

c = mean free path of lambda = 7.73 cm

E = energy of lambda in the laboratory frame

m = mass of lambda = 1.1156 GeV/c^2 .

(iii) C

The corrections include (a) efficiency of MWPC in detecting reconstructable tracks, (b) deadtime, (c) the efficiency and bias due to our triggering scheme, including prescale correction.

Our trigger requirements introduce several biases to the data. For example, events where charged particles (or electrons from $\pi^o(\gamma)$ converted by the one radiation length lead in front of the anticounters AB) were detected in the AB or AW counters were largely suppressed.

We can make only a crude estimate on this correction factor as we cannot determine either production or decay mechanism. This contributes the largest source of systematic errors.

(iv) $ER(E_k > 90) = 0.13$.

The acceptance is negligible for R_1 with energy less than 70 GeV. If we assume the associated production mechanism, a photon of over 90 GeV energy is needed. Hence, we use $EF(E_k > 90)$ which is measured to be 0.13.

Therefore, we have

$$\sigma(\gamma + Be \rightarrow R_1 + X$$
$$\hookrightarrow \bar{\Lambda}\pi^+\pi^-\pi^- \quad (2.26)$$
$$\hookrightarrow p\pi^+$$

$$= \frac{N}{A \times B \times C \times ER(E_k > 90) \times F \times L}$$

$$= \frac{50}{0.052 \times 1.236 \times 10^{+23} \times C \times 0.13 \times 1.1 \times 10^{12} \times 2.46}$$

if $C = 1$, $\sigma = 22 \times 10^{-33}$ cm^2/Be nucleus;

if $C = 0.1$, $\sigma = 220 \times 10^{-33}$ cm^2/Be nucleus.

The cross section

$$(\gamma + Be \rightarrow \bar{\Lambda}_{C^-} + X \quad)$$
$$\hookrightarrow \bar{\Lambda}\pi^+\pi^-\pi^-$$

will be obtained by multiplying R_1 by 1/0.642 to correct for the unobserved decay modes of lambda. We found

$(\gamma + Be \rightarrow \bar{\Lambda}_{\bar{c}} + X$

$\hookrightarrow \bar{\Lambda}\pi^+\pi^-\pi^-$ (2.26)

$= (34 \rightarrow 340) \times 10^{-33}$ cm^2/Be nucleus.

(c) $\gamma + Be \rightarrow R_2$ + all neutrals

$\hookrightarrow K_S^0\pi^+\pi^-\pi^+\pi^-$ (1.86)

$\hookrightarrow \pi^+\pi^-$.

(i) N = 30

(ii) A = 0.057 .

The acceptance is similar to that employed in the previous section. The decay vertex distribution function is changed to $e^{-z/c\tau_k(E_k/m_k)}$

where:

$c\tau_k$ = mean free path of K_S^0 = 2.68 cm

E_k = energy of K_S^0 in the laboratory frame

m_k = mass of K_S^0 = 0.498 GeV/c^2 .

(iii) $ER(E_k) = ER(E_k > 90) = 0.13$.

(iv) C

It is noted that in this case the calculation of the cross section is more reliable. This arises from the fact that the decay products seem to share the energy more uniformly and the additional requirement that no additional charged tracks accompany the resonance. The latter is particularly important as the trigger bias is reduced substantially.

Therefore, we have

$$\sigma(\gamma + Be \rightarrow R_2 + \text{all neutrals}$$
$$\hookrightarrow K_S^0 \pi^+\pi^-\pi^+\pi^-$$
$$\hookrightarrow \pi^+\pi^-$$

$$= \frac{N}{A \times B \times C \times ER \times F \times L}$$

$$= \frac{30}{0.057 \times 1.236 \times 10^{23} \times C \times 0.13 \times 1.1 \times 10^{12} \times 2.46}$$

$\sigma = 12 \times 10^{-33}$ cm^2/Be nucleus if C = 1;

$\sigma = 120 \times 10^{-33}$ cm^2/Be nucleus if C = 0.1 .

The value of C, determined mostly by the prescale corrections, is more likely to be 0.5.

The cross section

$$(\gamma + Be \rightarrow D^0 + \text{all neutrals})$$
$$\hookrightarrow K_S^0 \pi^+\pi^-\pi^+\pi^-$$

will be obtained by multiplying R_2 by 1/0.689 to correct for the unobserved decay modes of K_S^0 .

We found

$$(\gamma + Be \rightarrow D^0 + \text{all neutrals})$$
$$\hookrightarrow K_S^0 \pi^+\pi^-\pi^+\pi^-$$

$= (18 \rightarrow 180) \times 10^{-33}$ cm^2/Be nucleus.

APPENDIX VI

In this section, we shall estimate the upper limit for the ratio: $\Gamma(D^0 \to K_S^0\pi^+\pi^-)/(D^0 \to K_S^0\pi^+\pi^-\pi^+\pi^-)$. The acceptance calculation is the same as the one employed in Appendix II(c)(ii). The acceptances for $K_S^0\pi^+\pi^-$ and $K_S^0\pi^+\pi^-\pi^+\pi^-$ are 0.075 and 0.057, respectively. Assuming the same measured full width for the two states and an upper limit corresponding to a five-standard deviation effect, we obtain:

$$\frac{\Gamma(D \to K_S^0\pi^+\pi^-)}{\Gamma(D \to K_S^0\pi^+\pi^-\pi^+\pi^-)} < 2.0.$$

TABLE I

Modes of Running

Run	Deuterium		Lead Absorbers
	35 ft.	70 ft.	6 radiation lengths
Photon	Full	Full	Out
K_L	Full	Full	In
Neutron	Full	Empty	In

TABLE II

Bus Lines

Bus Lines	Symbol	Description
1	$A_0 + A_\mu > 2$	One or more charged particles in the anticounters upstream of the target.
2	AB + AW	One or more particles in the anticounters downstream of the target.
3	$E_V\ \bar{L}\cdot\bar{R}$	Energy deposited in vertical shower counters and no hits outside the central 16 wires in the X plane of P2 and P3.
4	MWPC > 0	$(>0)^3_{P2}\cdot(>0)^3_{P3}\cdot(>0)^3_{P4}\cdot P1(2/3)$
5	MWPC > 1	MWPC $> 0\cdot(>1)^2_{P2}\cdot(>1)^2_{P3}\cdot(>1)^2_{P4}$
6	MWPC > 2	MWPC $> 1\cdot(>2)^2_{P3}\cdot(>2)^2_{P4}$
		P1(2/3) = hits in two of the three planes of P1.
		$(>0)^3_{Pi}$ = at least one hit in each of the three signal planes of chamber Pi .
		$(>1)^2_{Pi}$ = more than one hit in any two planes of chamber Pi.
		$(>2)^2_{Pi}$ = more than two hits in any two planes of chamber Pi.
7	$\bar{L}\cdot\bar{R}$	No hits outside the central 16 wires in the X plane of P2 and P3.
8	2μ	Two or more coincidences between μH and μV hodoscopes.
9	1μ	One or more coincidences between μH and μV hodoscopes.

10	2e	Two or more coincidences between electron hodoscopes and energy deposited in corresponding shower counters on both banks.
11	1e	One or more coincidences between electron hodoscopes and energy deposited in corresponding front shower counter.
12	E_{LO}	Medium energy deposit (~ 30 GeV) in showers and hadron calorimeter.
13	E_{HI}	Large energy deposit (~ 60 GeV) in shower counters and hadron calorimeter.
14		
15	$E_{V1} \cdot E_{V2}$	Energy deposit in both vertical shower counters.
16	$E_{V1} \cdot E_{V2}$	Energy deposit in either vertical shower counter.

TABLE III

Pin Logic

	2e	1e	μe	2μ	2μ+h	1μ	2	4	2HI	4HI
Bus Lines	1	2	3	4	5	6	7	8	12	14
1. $A_0+A_\mu > 2$	F	F	F	F	F	F	F	F	F	F
2. AB + AW	F	F				F	F	F	F	F
3. $E_V \cdot \bar{L} \cdot \bar{R}$		F			F	F	F	F	F	F
4. MWPC > 0										
5. MWPC > 1	T	T	T	T	T	T	T		T	
6. MWPC > 2								T		T
7. $\bar{L} \cdot \bar{R}$	F									
8. 2μ				T	T					
9. 1μ			T			T				
10. 2e	T									
11. 1e		T	T							
12. E_{L0}					T	T	T	T		
13. E_{HI}		T							T	T
14.										
15. $E_{V1} \cdot E_{V2}$										
16. $E_{V1}+E_{V2}$				F						

T: True F: False : Don't Care

REFERENCES

1 J.J. Aubert, U. Becker, P.J. Biggs, J. Burger, M. Chen, G. Everhart, P. Goldhagen, J. Leong, T. McCorriston, T.G. Rhoades, M. Rohde, Samuel C.C. Ting, Sau Lan Wu, Y.Y. Lee, Phys. Rev. Lett. 33, 1404 (1974).

J.E. Augustin, A.M. Boyarski, M. Breidenbach, F. Bulos, J.T. Kakin, G.J. Feldman, G.E. Fischer, D. Fryberger, G. Hanson, B. Jean-Marie, R.R. Larsen, V. Lüth, H.L. Lynch, D. Lyon, C.C. Morehouse, J.M. Paterson, M.L. Perl, B. Richter, P. Rapidis, R.F. Schwitters, W.M. Tanenbaum, P. Vannucci, G.S. Abrams, D. Briggs, W. Chinowsky, C.E. Friedberg, G. Goldhaber, R.J. Hollebeek, J.A. Kadyk, B. Lulu, F. Pierre, G.H. Trilling, J.S. Whitaker, J. Wiss, J.E. Zipse, Phys. Rev. Lett. 33, 1406 (1974).

C. Bacci, R. Balbini Celio, M. Berna-Rodini, G. Caton, R. DelFabbro, M. Grilli, E. Iarocci, M. Locci, C. Mencuccini, G.P. Murtas, G. Penso, G.S.M. Spinetti, M. Spano, B. Stella, V. Valente, B. Bartoli, D. Bisello, B. Esposito, F. Felicetti, P. Monacelli, M. Nigro, L. Paolufi, I. Peruzzi, G. Piano Mortemi, M. Piccolo, F. Ronga, F. Sebastiani, L. Trasatti, F. Vanoli, G. Barbarino, G. Barbiellini, C. Bemporad, R. Biancastelli, F. Cevenini, M. Celvetti, F. Costantini, P. Lariccia, P. Parascandalo, E. Sassi, C. Spenser, L. Tottora, U. Troya, S. Vitale, Phys. Rev. Lett. 33, 1408 (1974).

2 A.M. Boyarski, M. Breidenbach, F. Bulos, G.J. Feldman, G.E. Fischer, D. Fryberger, G. Hanson, B. Jean-Marie, R.R. Larsen, D. Luke, V. Lüth, H.L. Lynch, D. Lyon, C.C. Morehouse, J.M. Paterson, M.L. Perl, P. Rapidis, B. Richter, R.F. Schwitters, W. Tanenbau, F. Vannucci, G.S. Abrams, D.D. Briggs, W. Chinowsky, C.E. Friedberg, G. Goldhaber, J.A. Kadyk, A.M. Litke, B.A. Lulu, F.M. Pierre, B. Sadoulet, G.H. Trilling, J.S. Whitaker, F. Winkelmann, J.E. Wiss, Phys. Rev. Lett. 34, 1357 (1975).

3 J.D. Bjorken, S.L. Glashow, Phys. Lett. 11, 255 (1964).
Y. Hara, Phys. Rev. 134B, 701 (1964).
S.L. Glashow, J. Iliopoulous, L. Maiani, Phys. Rev. D2, 1285 (1970).
M.K. Gaillard, B.W. Lee, J.L. Rosner, Rev. Mod. Phys. 47, 277 (1975).
A. DeRujula, H. Georgi, S.L. Glashow, Phys. Rev. D12, 147 (1975).

4 T. Appelquist, H.D. Politzer, Phys. Rev. Lett. 34, 43 (1975).
A. DeRujula, S.L. Glashow, Phys. Rev. Lett. 34, 46 (1975).
E. Eichten, K. Gottfried, T. Kinoshita, J. Kogut, K.D. Lane, T.M. Lane, Phys. Rev. Lett. 34, 369 (1975).

5 B. Knapp, W. Lee, P. Leung, S.D. Smith, A. Wijangco, J. Knauer, D. Yount, D. Nease. J. Bronstein, R. Coleman, L. Cormell, G. Gladding, M. Gormley, R. Messner, T. O'Halloran, J. Sarracino, A. Wattenberg, D. Wheeler, M. Binkley, R. Orr, J. Peoples, L. Read, Phys. Rev.

Lett. 34, 1040 (1975).

W. Lee, Proceedings of the 1975 International Symposium on Lepton and Photon Interactions at High Energies, W.T. Kirk, editor (Stanford Linear Accelerator Center, Stanford, 1975).

6 U. Camerini, J.G. Learned, R. Prepost, C.M. Spenser, D.E. Wiser, W.W. Ash, R.L. Anderson, D.M. Ritson, D.J. Sherden, C.K. Sinclair, Phys. Rev. Lett. 35, 483 (1975).

B. Gittelman, K.M. Hanson, D. Larson, E. Loh, A. Silverman, G. Theodosiou, Phys. Rev. Lett. 35, 1616 (1975).

T. Nash, A. Belousov, B. Govorkov, D.O. Caldwell, J.P. Cumalat, A.M. Eisner, R.J. Morrison, F.V. Murphy, S.J. Yellin, P.J. Davis, R.M. Egloff, G. Luste, J.D. Prentice, Phys. Rev. Lett. 36, 1233 (1976).

7 V. Barger, R. Phillips, Phys. Rev. D12, 2623 (1975).

T.K. Gaisser, F. Halzen, Phys. Rev. D11, 3157 (1975).

R. Field, C. Quigg, Fermilab Preprint 75/15 THY.

D. Sivers, Nucl. Phys. B106, 95 (1976).

8 B. Knapp, W. Lee, P. Leung, S.D. Smith, A. Wijangco, J. Knauer, D. Yount, D. Nease, J. Bronstein, R. Coleman, L. Cormell, G. Gladding, M. Gormley, R. Messner, T. O'Halloran, J. Sarracino, A. Wattenberg, D. Wheeler, M. Binkley, R. Orr, J. Peoples, L. Read, Phys. Rev. Lett. 34, 1044 (1975).

G.J. Blanar, C.F. Boyer, W.L. Faissler, D.A. Garelick, M.W. Gettner, M.J. Glaubman, J.R. Johnson, H. Johnstad,

M.L. Mallary, E.L. Pothier, D.M. Potter, M.T. Ronan, M. F. Tautz, E. von Goeler, Roy Weinstein, Phys. Rev. Lett. 35, 346 (1975).

K.J. Anderson, G.G. Henry, K.T. McDonald, J.E. Pilcher, E.I. Rosenberg, J.G. Branson, G.H. Sanders, A.J.S. Smith, J.J. Thaler, Phys. Rev. Lett. 36, 237 (1976); Phys. Rev. Lett. 37, 799 (1976).

Columbia-Illinois-FNAL Group, Phys. Rev. Lett. 37, 574 (1976).

Yu. M. Antipov, V.A. Bessubov, N.P. Budanov, Yu. B. Bushnin, S.P. Denisov, Yu. P. Gorin, A.A. Lebedev, A.A. Lednev, Yu. M. Mikhailov, A.I. Petrukhin, S.A. Polovnikov, V.N. Roinishvili, V.S. Selesnev, V.I. Sergienko, D.A. Stoyanova, A.N. Sytin, Ya. A. Vazdik, F.A. Yotch, Phys. Lett. 60B, 309 (1976).

9 The literature on this subject is quite extensive. For example, see: K.C. Stanfield, Proceedings APS Particles and Fields, Brookhaven National Laboratory (1975).

J.J. Aubert, U. Becker, P.J. Biggs, J. Burger, M. Chen, G. Everhart, J. Leong, T.G. Rhoades, M. Rohde, T. Sanford, Samuel C.C. Ting, W.H. Toki, Sau Lan Wu, J.W. Glen, III, Y.Y. Lee, Phys. Rev. Lett. 35, 416 (1975).

M.A. Abolins, D. Cardimona, J.A.J. Matthews, R.A. Sidwell, H.R. Barton, Jr., N.W. Reay, K. Reibel, N. Stanton, K.W. Edwards, G. Luxton, Phys. Rev. Lett. 37, 417 (1976).

D. Bintinger, R.A. Lundy, D.D. Yovanovitch, C.W. Alcerlof, P. Alley, D. Koltick, R.L. Loveless, D.I. Meyer, R. Thun, W.R. Ditzler, D.A. Finley, F.J. Loeffler, E.I. Shibata,

K.C. Stanfield, Phys. Rev. Lett. 37, 732 (1976).

[10] E. Fermi, C.N. Yang, Phys. Rev. 76, 1739 (1949).

[11] Sakata, Progr. Theor. Phys. 16, 686 (1956).

[12] M. Gell-Mann, Phys. Lett. 8, 214 (1964).

M. Gell-Mann, Y. Ne'eman, The Eightfold Way, Benjamin, 1964.

[13] V.E. Barnes, P.L. Connolly, D.J. Crennell, B.B. Culwick, W.C. Delaney, W.B. Fowler, P.E. Hagerty, E.L. Hart, N. Horwitz, P.V.C. Hough, J.E. Jensen, J.K. Kopp, K.W. Lai, J. Leitner, J.L. Lloyd, G.W. London, T.W. Morris, Y. Oren, R.B. Palmer, A.G. Prodell, D. Radojicic, D.C. Rahm, C.R. Richardson, N.P. Samios, J.R. Sanford, R.P. Shutt, J.R. Smith, D.L. Stonehill, R.C. Strand, A.M. Thorndike, M.S. Webster, W.J. Willis, S.S. Yamamoto, Phys. Rev. Lett. 12, 204 (1964).

[14] Alan R. Clark, T. Eliot, R.C. Field, H.J. Frisch, Rolland P. Johnson, Leroy T. Kerth, W.A. Wenzel, Phys. Rev. Lett. 26, 1667 (1971).

L.T. Kerth, Bull. Am. Phys. Soc. 18, 639 (1973).

W.C. Carithers, T. Modis, D.R. Nygren, T.P. Pun, E.L. Schwartz, H. Sticker, J. Steinberger, P. Weilhammer, J.H. Christenson, Phys. Rev. Lett. 30, 1336 (1973).

W.C. Carithers, D.R. Nygren, H.A. Gordon, M.L. Ioffredo, Kwan-Wu Lai, P. Weilhammer, Phys. Rev. Lett. 31, 1025 (1973).

Y. Fukushima, D.A. Jensen, P. Surko, J.J. Thaler, M.N. Kreisler, A.M. Lopez, P. Shah, Phys. Rev. Lett. 36, 348 (1976).

J.H. Klems, R.H. Hildebrand, R. Stiening, Phys. Rev. D4, 66 (1971).

G.D. Cable, R.H. Hildebrand, C.Y. Pang, R. Stiening, Phys. Rev. D8, 3807 (1973).

P. Bloch, S. Brehin, G. Bunce, B. Devaux, A.M. Diamant-Berger, N. Do-Duc, G. Marel, R. Turlay, P. Extermann, J. Rischer, O. Guisan, R. Mermod, L. Rosselet, R. Sachot, Phys. Lett. 56B, 201 (1975).

15 S. Weinberg, Phys. Rev. Lett. 19, 1264 (1967).

A. Salam, Proceedings of the 8th Nobel Symposium, Stockholm, 1968.

16 G. Zweig, CERN Report No. TH401, 1964, unpublished.

CERN Report, No. TH412, 1964, unpublished.

S. Okubo, Phys. Lett. 5, 165 (1963).

J. Iizuka, Suppl. to Prog. Theor. Phys. 37-38, 21 (1966).

17 W. Braunschweig, H.-U. Martyn, H.G. Sander, D. Schmitz, W. Sturm, W. Wallraff, K. Berkelman, D. Cords, R. Felst, E. Gadermann, G. Grindhammer, H. Hultschig, P. Joos, W. Koch, U. Kötz, H. Krehbiel, D. Kreinick, J. Ludwig, K.-H. Mess, K.C. Moffeit, A. Petersen, G. Poelz, J. Ringel, K. Sauerberg, P. Schmüser, G. Vogel, B.H. Wiik, G. Wolf, G. Buschhorn, R. Kotthaus, U.E. Kruse, H. Lierl, H. Oberlack, K. Pretzl, M. Schliwa, S. Orito, T. Suda, Y. Totsuka, S. Yamada, Phys. Lett. 57B, 407 (1975).

LBL-SLAC Group, Phys. Rev. Lett. 35, 821 (1975).

SLAC-LBL Group, Phys. Rev. Lett. 35, 1323 (1975).

SLAC-LBL Group, Phys. Rev. Lett. 37, 1596 (1976).

[18] G. Geldman, Lectures at the SLAC Summer Institute in Particle Physics, 1976, unpublished.

[19] B. Wiik, Rapporteur talk at the 18th International Conference on High Energy Physics, Tbilisi, USSR, July 1976, unpublished.

[20] A. Benvenuti, D. Cline, W.T. Ford, R. Imlay, T.Y. Ling, A.K. Mann, R. Orr, D.D. Reeder, C. Rubbia, R. Stefanski, L. Sulak, P. Wanderer, Phys. Rev. Lett. 35, 1199; 1203; 1249 (1975).

B.C. Barish, J.F. Bartlett, A. Bodek, K.W. Brown, D. Buchholz, F. Jacquet, J. Lee, F.S. Merritt, F.J. Sciulli, L. Stutte, H. Suter, H.E. Fisk, G. Krafczyk, Phys. Rev. Lett. 36, 939 (1976).

[21] H. Deden, F.J. Hasert, W. Krenz, J. von Krogh, D. Lanske, J. Morfin, M. Pohl, K. Schultze, H. Weerts, G.H. Bertrand-Coremans, M. Goossens, H. Mulkens, J. Sacton, W. Van Doninck, P. Vilain, H. Burmeister, D.C. Cundy, D. Haidt, A. Lloret, P. Musset, J.B.M. Pattison, D.H. Perkins, F. Romano, A. Rousset, H. Wachsmuth, L. Behr, V. Brisson, A. Comtet, B. Degrange, M. Haguenauer, L. Kluberg, U. Nguyen-Khac, P. Petiau, E. Bellotti, S. Conetti, D. Cavalli, E. Fiorini, A. Pullia, M. Rollier, B. Aubert, L.M. Chounet, J. Grandsman, P. Heusse, M. Jaffre, L. Jauneau, C. Louguemare, A.M. Lutz, C. Pascaud, J.P. Vialle, F.W. Bullock, T.W. Jones, A.G. Michette, G. Myatt, J. Pinfold, Phys. Lett. 58B, 361 (1975).

J. von Krogh, W. Fry, U. Camerini, D. Cline, R.J. Loveless, J. Mapp, R.H. March, D.D. Reeder, A. Barbaro-Galtiere, P. Bosetti, G. Lynch, J. Marriner, F. Solmitz, M.L. Stevenson, D. Haidt, G. Harigel, H. Wachsmuth, R. Cence, F. Harris, S.I. Parker, M. Peters, V. Peterson, V. Stenger, Phys. Rev. Lett. 36, 710 (1976).

Aachen-Brussels-CERN-Palaiseau-Milan-Orsay-London Group, Phys. Lett. 60B, 207 (1976).

W. Lee, Proceedings of the International Neutrino Conference, Aachen, Germany (1976).

C. Baltay, Proceedings of the International Neutrino Conference, Aachen, Germany (1976).

22 H. Meyer, Proceedings of the Summer Institute on Particle Physics, SLAC, Stanford, November 1976.

23 E.G. Cazzoli, A.M. Cnops, P.L. Connolly, R.L. Louttit, W.J. Murtagh, R.B. Palmer, N.P. Samios, T.T. Tso, H.H. Williams, Phys. Rev. Lett. 34, 1125 (1975); BNL Report No. BNL-19931 (1975).

24 LBL-SLAC Group, Phys. Rev. Lett. 37, 255 (1976).

LBL-SLAC Group, Phys. Rev. Lett. 37, 569 (1976).

LBL-SLAC Group, Phys. Rev. Lett. 37, 1531 (1976).

R.F. Schwitters, Talk presented at Meeting of Division of Particles and Fields, APS, Brookhaven National Laboratory (1976).

25 LBL-SLAC Group, Phys. Rev. Lett. 34, 764 (1975).

LBL-SLAC Group, Phys. Rev. Lett. 36, 700 (1976).

[26] H. Sugimoto, Y. Sato, T. Saito, Prog. Theor. Phys. 53, 1541 (1975).

[27] A. Wijangco, Ph.D. Thesis, Columbia University (1976), unpublished.

[28] D. Nease, Ph.D. Thesis, Cornell University (1976), unpublished.

L. Cormell, Ph.D. Thesis, University of Illinois (1976), unpublished.

D. Wheeler, Ph.D. Thesis, University of Illinois (1976), unpublished.

J. Knauer, D. Yount, Some Photon and Neutron Calorimeter for FNAL Expt. 87A, Proceedings of the Calorimeter Workshop, FNAL, May (1975).

[29] J. Sarracino, Ph.D. Thesis, University of Illinois (1976), unpublished.

[30] R.L. Cool, G. Giacomelli, T.F. Kycia, B.A. Leontic, K.K. Li, A. Lundy, J. Teiger, C. Wilkin, Phys. Rev. D1, 1887 (1970).

N. Samios, M. Goldberg, B.T. Meadows, "Hadrons and SU(3): A Critical Review", Brookhaven National Laboratory, (1973).

[31] SLAC-LBL Group, Phys. Rev. Lett. 34, 1357 (1975).

FIGURE CAPTIONS

Fig. 1 Beam line.

Fig. 2 Photon spectrum.

Fig. 3 Detector layout.

Fig. 4 Spectrum of predicted C = 1 baryons.

Fig. 5a Sketch of a typical V^o event.

5b Sketch of a V^o verticizing with another track downstream of the target.

Fig. 6a Invariant mass distribution for V^o's, assuming $\pi^+\pi^-$.

6b K_S^0 mass.

Fig. 7a Invariant mass distribution for V^o's, assuming $p\pi^-$.

7b Λ mass.

Fig. 8a Invariant mass distribution for V^o's, assuming $\bar{p}\pi^+$.

8b $\bar{\Lambda}$ mass.

Fig. 9 Mass of K_S^o as function of energy of $K_S^o(E)$: (a) $E < 40$ GeV; (b) $40 \text{ GeV} < E < 60$ GeV; (c) $E > 60$ GeV.

Fig. 10 Energy distribution of V^o: (a) K_S^o, (b) Λ, (c) $\bar{\Lambda}$.

Fig. 11 $P_\perp^2$ distribution of V^o: (a) K_S^o, (b) Λ, (c) $\bar{\Lambda}$.

Fig. 12 Total energy of all the reconstructed tracks of an event with a V^o: (a) K_S^o, (b) Λ, (c) $\bar{\Lambda}$.

Fig. 13 Mass of $\Lambda\pi^{\pm}$ from V^{o} which verticizes downstream of the target:
(a) $\Lambda\pi^{-}$, (b) $\Lambda\pi^{+}$.

Fig. 14 Mass of $\bar{\Lambda}\pi^{\pm}$ from V^{o} which verticizes downstream of the target:
(a) $\bar{\Lambda}\pi^{+}$, (b) $\bar{\Lambda}\pi^{-}$.

Fig. 15 $K_S^{o}\pi^{\pm}$ mass, photon data:
(a) $K_S^{o}\pi^{+}$ low mass, (b) $K_S^{o}\pi^{+}$ high mass,
(c) $K_S^{o}\pi^{-}$ low mass, (d) $K_S^{o}\pi^{-}$ high mass.

Fig. 16 $K_S^{o}\pi^{+}\pi^{-}$ mass, photon data.

Fig. 17 $K_S^{o}\pi^{+}\pi^{-}\pi^{\pm}$ mass, photon data:
(a) $K_S^{o}\pi^{+}\pi^{-}\pi^{+}$, (b) $K_S^{o}\pi^{+}\pi^{-}\pi^{-}$.

Fig. 18 $K_S^{o}\pi^{+}\pi^{-}\pi^{+}\pi^{-}$ mass, photon data.

Fig. 19 $\Lambda\pi^{+}$ mass, photon data:
(a) $\Lambda\pi^{+}$ low mass, (b) $\Lambda\pi^{+}$ high mass.

Fig. 20 $\Lambda\pi^{-}$ mass, photon data:
(a) $\Lambda\pi^{-}$ low mass, (b) $\Lambda\pi^{-}$ high mass.

Fig. 21 $\bar{\Lambda}\pi^{+}$ mass, photon data:
(a) $\bar{\Lambda}\pi^{+}$ low mass, (b) $\bar{\Lambda}\pi^{+}$ high mass.

Fig. 22 $\bar{\Lambda}\pi^{-}$ mass, photon data:
(a) $\bar{\Lambda}\pi^{-}$ low mass, (b) $\bar{\Lambda}\pi^{-}$ high mass.

Fig. 23 $\Lambda\pi\pi$ mass, photon data:
(a) $\Lambda\pi^{+}\pi^{+}$, (b) $\Lambda\pi^{+}\pi^{-}$, (c) $\Lambda\pi^{-}\pi^{-}$.

Fig. 24 $\bar{\Lambda}\pi\pi$ mass, photon data:
(a) $\bar{\Lambda}\pi^{+}\pi^{+}$, (b) $\bar{\Lambda}\pi^{+}\pi^{-}$, (c) $\bar{\Lambda}\pi^{-}\pi^{-}$.

Fig. 25 $\Lambda\pi^+\pi^-\pi^\pm$ mass, photon data:
(a) $\Lambda\pi^+\pi^-\pi^+$, (b) $\Lambda\pi^+\pi^-\pi^-$.

Fig. 26 $\bar{\Lambda}\pi^+\pi^-\pi^\pm$ mass, photon data:
(a) $\bar{\Lambda}\pi^+\pi^-\pi^+$, (b) $\bar{\Lambda}\pi^+\pi^-\pi^-$.

Fig. 27 $\Lambda\pi^+\pi^-\pi\pi$ mass, photon data:
(a) $\Lambda\pi^+\pi^-\pi^+\pi^+$, (b) $\Lambda\pi^+\pi^-\pi^+\pi^-$, (c) $\Lambda\pi^+\pi^-\pi^-\pi^-$.

Fig. 28 $\bar{\Lambda}\pi^+\pi^-\pi\pi$ mass photon data:
(a) $\bar{\Lambda}\pi^+\pi^-\pi^+\pi^+$, (b) $\bar{\Lambda}\pi^+\pi^-\pi^+\pi^-$, (c) $\bar{\Lambda}\pi^+\pi^-\pi^-\pi^-$.

Fig. 29 Number of reconstructed tracks for the events inside the $\bar{\Lambda}\pi^+\pi^-\pi^-$ peak.

Fig. 30 Angular distribution of $\bar{p}$ with respect to the $\bar{\Lambda}$ direction in the $\bar{\Lambda}\pi^+\pi^-\pi^-$ rest system (dashed curve: the same distribution for the events just outside the $\bar{\Lambda}\pi^+\pi^-\pi^-$ peak).

Fig. 31 Distribution of the variable, $F^\pm = P_{\pi^\pm} / (P_{\pi^+} + P_{\pi^-} + P_{\pi^-})$ in the rest frame of $\bar{\Lambda}\pi^+\pi^-\pi^-$.

Fig. 32 Study of $\bar{\Lambda}\pi^\pm$, $\bar{\Lambda}\pi^+\pi^-$ mass distributions from the $\bar{\Lambda}\pi^+\pi^-\pi^-$ combinations inside the peak:
(a) $\bar{\Lambda}\pi^+$, (b) $\bar{\Lambda}\pi^-$, (c) $\bar{\Lambda}\pi^+\pi^-$, (d) $\bar{\Lambda}\pi^-\pi^-$.

Fig. 33a Energy distribution of $\bar{\Lambda}\pi^+\pi^-\pi^-$ peak.
33b $P_\perp^2$ distribution of $\bar{\Lambda}\pi^+\pi^-\pi^-$ peak.

Fig. 34 Mass difference between $\bar{\Lambda}\pi^+\pi^-\pi^+\pi^-$ and $\bar{\Lambda}\pi^+\pi^-\pi^-$ within the 2.26 GeV/c^2 peak and immediately outside the peak (dashed curve).

Fig. 35a $\bar{\Lambda}p\pi^-\pi^-$ mass, assuming the positive track to be a proton.

Fig. 35b $\bar{\Lambda}K^+\pi^-\pi^-$ mass, assuming the positive track to be a kaon.

35c $\bar{\Lambda}K^-\pi^+\pi^-$ mass, assuming the negative track to be a kaon.

Fig. 36 $\bar{\Lambda}\pi^+\pi^-\pi^+$ mass, from runs with magnet polarity (a) positive, (b) negative.

Fig. 37 $\bar{\Lambda}\pi^+\pi^-\pi^-$ mass, from runs with magnet polarity (a) positive, (b) negative.

Fig. 38 $K_S^o\pi^+\pi^-\pi^+\pi^-$ mass, photon data: (a) 6-prong events only, (b) no anticounters and number of unused hits in chambers less than 10, (c) energy of $K_S^o\pi^+\pi^-\pi^+\pi^-$ less than 150 GeV.

Fig. 39 $K_S^o\pi^+\pi^-\pi^+\pi^-$ mass, K_L + neutron data shaded: K_L data only: (a) 6-prong events only, (b) no anticounters and number of unused hits in chambers less than 10, (c) energy of $K_S^o\pi^+\pi^-\pi^+\pi^-$ less than 150 GeV.

Fig. 40 $\Lambda\pi^+\pi^-\pi^\pm$ mass, K_L + neutron data: (a) $\Lambda\pi^+\pi^-\pi^+$, (b) $\Lambda\pi^+\pi^-\pi^-$.

Fig. 41 $\bar{\Lambda}\pi^+\pi^-\pi^\pm$ mass, K_L + neutron data: (a) $\bar{\Lambda}\pi^+\pi^-\pi^+$, (b) $\bar{\Lambda}\pi^+\pi^-\pi^-$.

Fig. 42 $\Lambda\pi^+\pi^-\pi\pi$ mass, K_L + neutron data: (a) $\Lambda\pi^+\pi^-\pi^+\pi^+$, (b) $\Lambda\pi^+\pi^-\pi^+\pi^-$, (c) $\Lambda\pi^+\pi^-\pi^-\pi^-$.

Fig. 43 $\bar{\Lambda}\pi^+\pi^-\pi\pi$ mass, K_L + neutron data: (a) $\bar{\Lambda}\pi^+\pi^-\pi^+\pi^+$, (b) $\bar{\Lambda};^+\pi^-\pi^+\pi^-$, (c) $\bar{\Lambda}\pi^+\pi^-\pi^-\pi^-$.

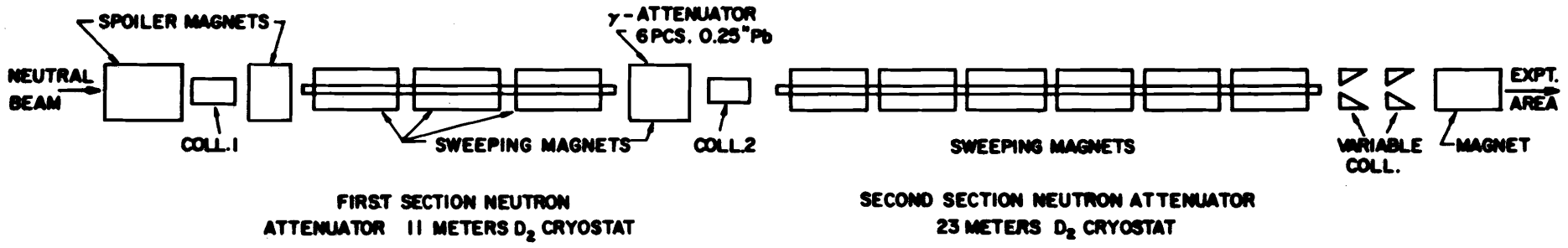
SPOILER MAGNETS
NEUTRAL BEAM
COLL.1
SWEEPING MAGNETS
γ-ATTENUATOR
6 PCS. 0.25" Pb
COLL.2
SWEEPING MAGNETS
VARIABLE COLL.
MAGNET
EXPT. AREA
FIRST SECTION NEUTRON ATTENUATOR 11 METERS D_2 CRYOSTAT
SECOND SECTION NEUTRON ATTENUATOR 23 METERS D_2 CRYOSTAT

FIG. 1

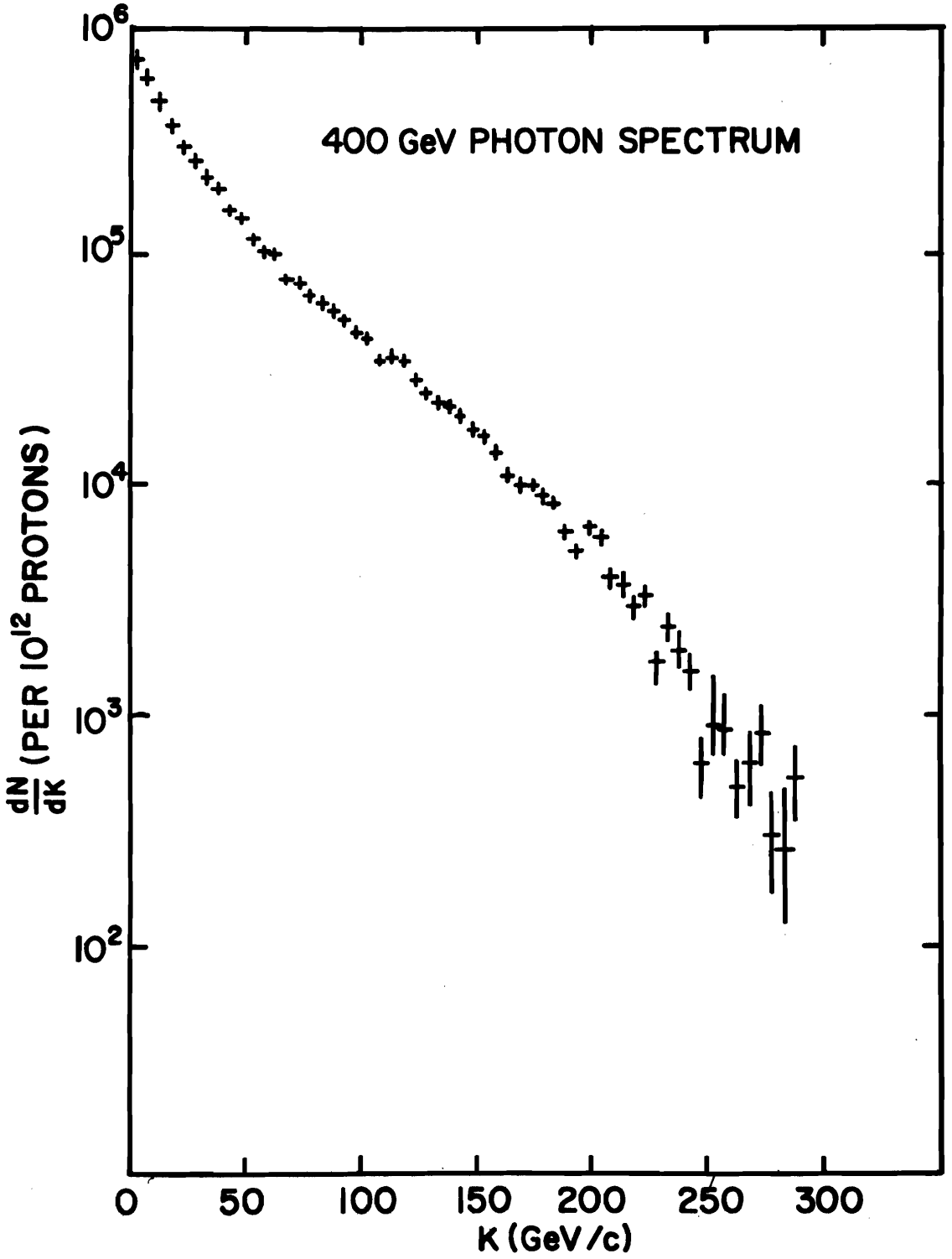
400 GeV PHOTON SPECTRUM
10^6
10^5
10^4
10^3
10^2
$\frac{dN}{dK}$ (PER 10^{12} PROTONS)
0
50
100
150
200
250
300
K (GeV/c)

FIG. 2

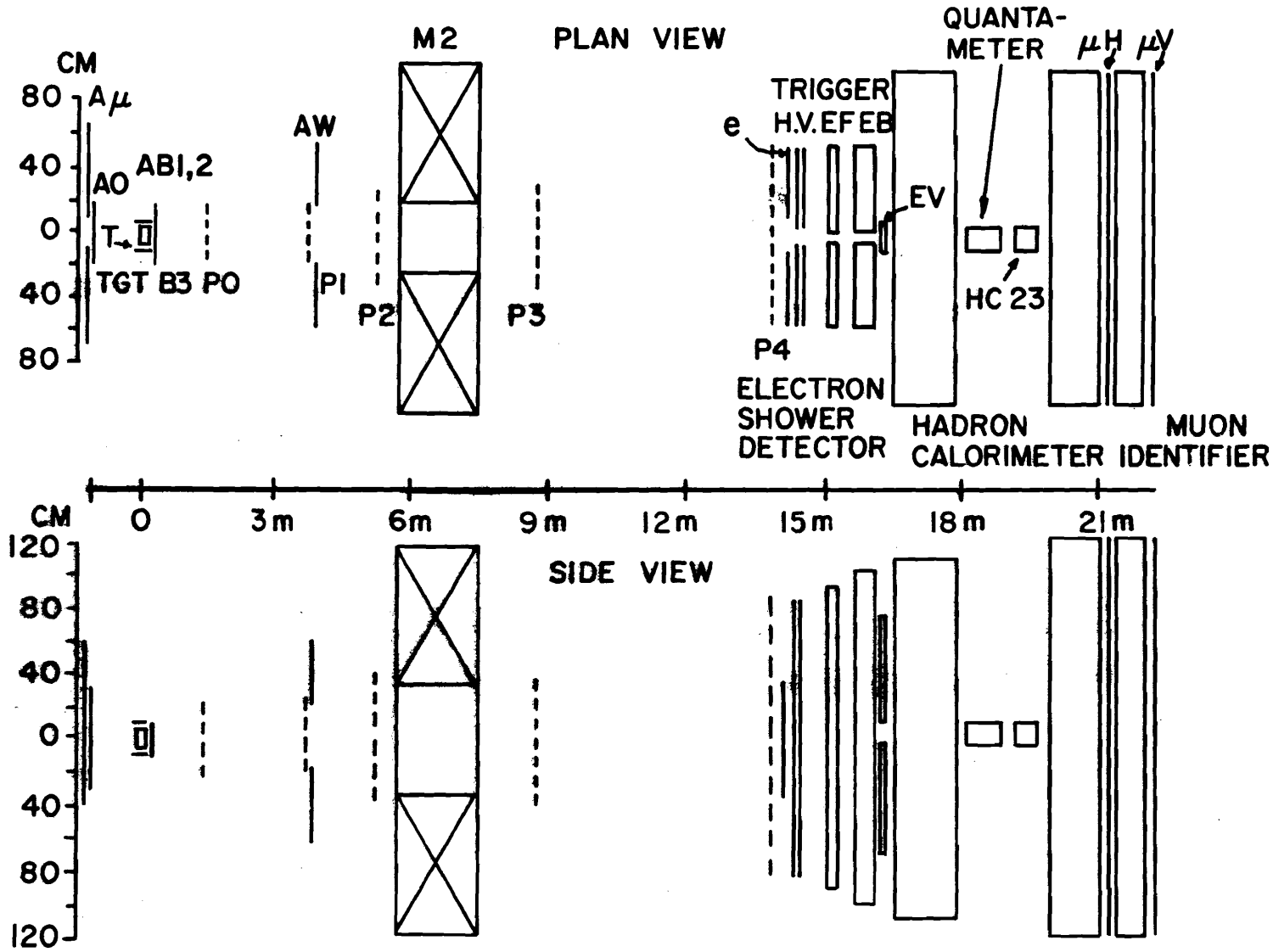

VIEWS OF MAGNETIC SPECTROMETER AND PARTICLE IDENTIFICATION SYSTEM

FIG. 3

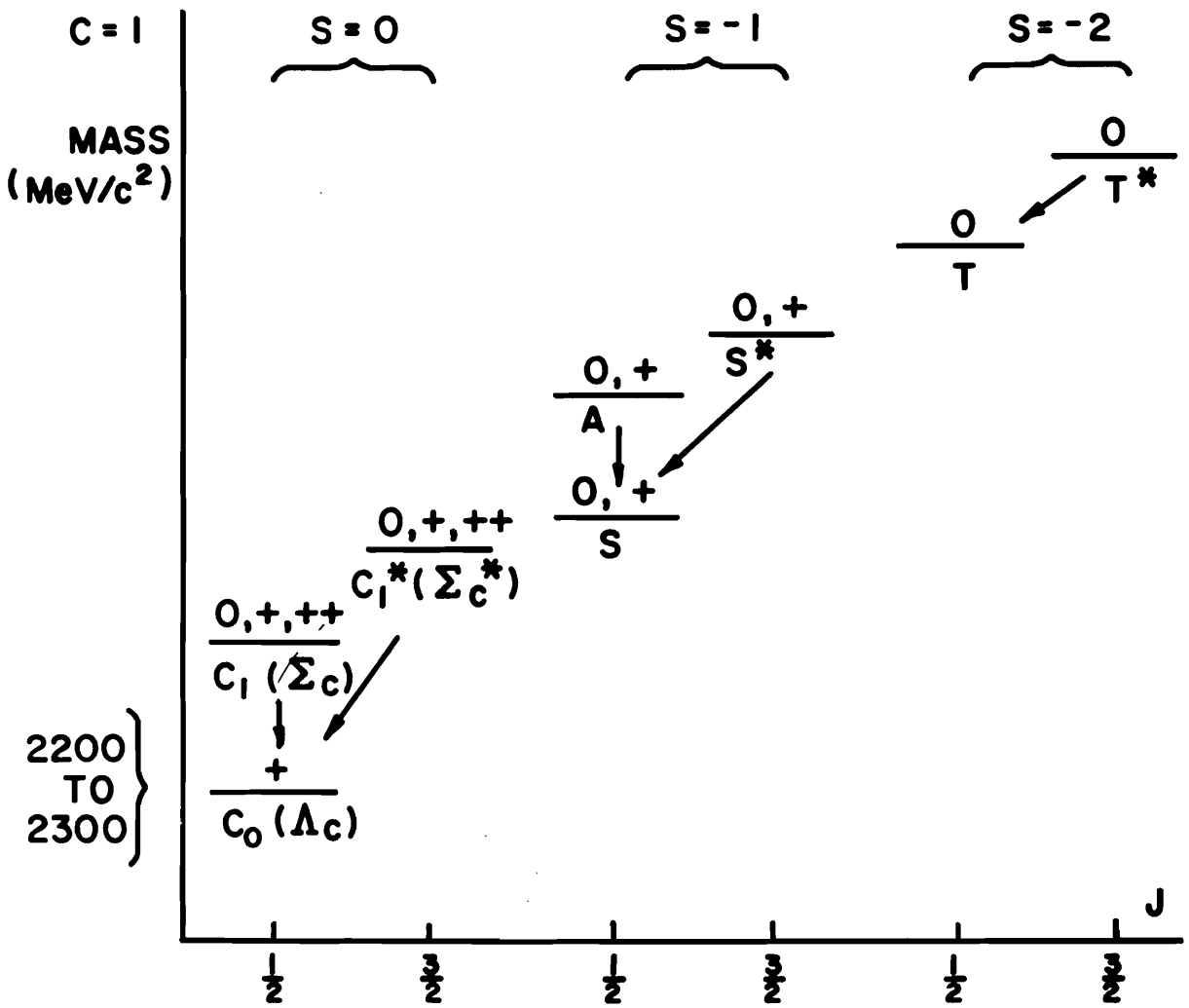
C = 1
S = 0
S = -1
S = -2
MASS
(MeV/c²)
0
T*
0
T
0, +
S*
0, +
A
0, +
S
0, +, ++
C₁*(Σc*)
0, +, ++
C₁ (Σc)
+
C₀ (Λc)
2200
TO
2300
J
1/2
3/2
1/2
3/2
1/2
3/2

FIG. 4

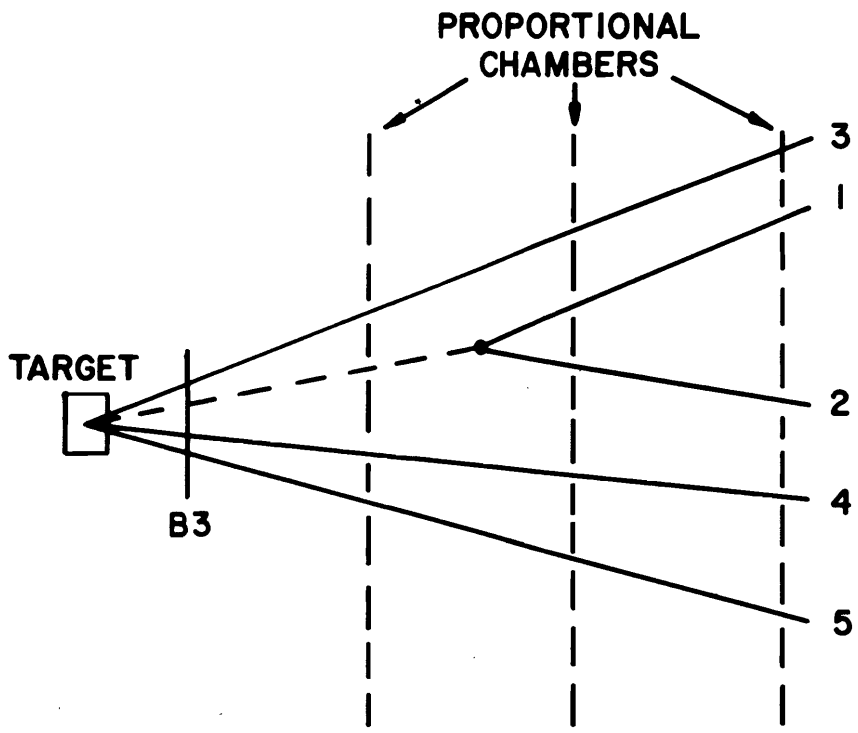

IF MASS OF $V = K_S \rightarrow K_S$
$(K_S \rightarrow \pi^+\pi^-)$
$M_{ks} = 498 \pm 15$ MeV

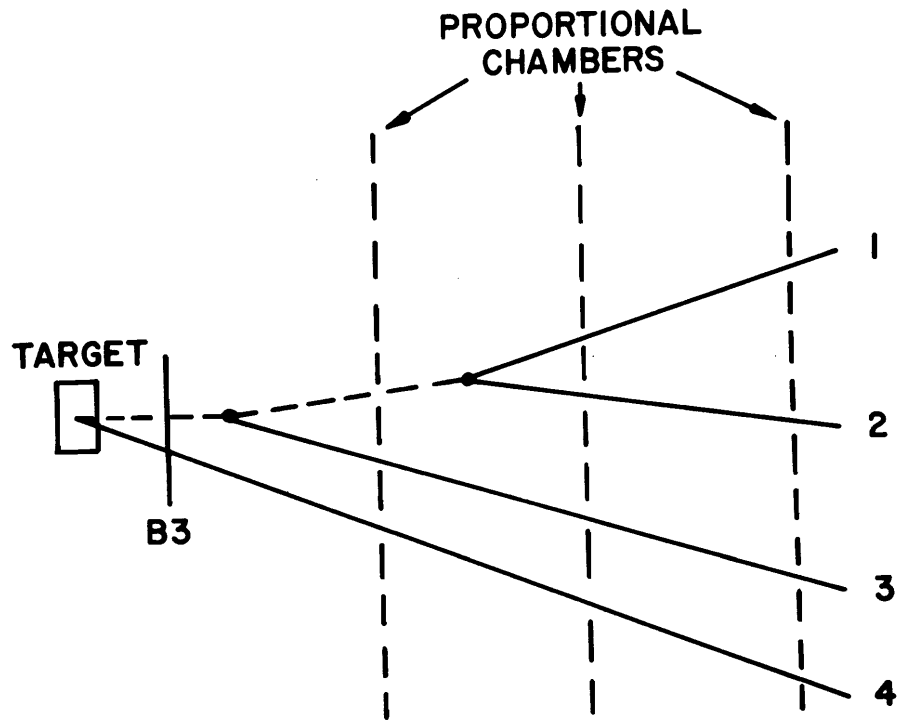

$1+2 = \Lambda(\bar{\Lambda})$
$(1+2)+3 = \Lambda(\bar{\Lambda})+\pi$

FIG. 5

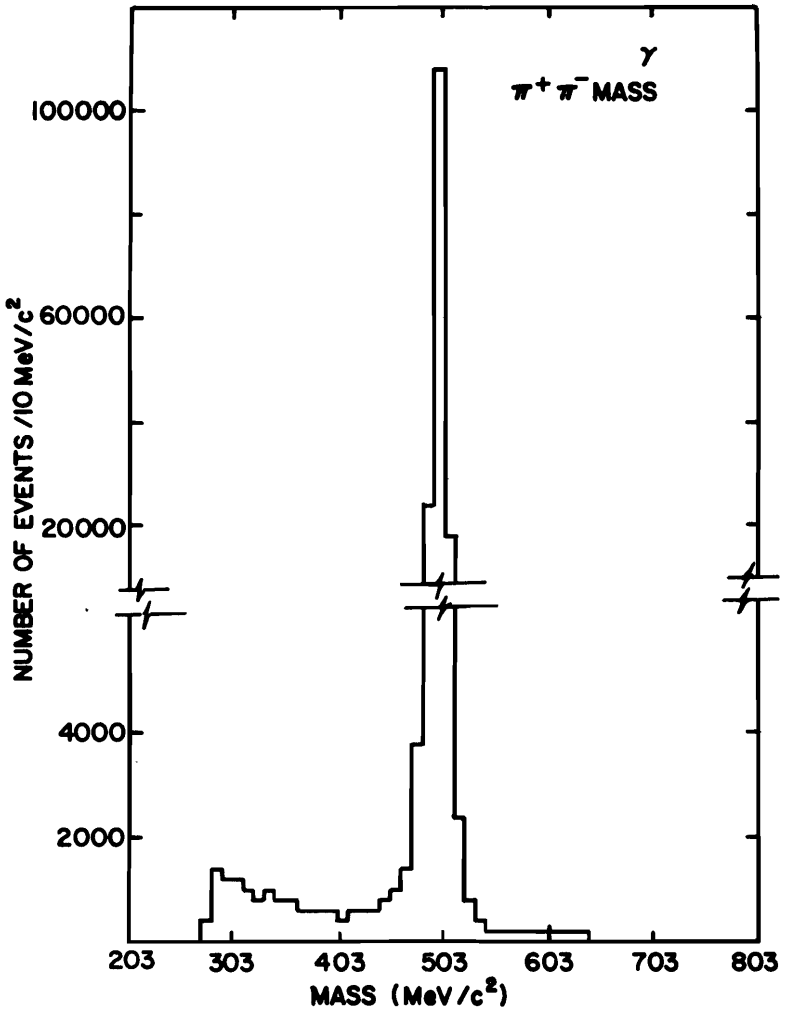
γ
π+π− MASS
100000
60000
20000
4000
2000
NUMBER OF EVENTS /10 MeV/c²
203
303
403
503
603
703
803
MASS (MeV/c²)

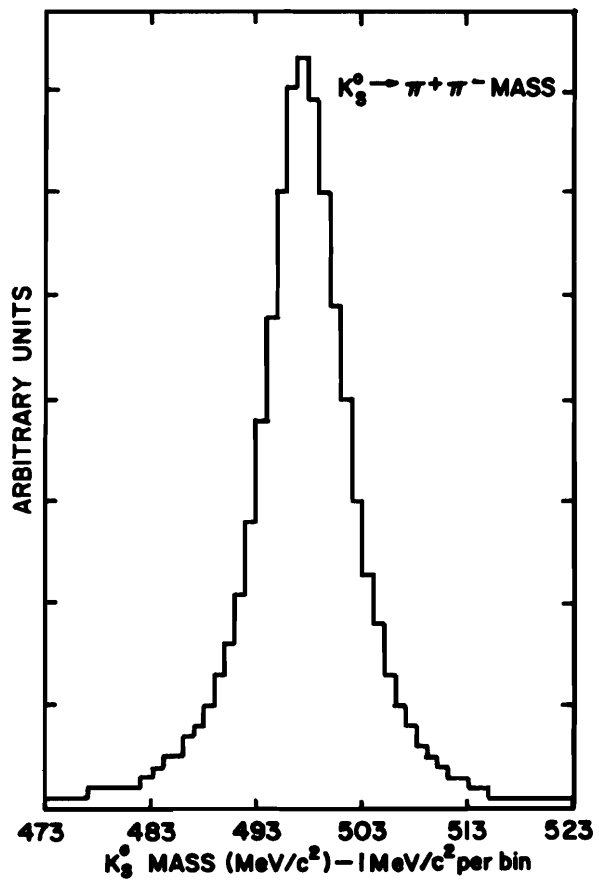
K⁰s → π+π− MASS
ARBITRARY UNITS
473
483
493
503
513
523
K⁰s MASS (MeV/c²) – 1 MeV/c² per bin

FIG. 6

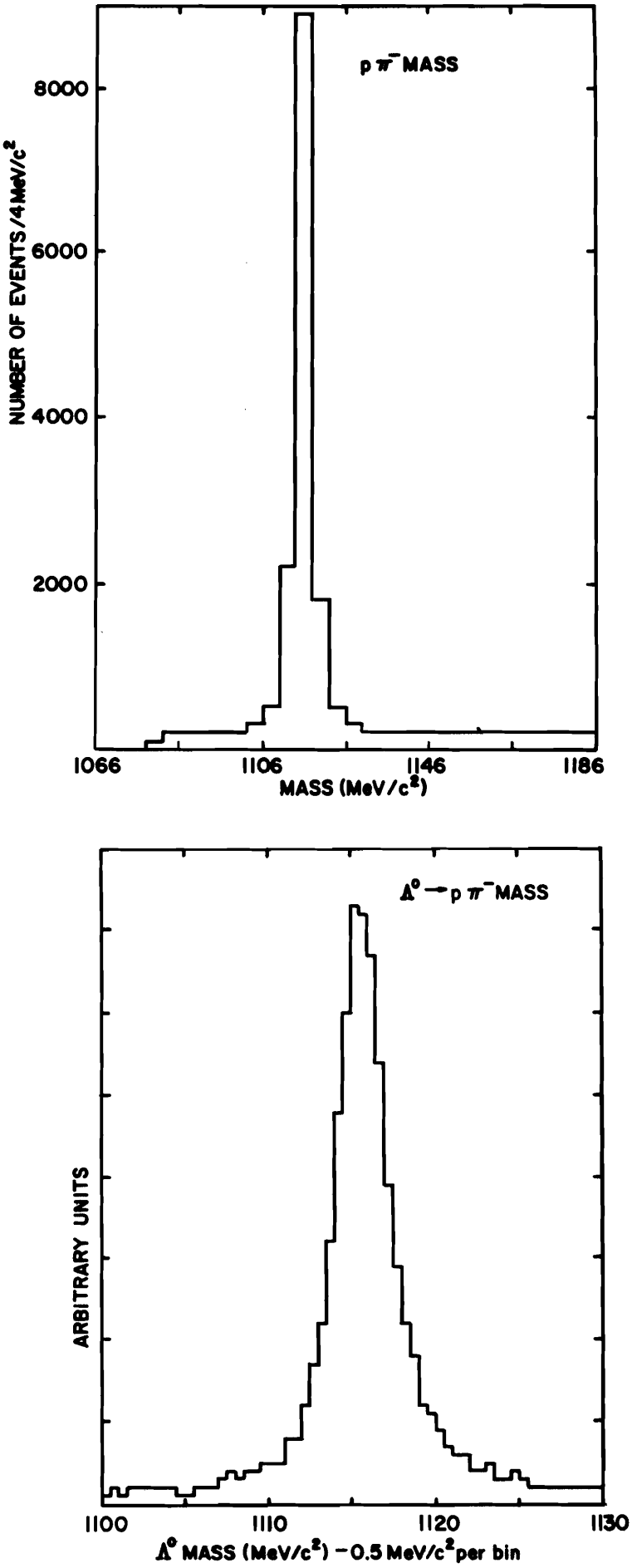
p π⁻ MASS
NUMBER OF EVENTS/4 MeV/c²
8000
6000
4000
2000
1066
1106
1146
1186
MASS (MeV/c²)
Λ⁰ → p π⁻ MASS
ARBITRARY UNITS
1100
1110
1120
1130
Λ⁰ MASS (MeV/c²) − 0.5 MeV/c² per bin

FIG. 7

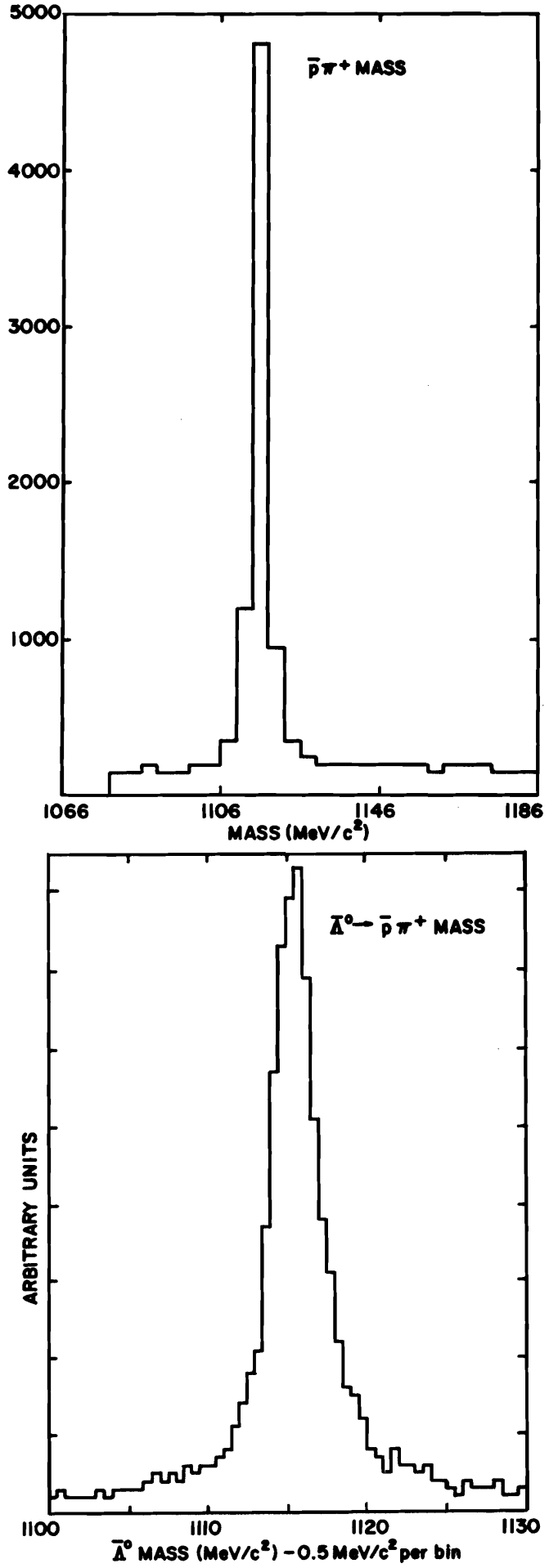
5000
4000
3000
2000
1000
$\bar{p}\pi^+$ MASS
1066
1106
1146
1186
MASS (MeV/c^2)
$\bar{\Lambda}^0 \to \bar{p}\pi^+$ MASS
ARBITRARY UNITS
1100
1110
1120
1130
$\bar{\Lambda}^0$ MASS (MeV/c^2) - 0.5 MeV/c^2 per bin

FIG. 8

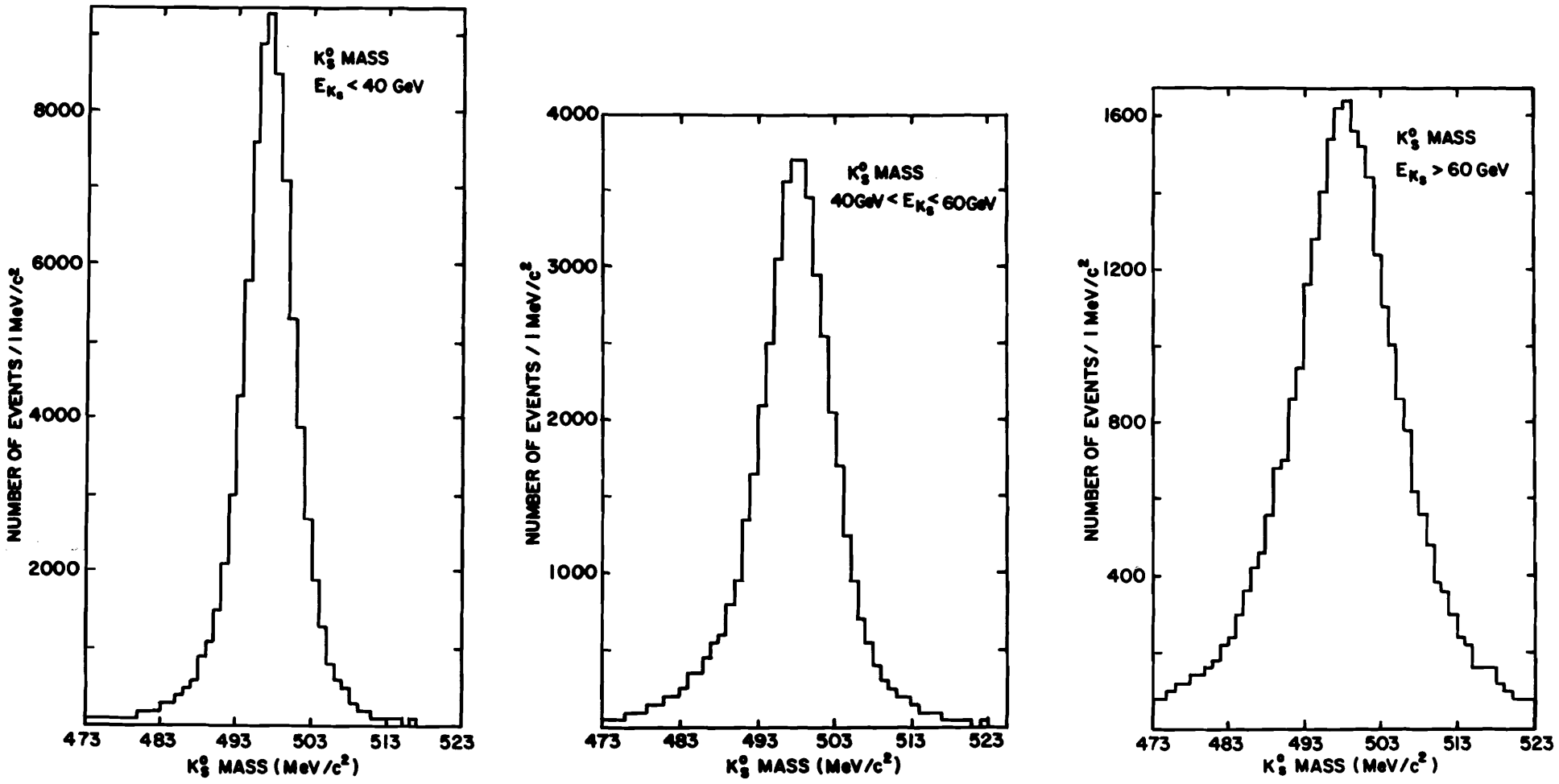
K_S^0 MASS
$E_{K_S} < 40$ GeV
NUMBER OF EVENTS / 1 MeV/c²
8000
6000
4000
2000
473
483
493
503
513
523
K_S^0 MASS (MeV/c²)
K_S^0 MASS
40GeV < E_{K_S} < 60GeV
NUMBER OF EVENTS / 1 MeV/c²
4000
3000
2000
1000
473
483
493
503
513
523
K_S^0 MASS (MeV/c²)
K_S^0 MASS
E_{K_S} > 60 GeV
NUMBER OF EVENTS / 1 MeV/c²
1600
1200
800
400
473
483
493
503
513
523
K_S^0 MASS (MeV/c²)

FIG. 9

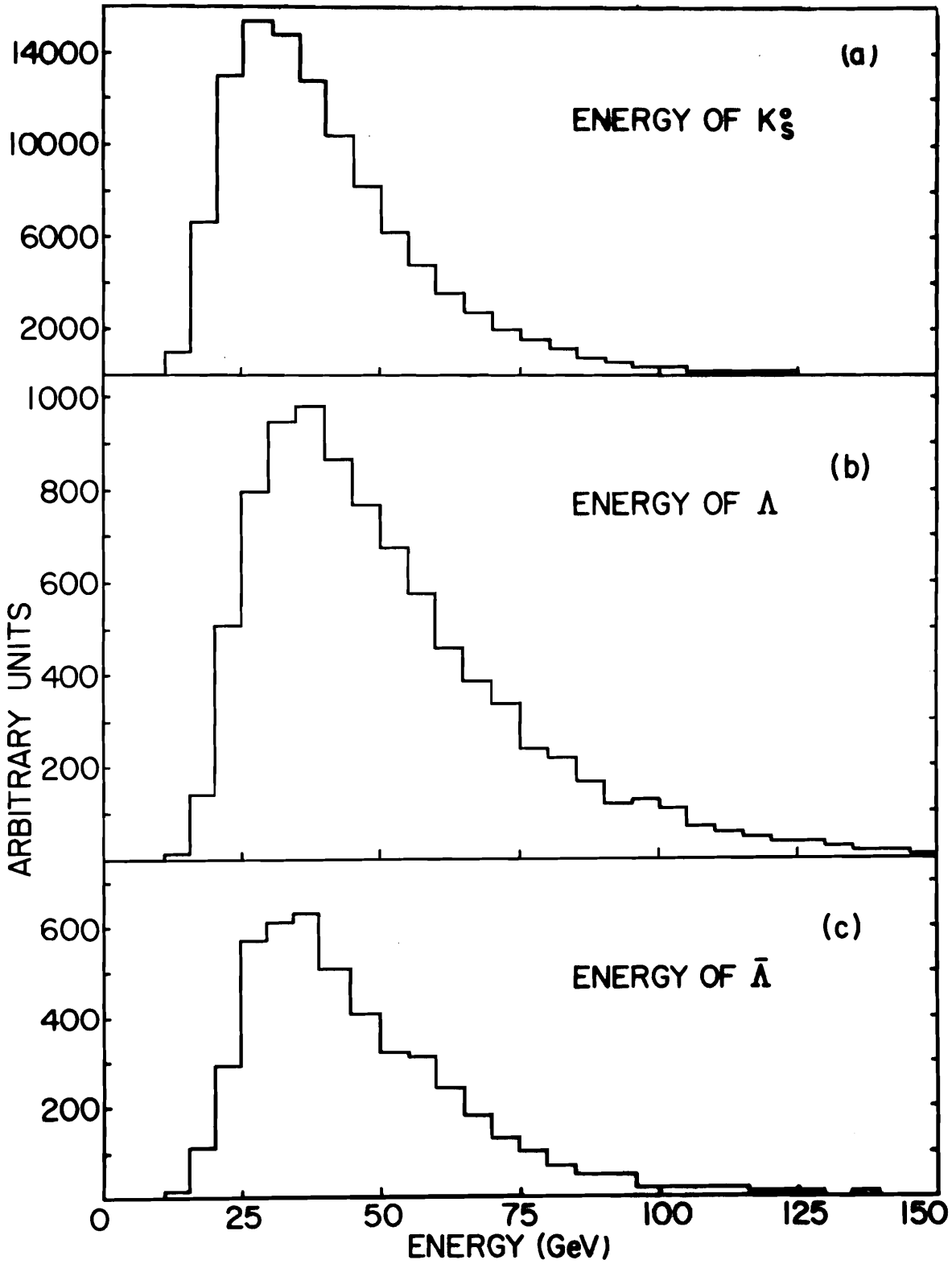
14000
10000
6000
2000
(a)
ENERGY OF K_S^0
1000
800
600
400
200
(b)
ENERGY OF Λ
ARBITRARY UNITS
600
400
200
(c)
ENERGY OF $\bar{\Lambda}$
0
25
50
75
100
125
150
ENERGY (GeV)

FIG. 10

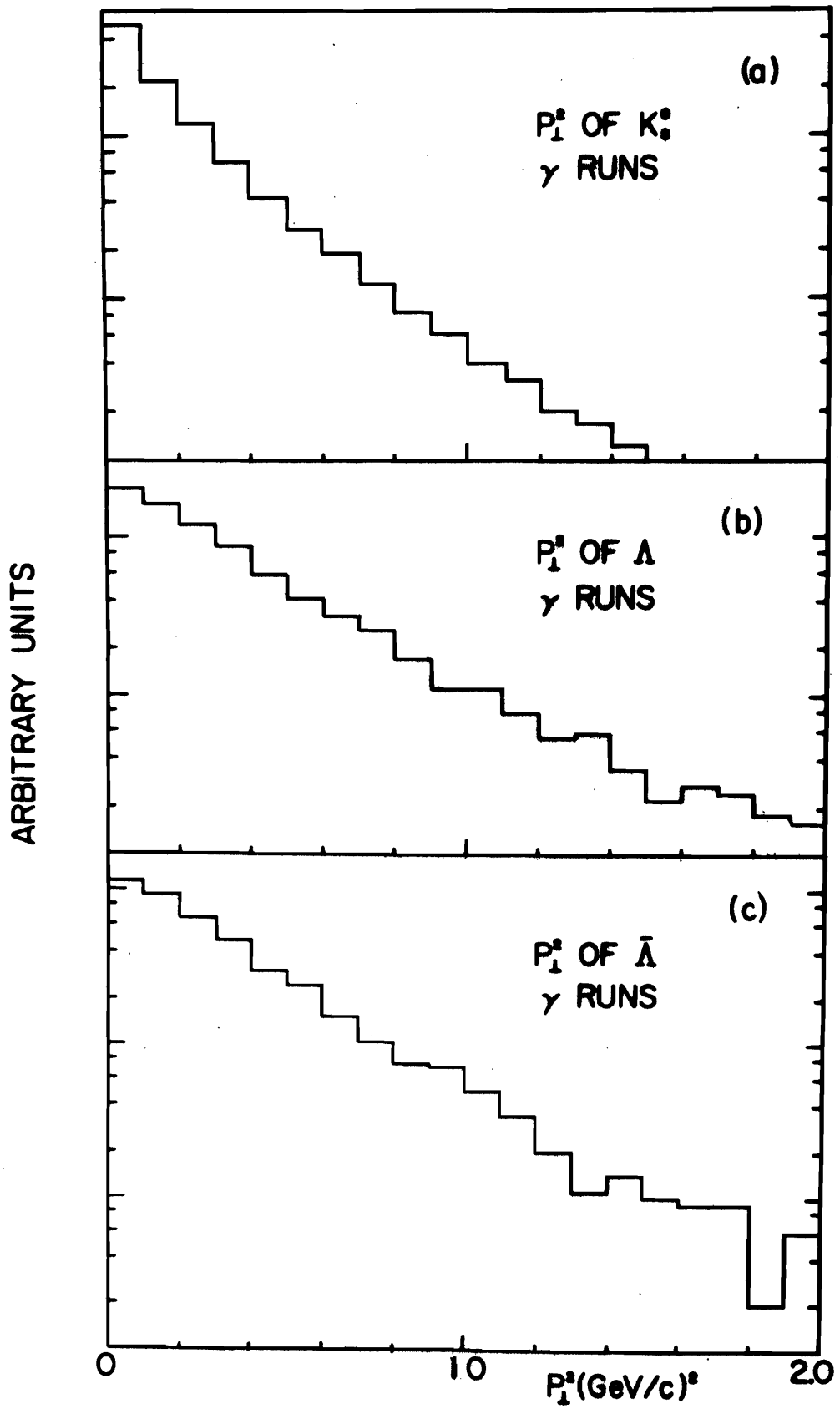
(a)
$P_\perp^2$ OF K_s^0
γ RUNS
(b)
$P_\perp^2$ OF Λ
γ RUNS
(c)
$P_\perp^2$ OF $\bar{\Lambda}$
γ RUNS
ARBITRARY UNITS
0
1.0
2.0
$P_\perp^2$(GeV/c)^2

FIG. 11

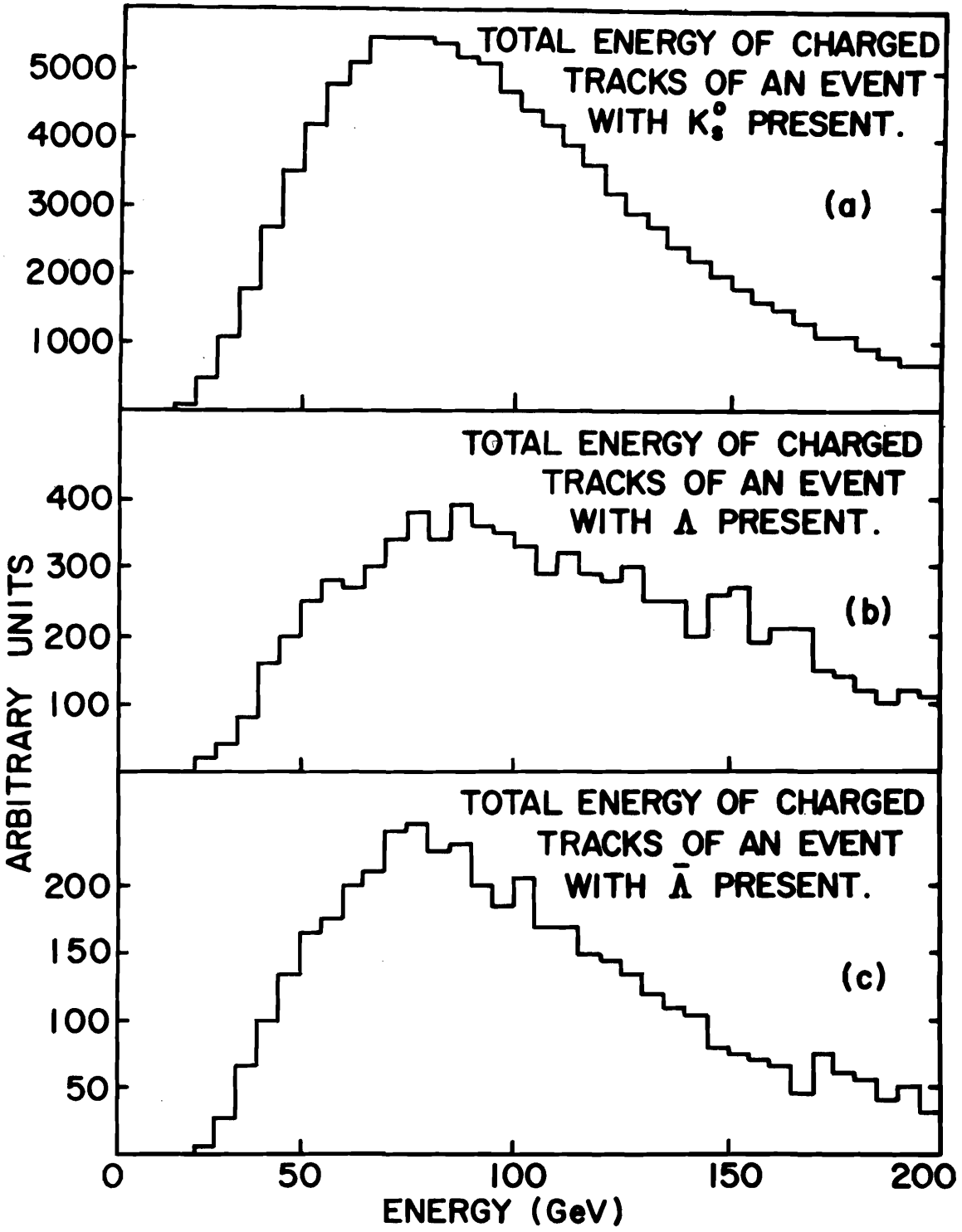
TOTAL ENERGY OF CHARGED TRACKS OF AN EVENT WITH K_s^0 PRESENT.
(a)
TOTAL ENERGY OF CHARGED TRACKS OF AN EVENT WITH Λ PRESENT.
(b)
TOTAL ENERGY OF CHARGED TRACKS OF AN EVENT WITH $\bar{\Lambda}$ PRESENT.
(c)
ARBITRARY UNITS
5000
4000
3000
2000
1000
400
300
200
100
200
150
100
50
0
50
100
150
200
ENERGY (GeV)

FIG. 12

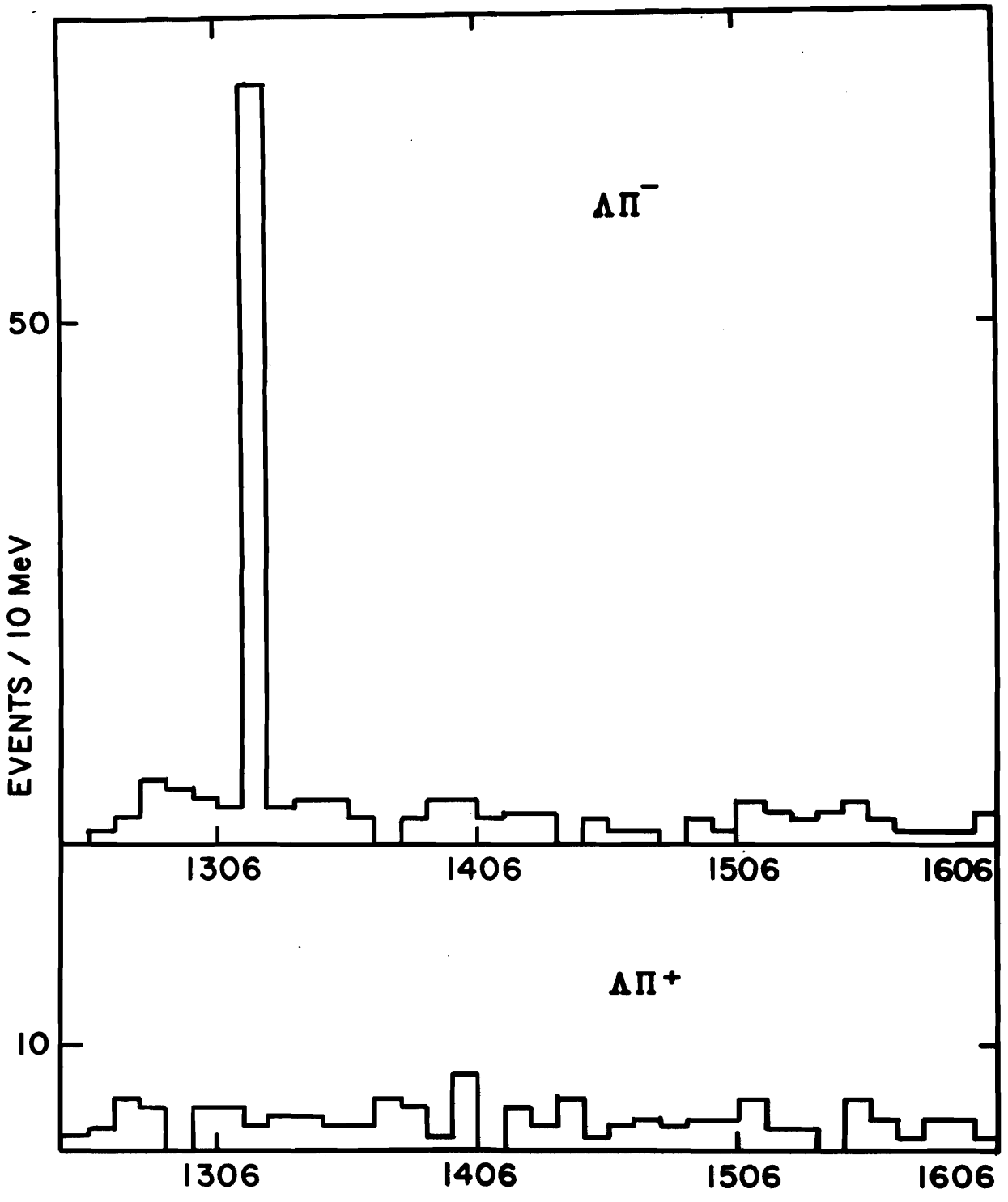
ΛΠ⁻
50
EVENTS / 10 MeV
1306
1406
1506
1606
ΛΠ⁺
10
1306
1406
1506
1606

FIG. 13

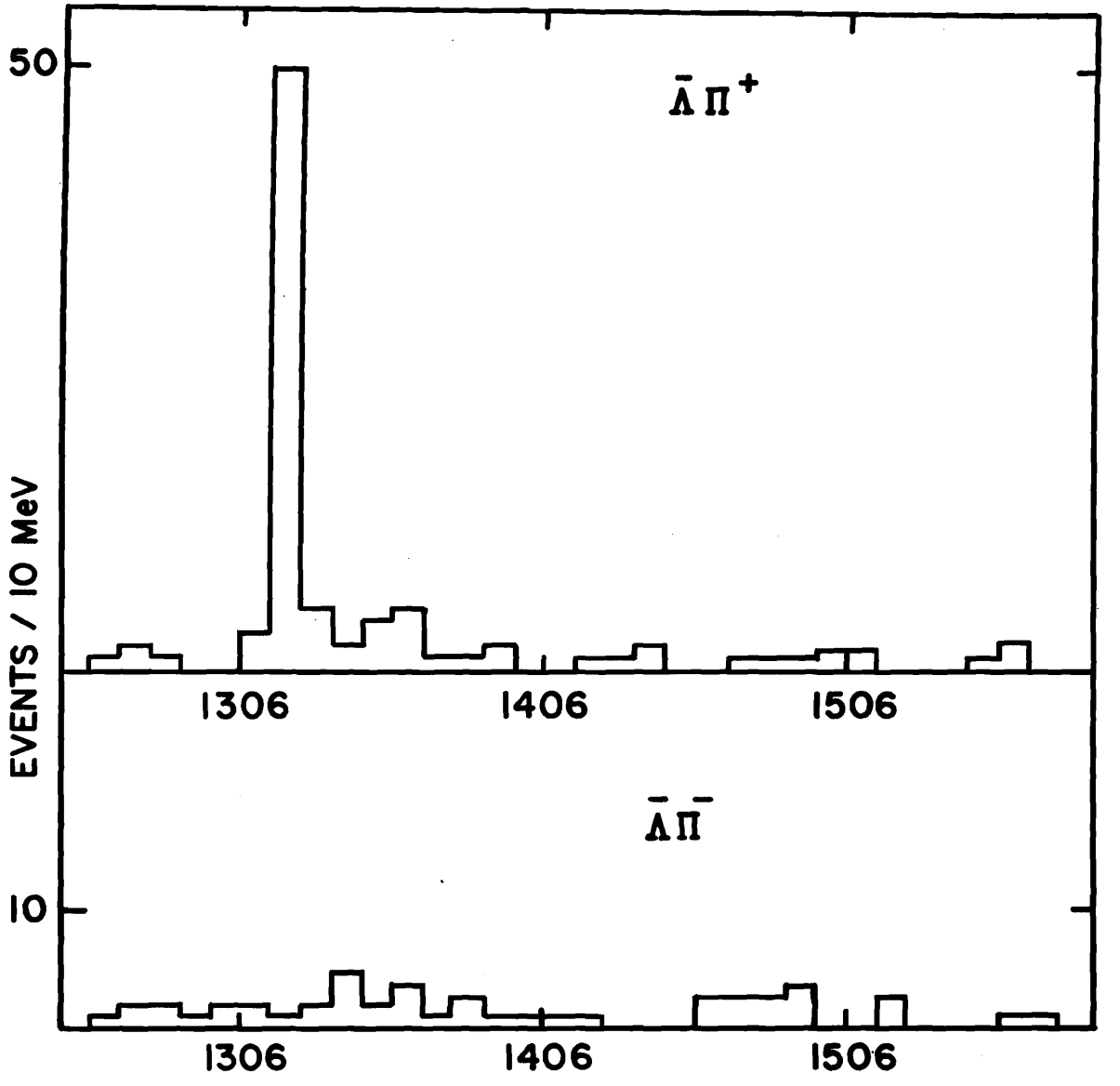
50
10
EVENTS / 10 MeV
$\bar{\Lambda}\Pi^+$
$\bar{\Lambda}\Pi^-$
1306
1406
1506
1306
1406
1506

FIG. 14

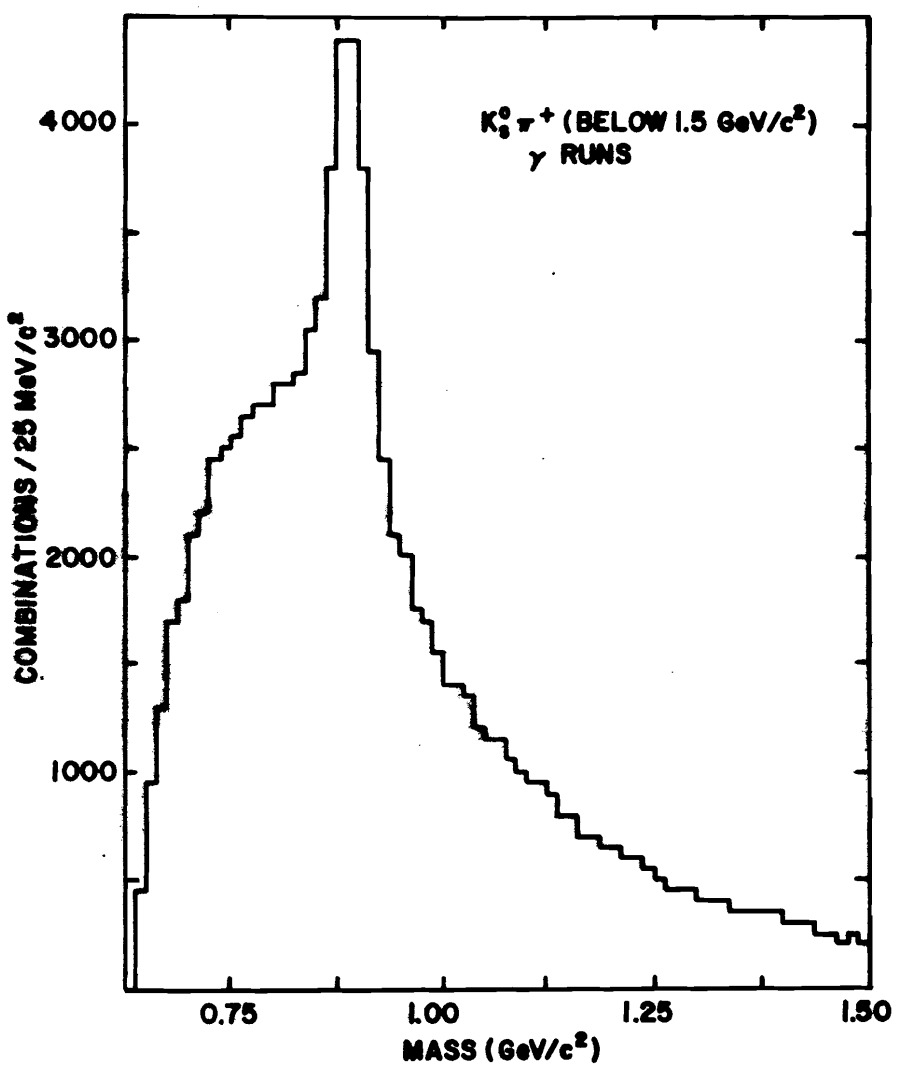
$K_s^0 \pi^+$ (BELOW 1.5 GeV/c²)
γ RUNS
COMBINATIONS / 25 MeV/c²
4000
3000
2000
1000
0.75
1.00
1.25
1.50
MASS (GeV/c²)

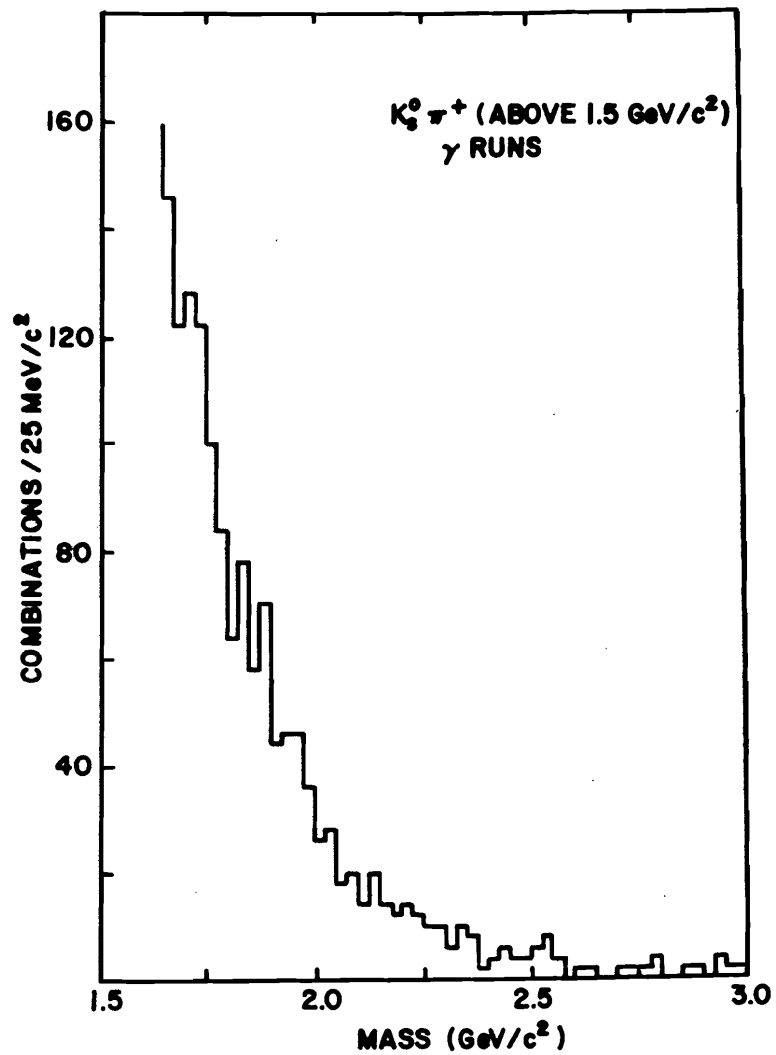
$K_s^0 \pi^+$ (ABOVE 1.5 GeV/c²)
γ RUNS
COMBINATIONS / 25 MeV/c²
160
120
80
40
1.5
2.0
2.5
3.0
MASS (GeV/c²)

FIG. 15
a, b

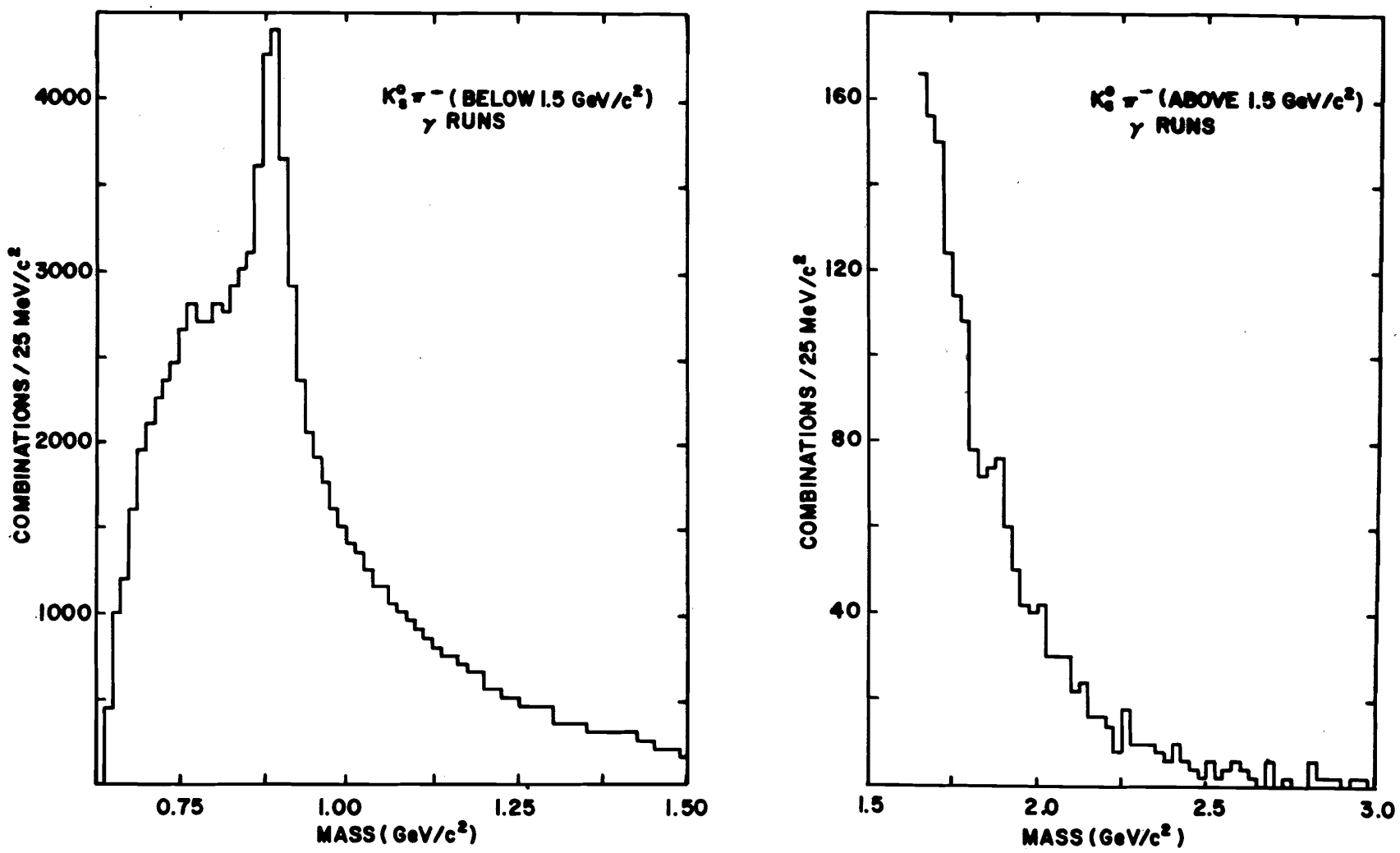
$K_s^0\pi^-$ (BELOW 1.5 GeV/c²)
γ RUNS
COMBINATIONS / 25 MeV/c²
4000
3000
2000
1000
0.75
1.00
1.25
1.50
MASS (GeV/c²)
$K_s^0\pi^-$ (ABOVE 1.5 GeV/c²)
γ RUNS
COMBINATIONS / 25 MeV/c²
160
120
80
40
1.5
2.0
2.5
3.0
MASS (GeV/c²)

FIG. 15
c,d

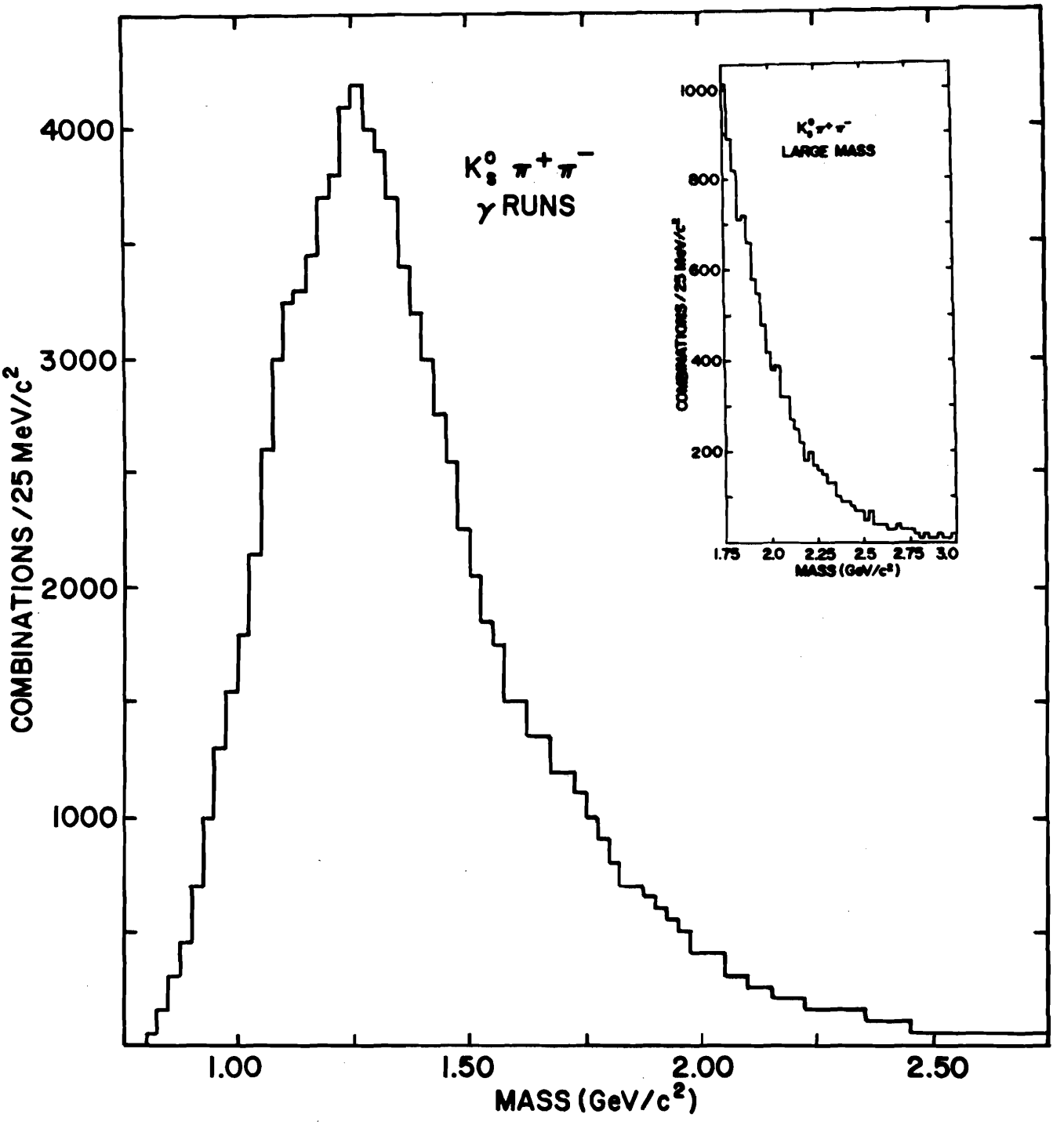
$K_s^0\ \pi^+\pi^-$
γ RUNS
COMBINATIONS/25 MeV/c^2
4000
3000
2000
1000
1.00
1.50
2.00
2.50
MASS (GeV/c^2)
$K_s^0\pi^+\pi^-$
LARGE MASS
1000
800
600
400
200
1.75
2.0
2.25
2.5
2.75
3.0
MASS (GeV/c^2)

FIG. 16

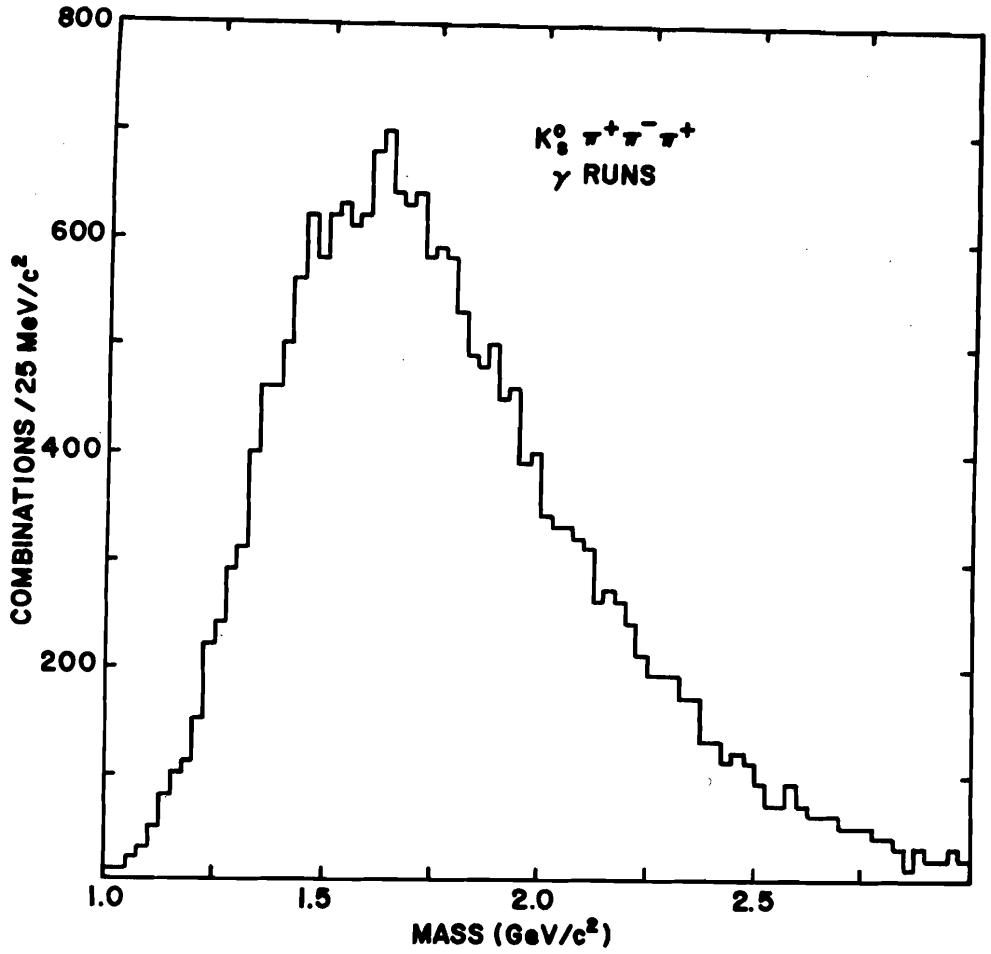
800
600
400
200
COMBINATIONS /25 MeV/c²
$K_s^0\ \pi^+\pi^-\pi^+$
γ RUNS
1.0
1.5
2.0
2.5
MASS (GeV/c²)

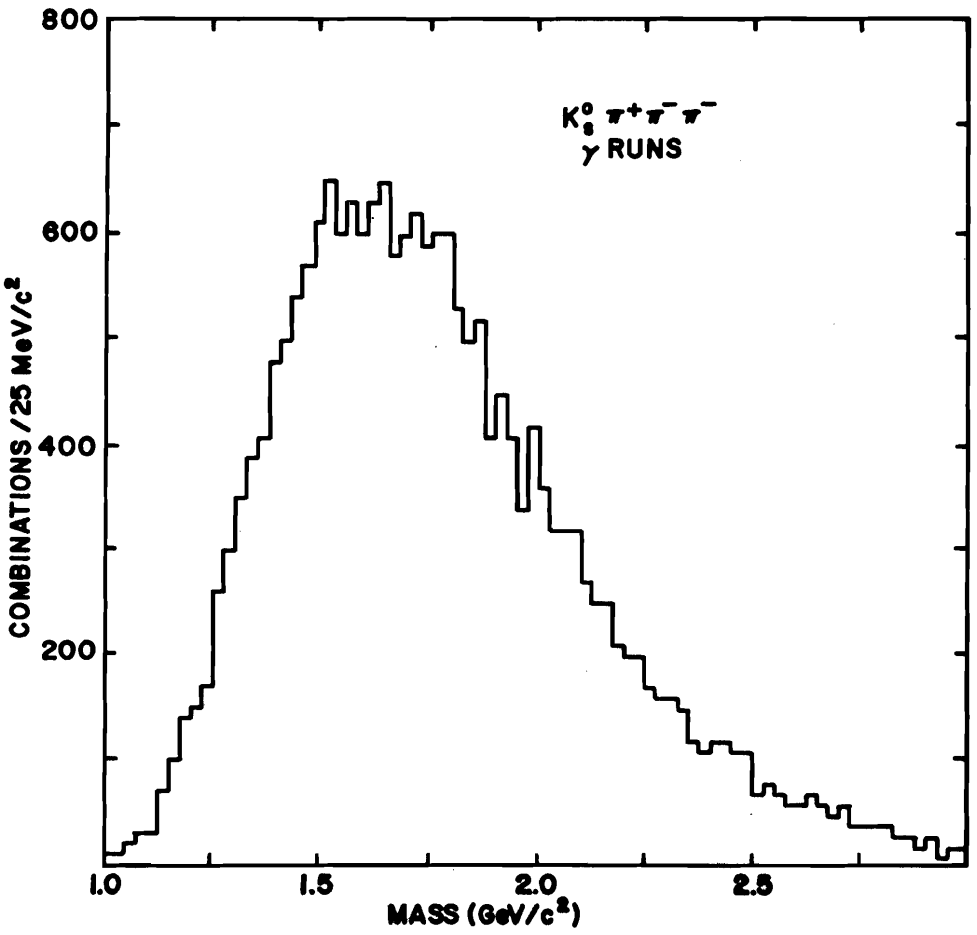
800
600
400
200
COMBINATIONS /25 MeV/c²
$K_s^0\ \pi^+\pi^-\pi^-$
γ RUNS
1.0
1.5
2.0
2.5
MASS (GeV/c²)

FIG. 17

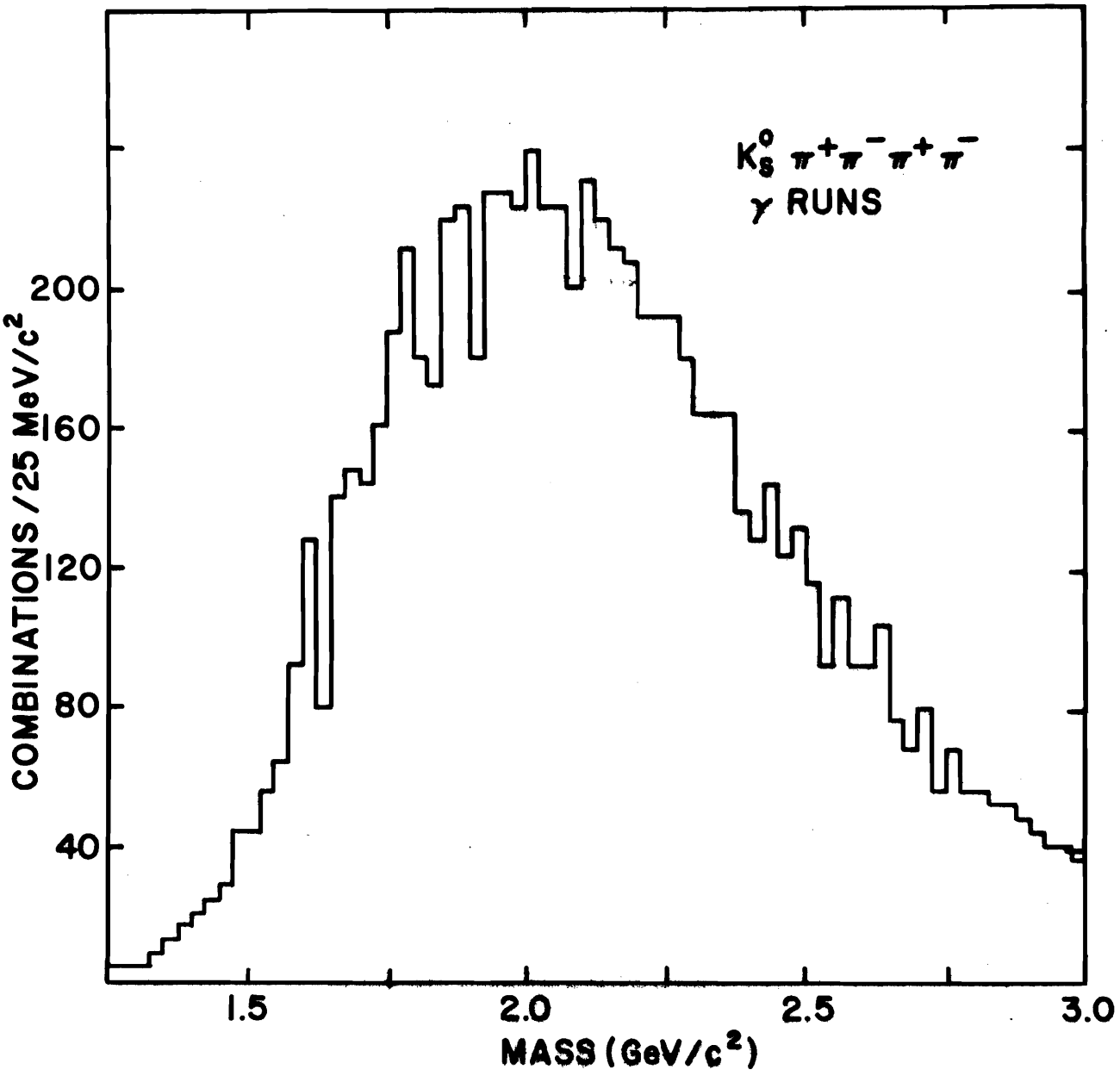
$K_S^0\ \pi^+\pi^-\pi^+\pi^-$
γ RUNS
COMBINATIONS /25 MeV/c^2
200
160
120
80
40
1.5
2.0
2.5
3.0
MASS (GeV/c^2)

FIG. 18

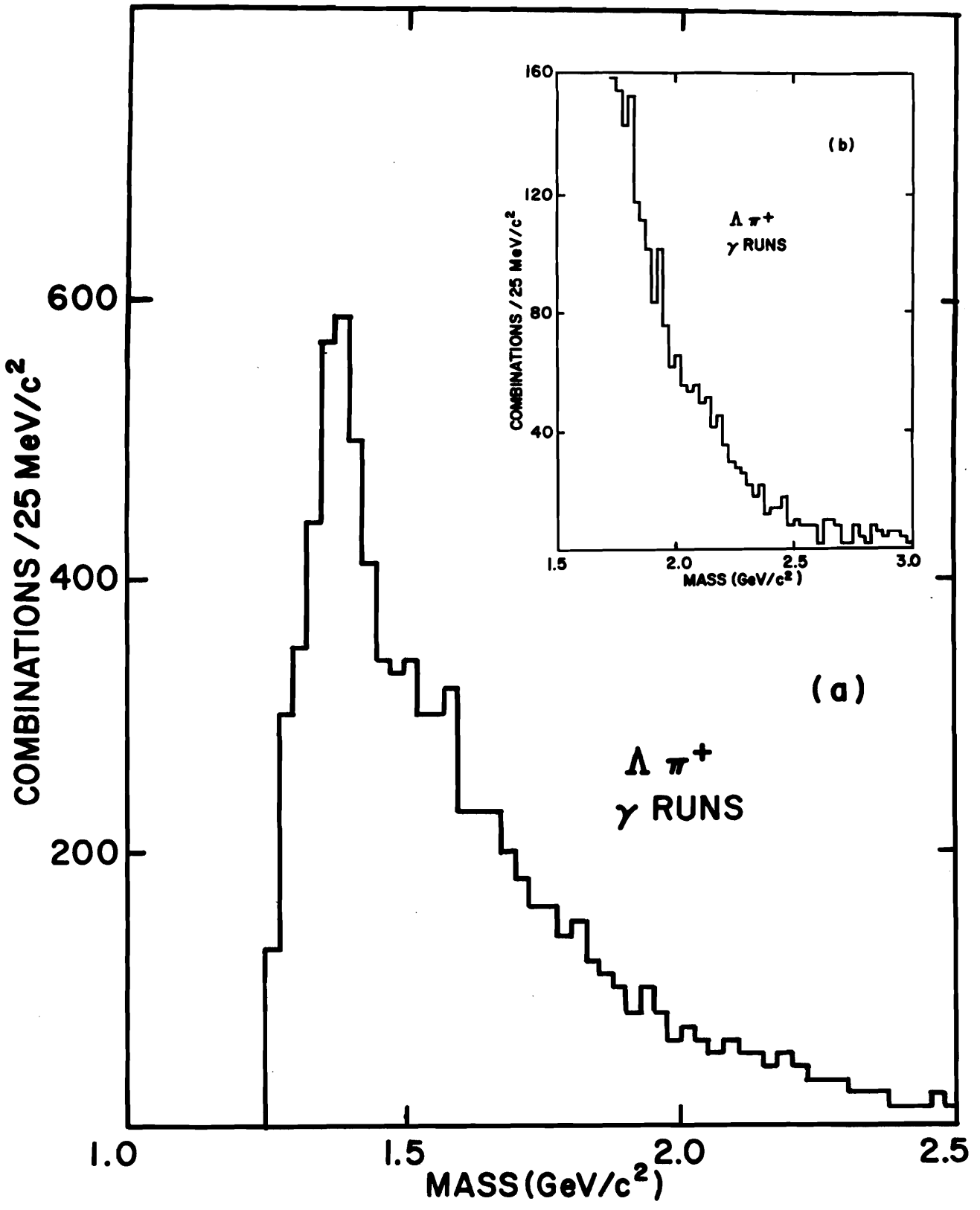
COMBINATIONS /25 MeV/c²
600
400
200
1.0
1.5
2.0
2.5
MASS (GeV/c²)
(a)
Λ π+
γ RUNS
160
120
80
40
COMBINATIONS / 25 MeV/c²
1.5
2.0
2.5
3.0
MASS (GeV/c²)
(b)
Λ π+
γ RUNS

FIG. 19

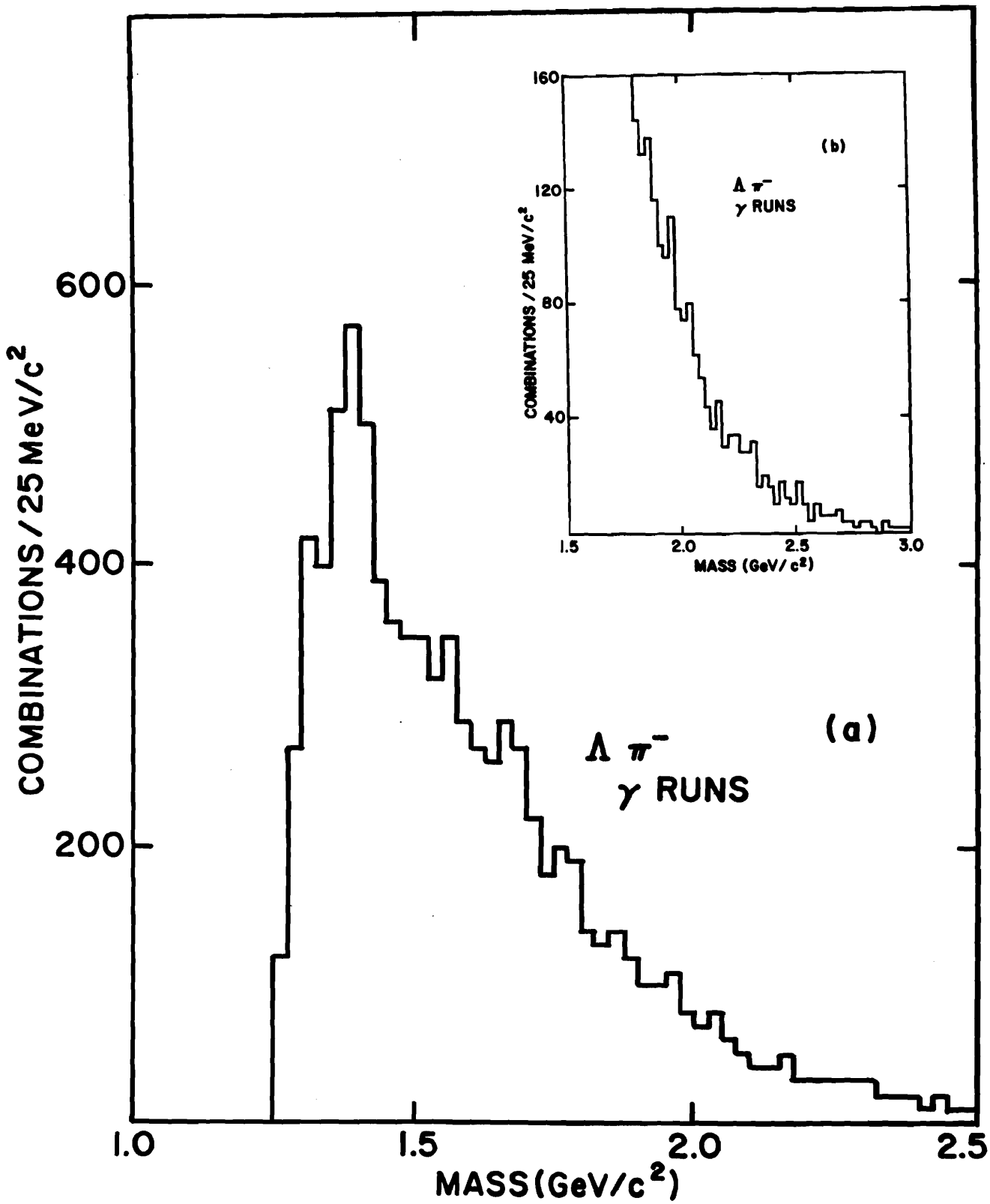
COMBINATIONS / 25 MeV/c²
600
400
200
1.0
1.5
2.0
2.5
MASS(GeV/c²)
Λ π⁻
γ RUNS
(a)
160
120
80
40
COMBINATIONS / 25 MeV/c²
1.5
2.0
2.5
3.0
MASS (GeV/c²)
(b)
Λ π⁻
γ RUNS

FIG. 20

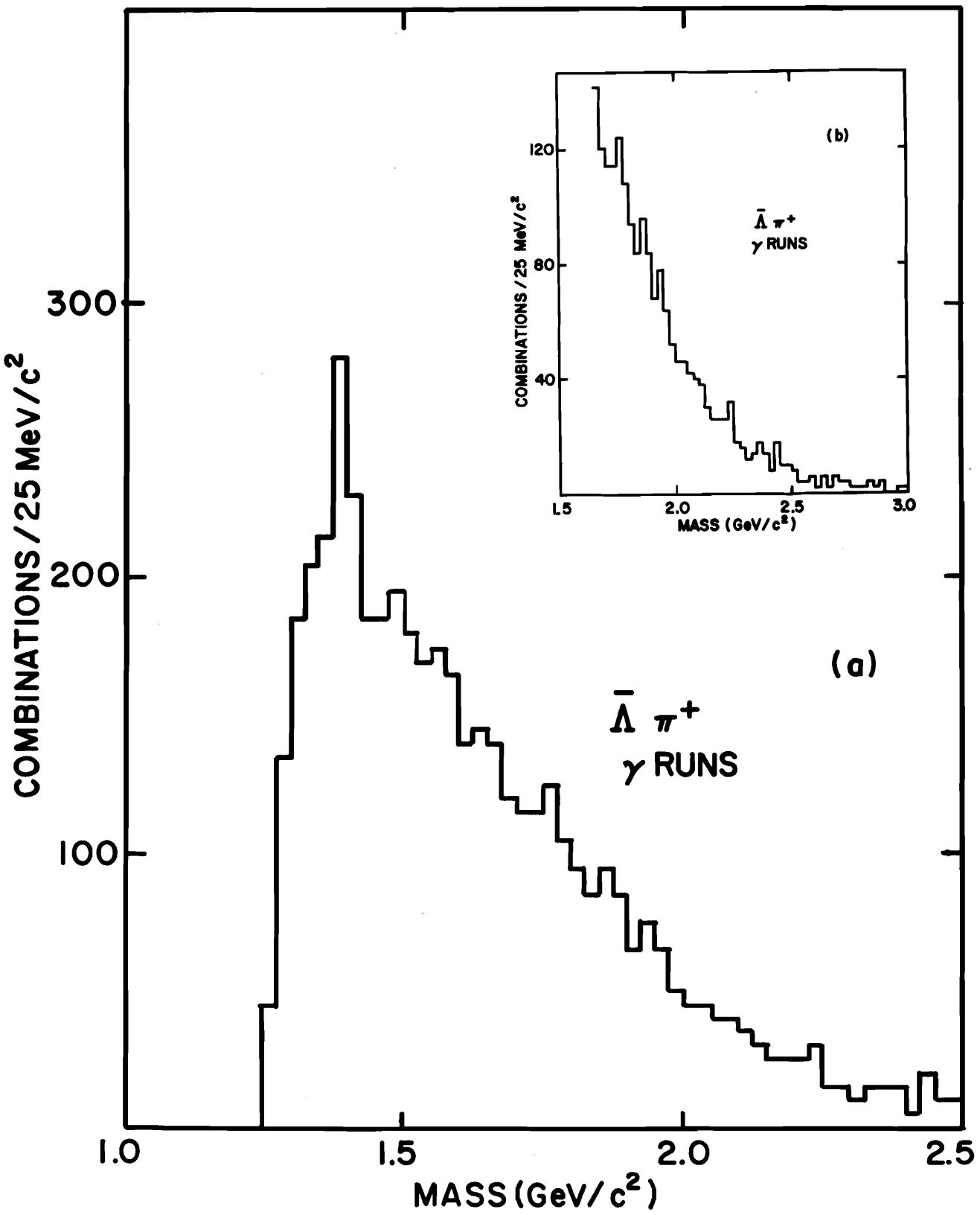
COMBINATIONS / 25 MeV/c²
300
200
100
1.0
1.5
2.0
2.5
MASS (GeV/c²)
(a)
Λ̄ π⁺
γ RUNS
(b)
120
80
40
COMBINATIONS / 25 MeV/c²
1.5
2.0
2.5
3.0
MASS (GeV/c²)
Λ̄ π⁺
γ RUNS

FIG. 21

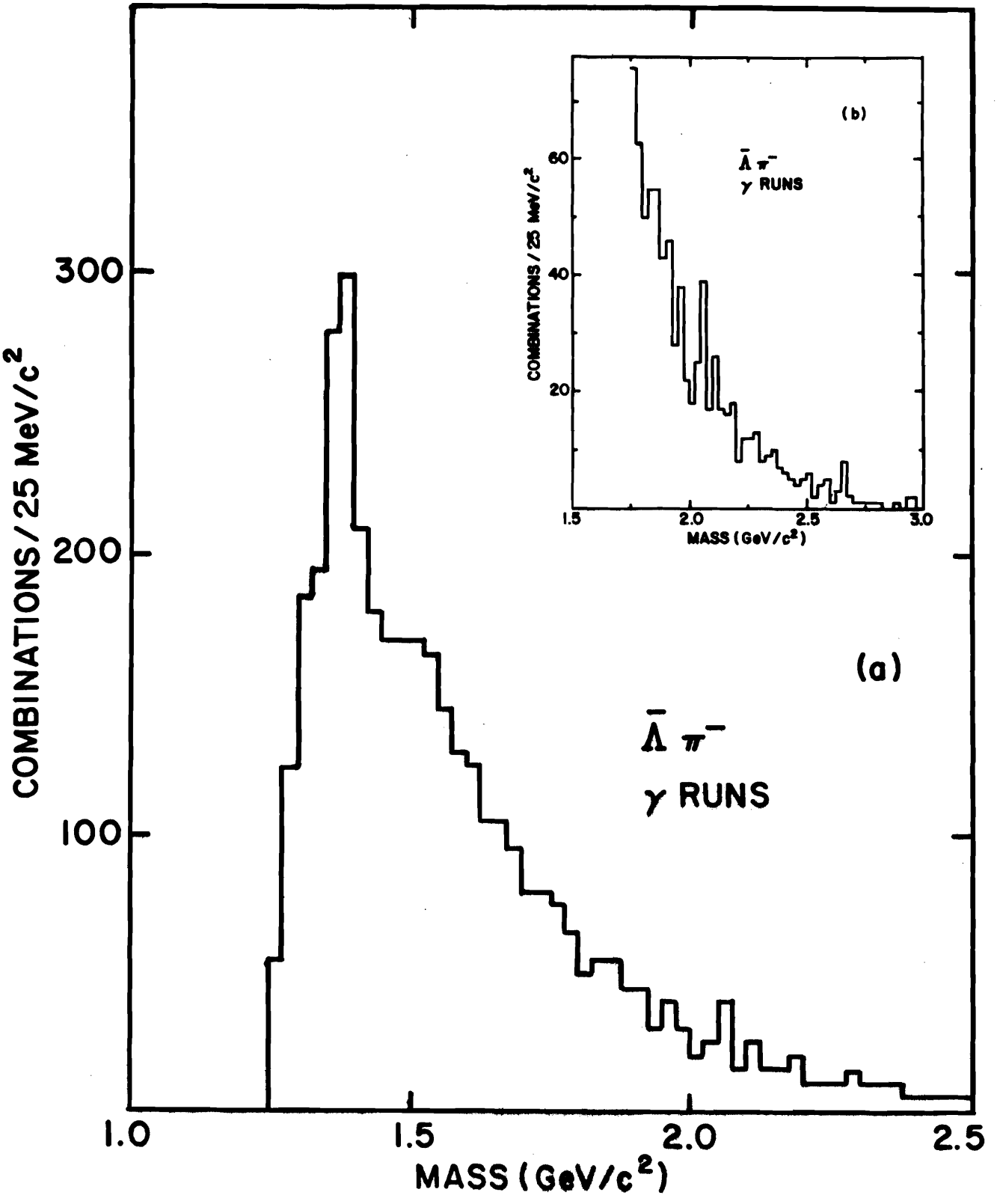
COMBINATIONS / 25 MeV/c²
300
200
100
1.0
1.5
2.0
2.5
MASS (GeV/c²)
(a)
Λ̄ π⁻
γ RUNS
(b)
Λ̄ π⁻
γ RUNS
COMBINATIONS / 25 MeV/c²
60
40
20
1.5
2.0
2.5
3.0
MASS (GeV/c²)

FIG. 22

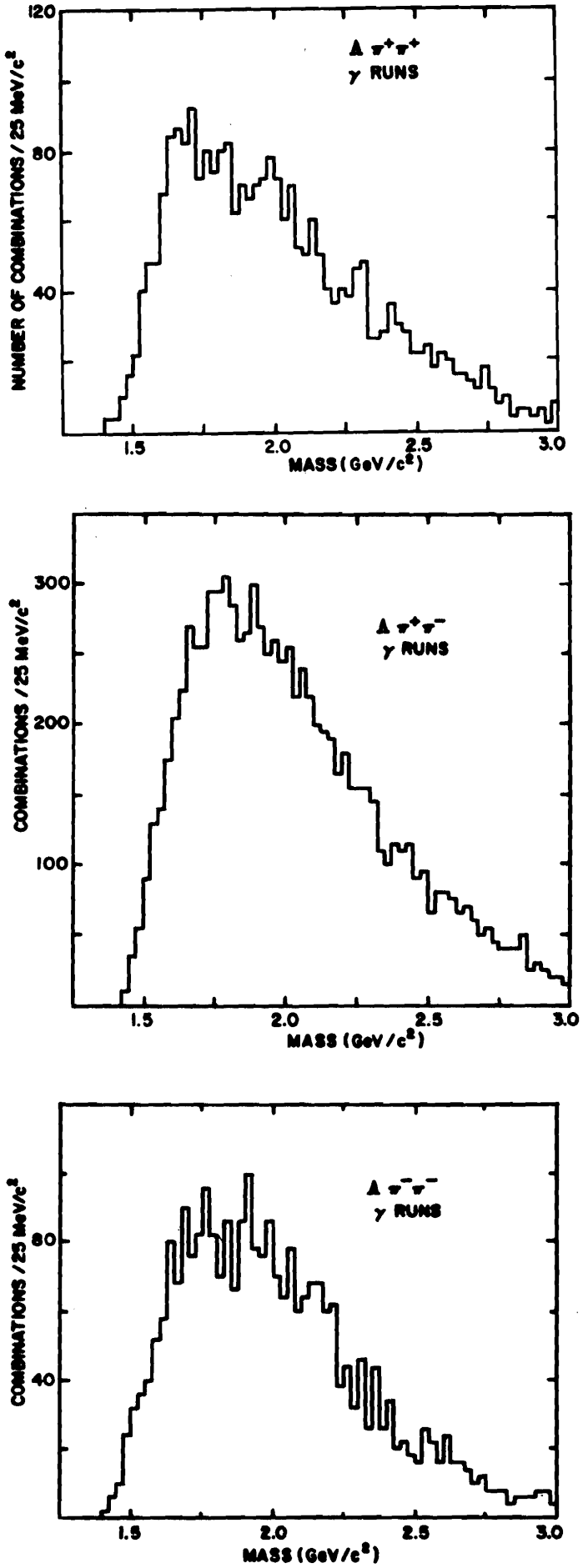
Λ π⁺π⁺
γ RUNS
NUMBER OF COMBINATIONS / 25 MeV/c²
120
80
40
1.5
2.0
2.5
3.0
MASS (GeV/c²)
Λ π⁺π⁻
γ RUNS
COMBINATIONS / 25 MeV/c²
300
200
100
1.5
2.0
2.5
3.0
MASS (GeV/c²)
Λ π⁻π⁻
γ RUNS
COMBINATIONS / 25 MeV/c²
80
40
1.5
2.0
2.5
3.0
MASS (GeV/c²)

FIG. 23

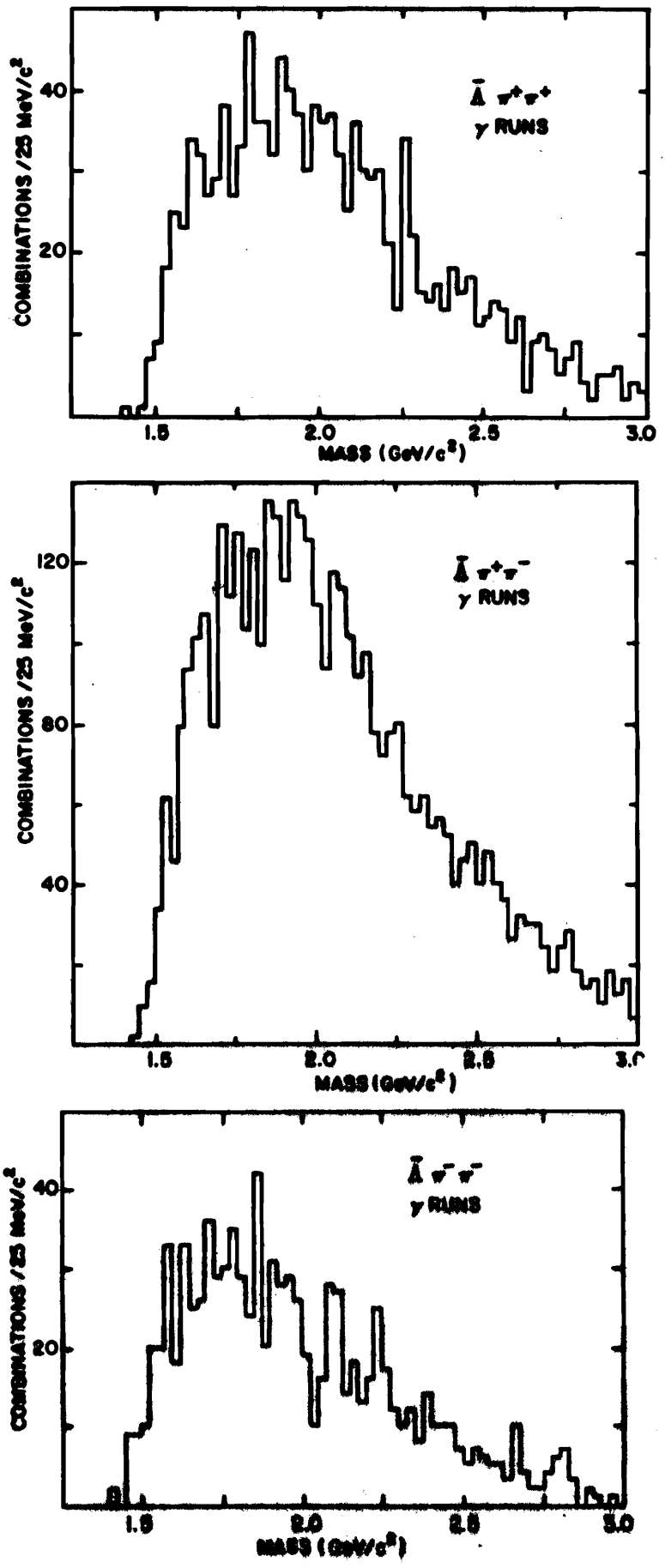
$\bar{\Lambda}\ \pi^+\pi^+$
γ RUNS
COMBINATIONS /25 MeV/c²
MASS (GeV/c²)
$\bar{\Lambda}\ \pi^+\pi^-$
γ RUNS
COMBINATIONS /25 MeV/c²
MASS (GeV/c²)
$\bar{\Lambda}\ \pi^-\pi^-$
γ RUNS
COMBINATIONS /25 MeV/c²
MASS (GeV/c²)

FIG. 24

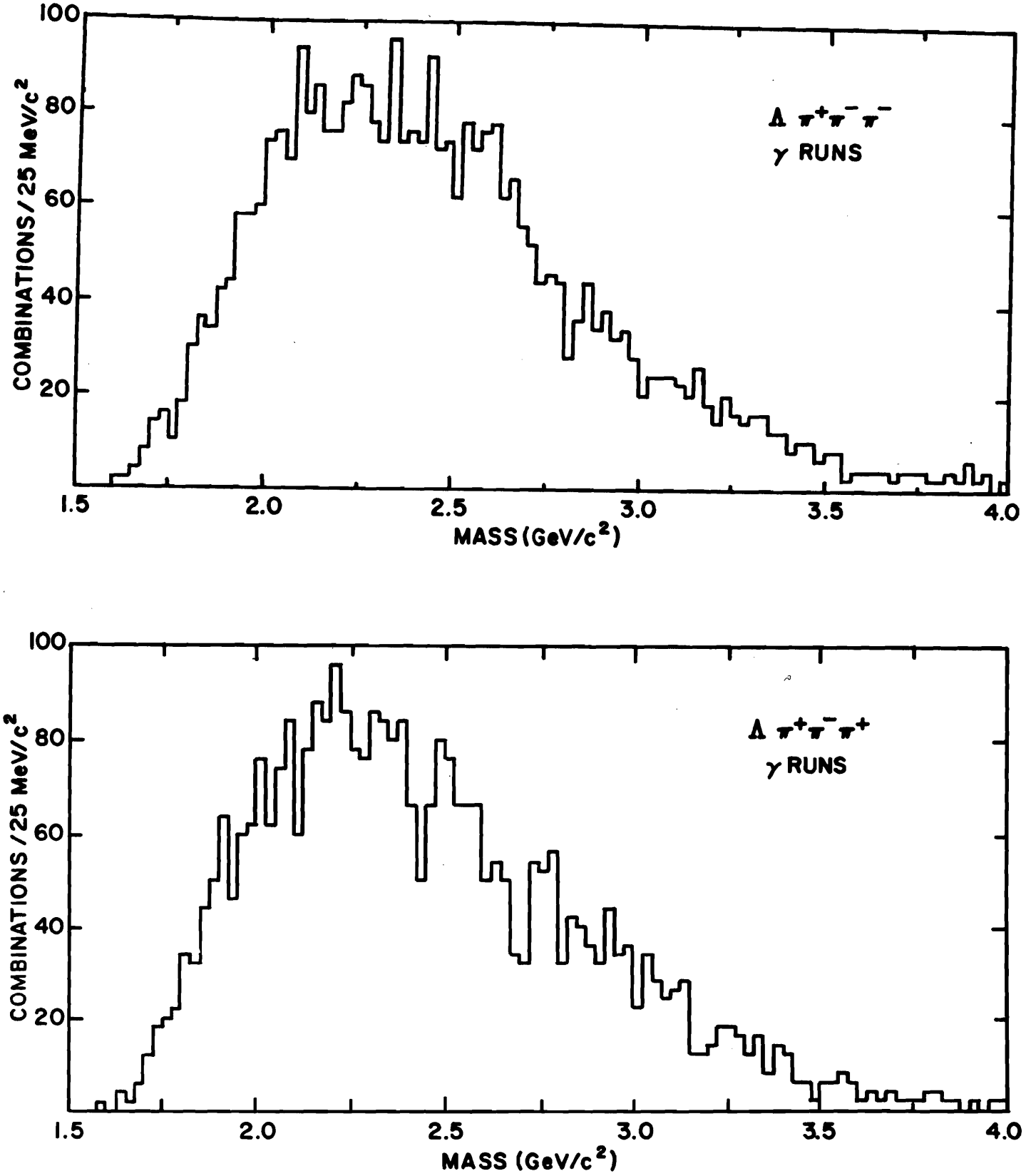
100
80
60
40
20
COMBINATIONS / 25 MeV/c²
Λ π⁺π⁻π⁻
γ RUNS
1.5
2.0
2.5
3.0
3.5
4.0
MASS (GeV/c²)
100
80
60
40
20
COMBINATIONS / 25 MeV/c²
Λ π⁺π⁻π⁺
γ RUNS
1.5
2.0
2.5
3.0
3.5
4.0
MASS (GeV/c²)

FIG. 25

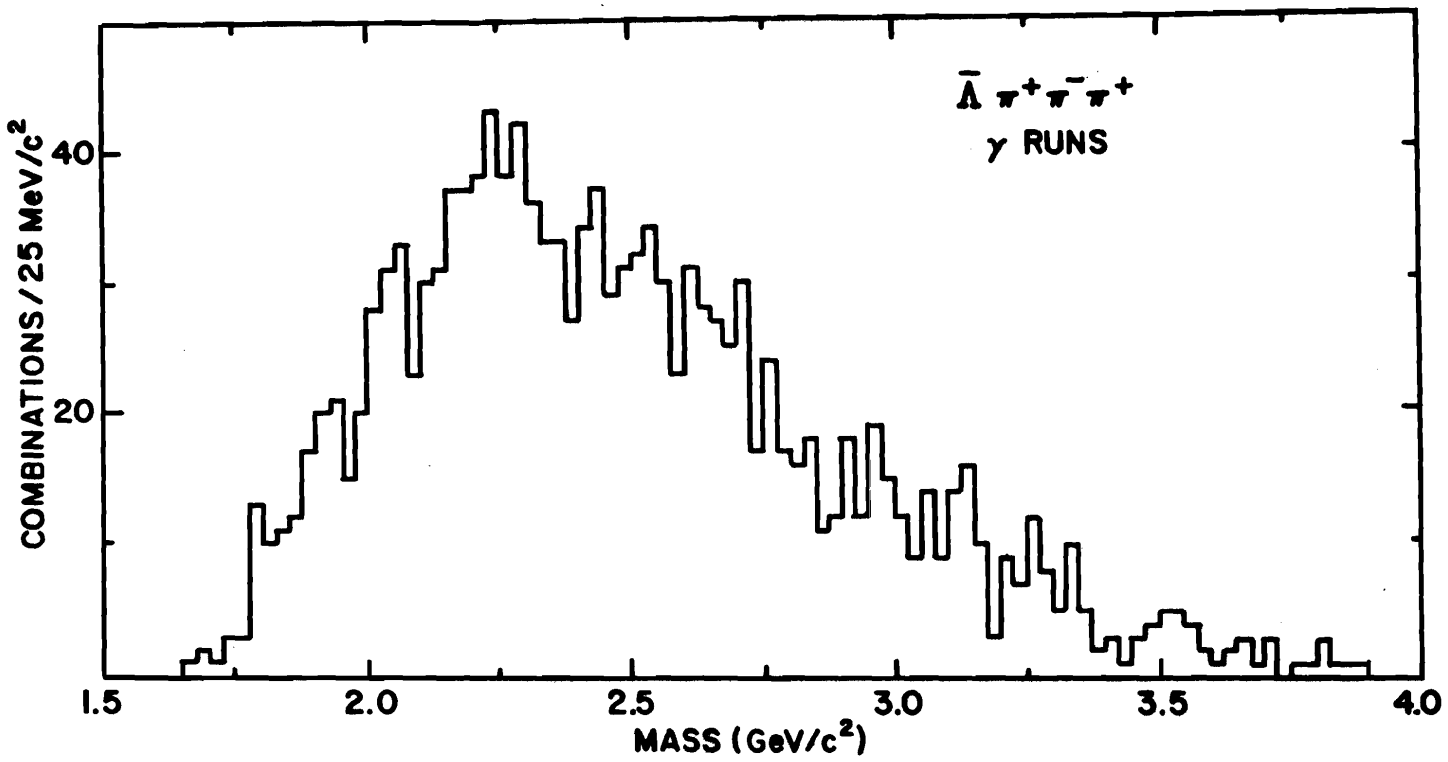
$\bar{\Lambda}\,\pi^+\pi^-\pi^+$
γ RUNS
COMBINATIONS / 25 MeV/c^2
40
20
1.5
2.0
2.5
3.0
3.5
4.0
MASS (GeV/c^2)

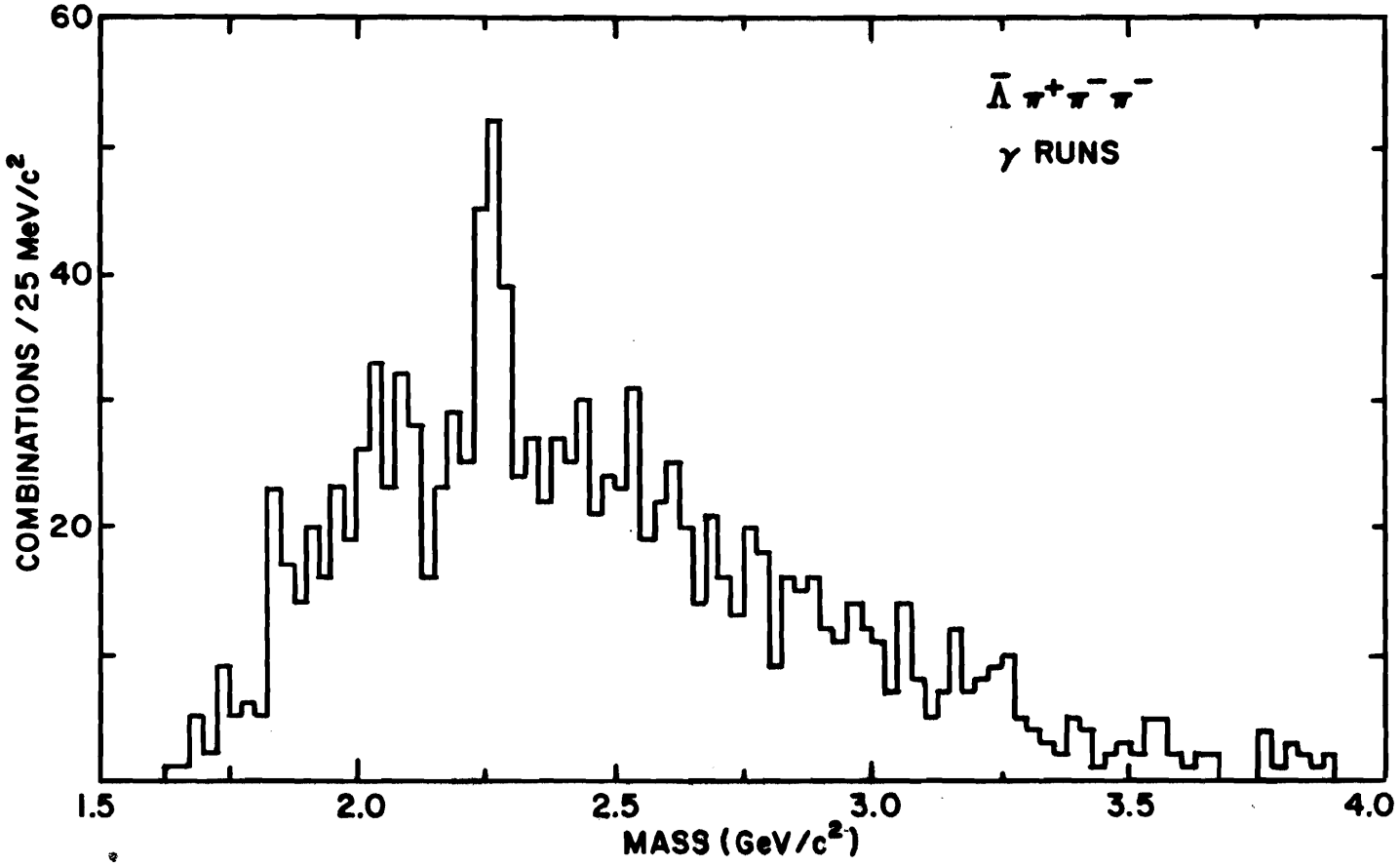
$\bar{\Lambda}\,\pi^+\pi^-\pi^-$
γ RUNS
COMBINATIONS / 25 MeV/c^2
60
40
20
1.5
2.0
2.5
3.0
3.5
4.0
MASS (GeV/c^2)

FIG. 26

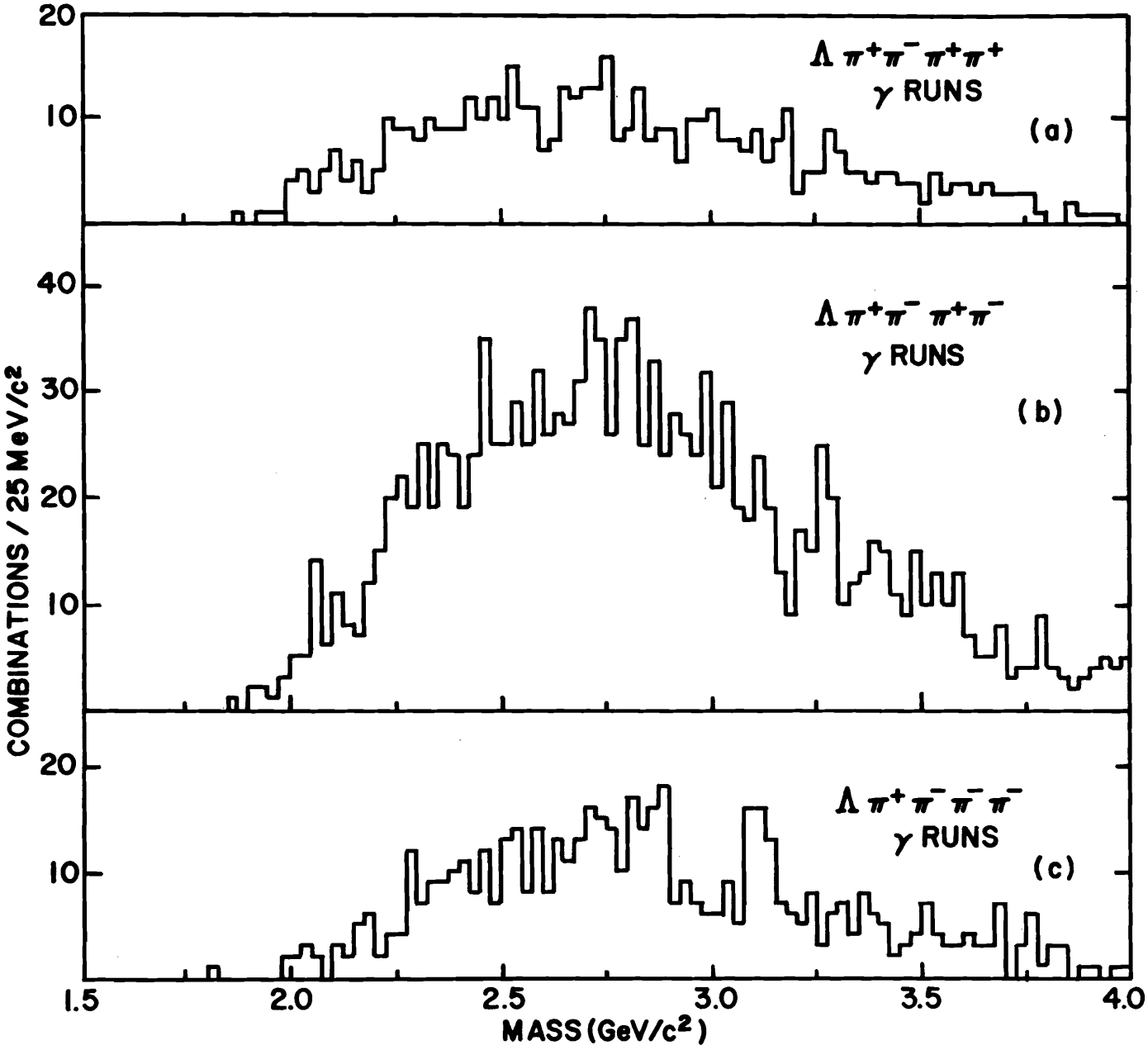
Λ π+π− π+π+
γ RUNS
(a)
Λ π+π− π+π−
γ RUNS
(b)
Λ π+π− π−π−
γ RUNS
(c)
COMBINATIONS / 25 MeV/c²
MASS (GeV/c²)
20
10
40
30
20
10
20
10
1.5
2.0
2.5
3.0
3.5
4.0

FIG. 27

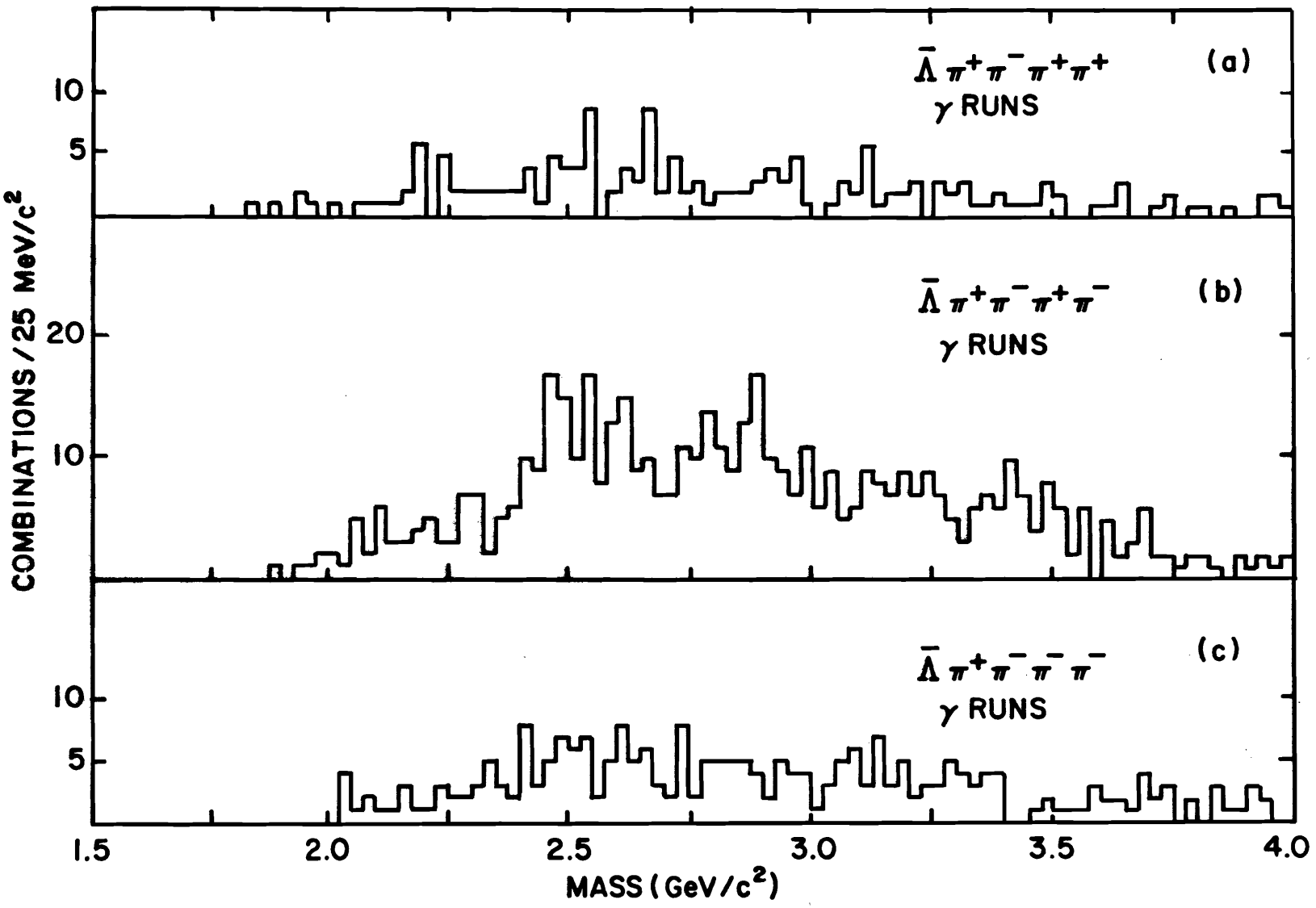
$\bar{\Lambda}\pi^+\pi^-\pi^+\pi^+$
γ RUNS
(a)
$\bar{\Lambda}\pi^+\pi^-\pi^+\pi^-$
γ RUNS
(b)
$\bar{\Lambda}\pi^+\pi^-\pi^-\pi^-$
γ RUNS
(c)
COMBINATIONS / 25 MeV/c^2
10
5
20
10
10
5
1.5
2.0
2.5
3.0
3.5
4.0
MASS (GeV/c^2)

FIG. 28

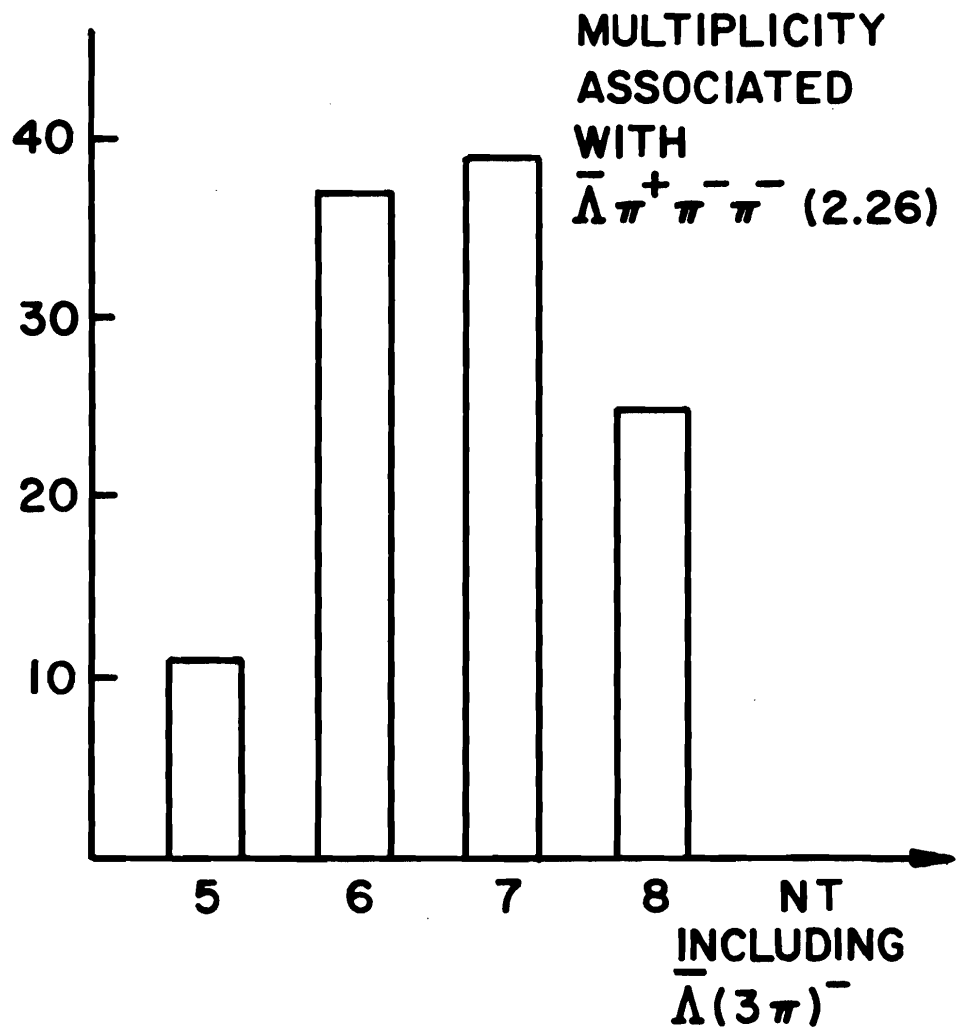
MULTIPLICITY
ASSOCIATED
WITH
$\bar{\Lambda}\pi^+\pi^-\pi^-$ (2.26)
40
30
20
10
5
6
7
8
NT
INCLUDING
$\bar{\Lambda}(3\pi)^-$

FIG. 29

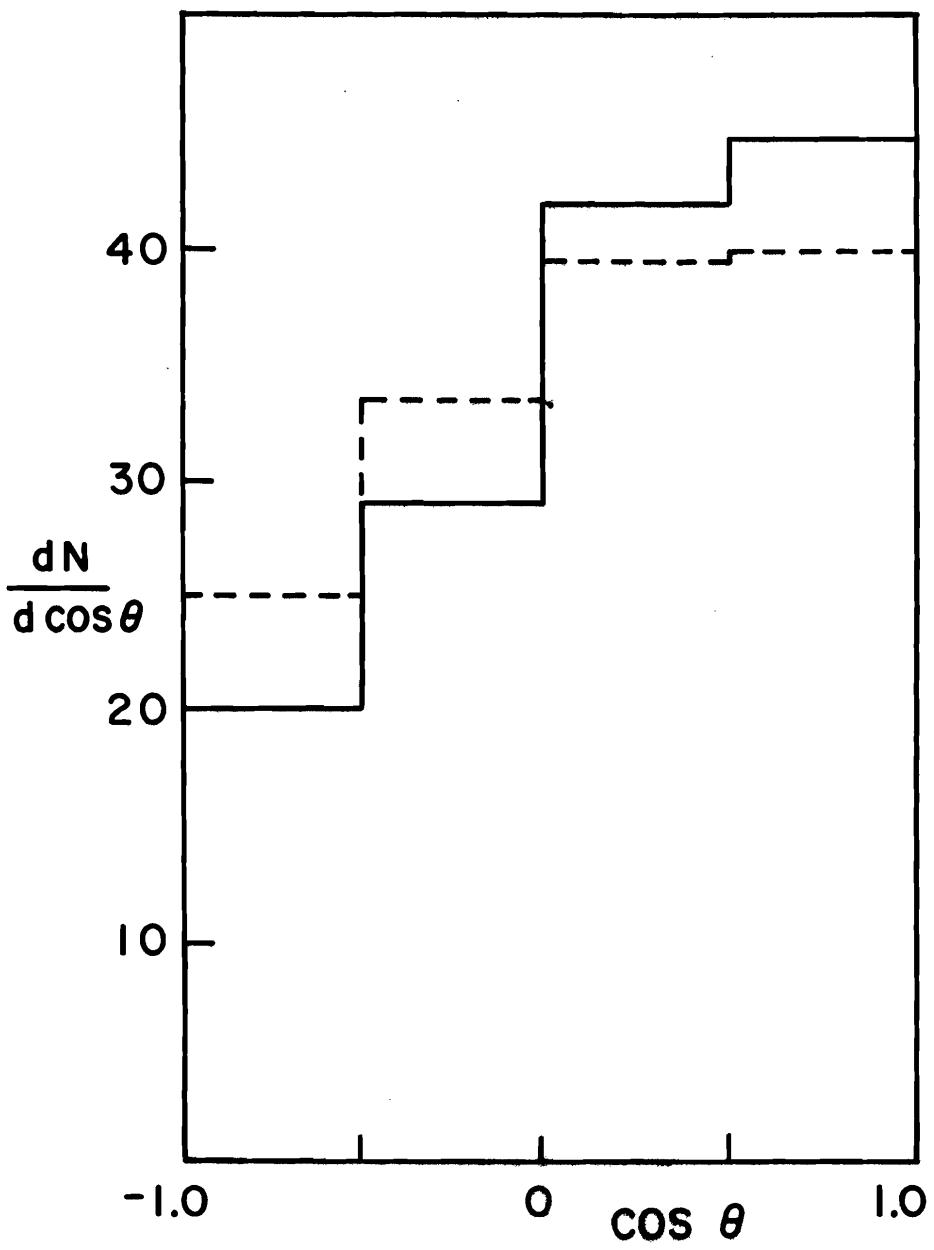

FIG. 30

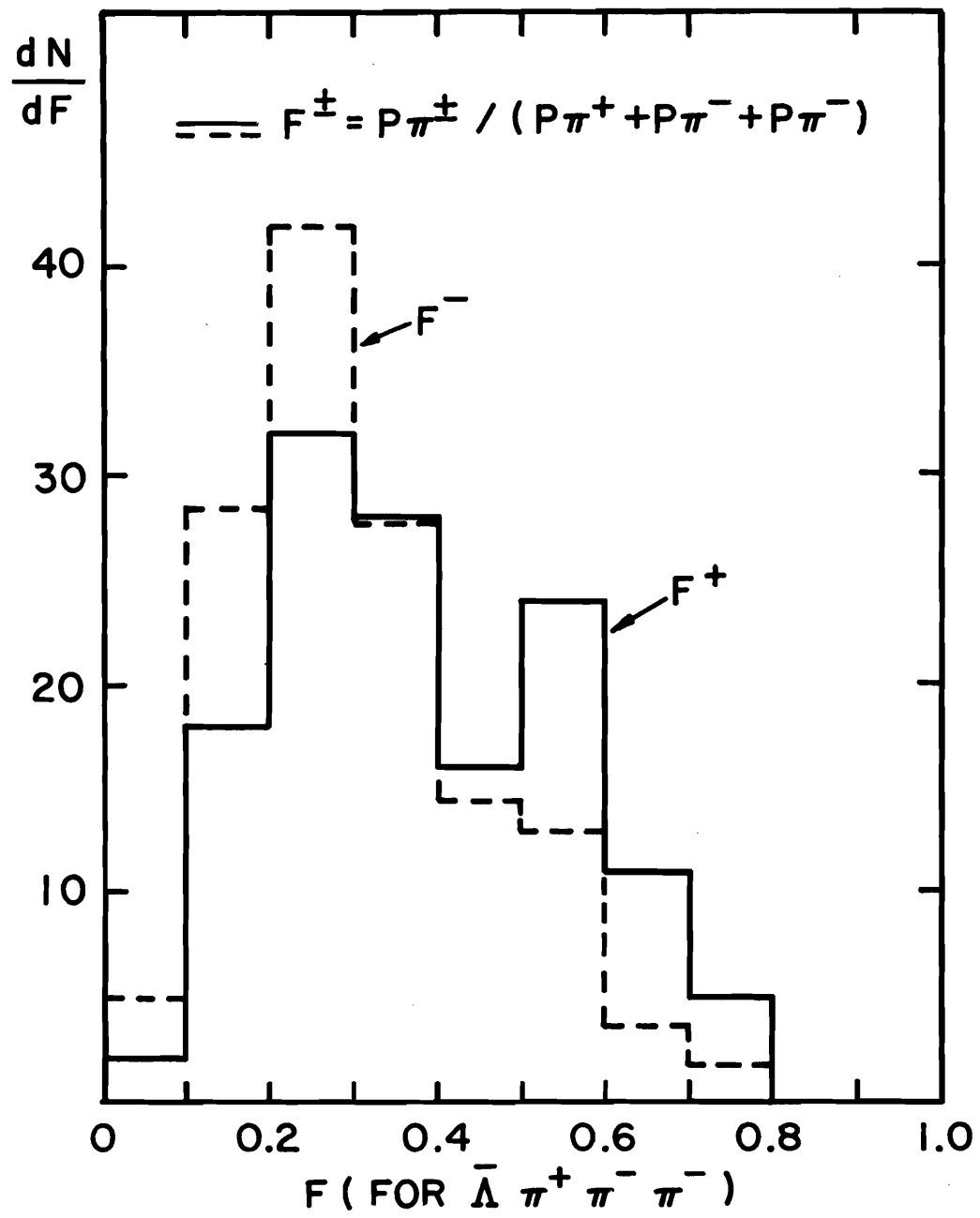

FIG. 31

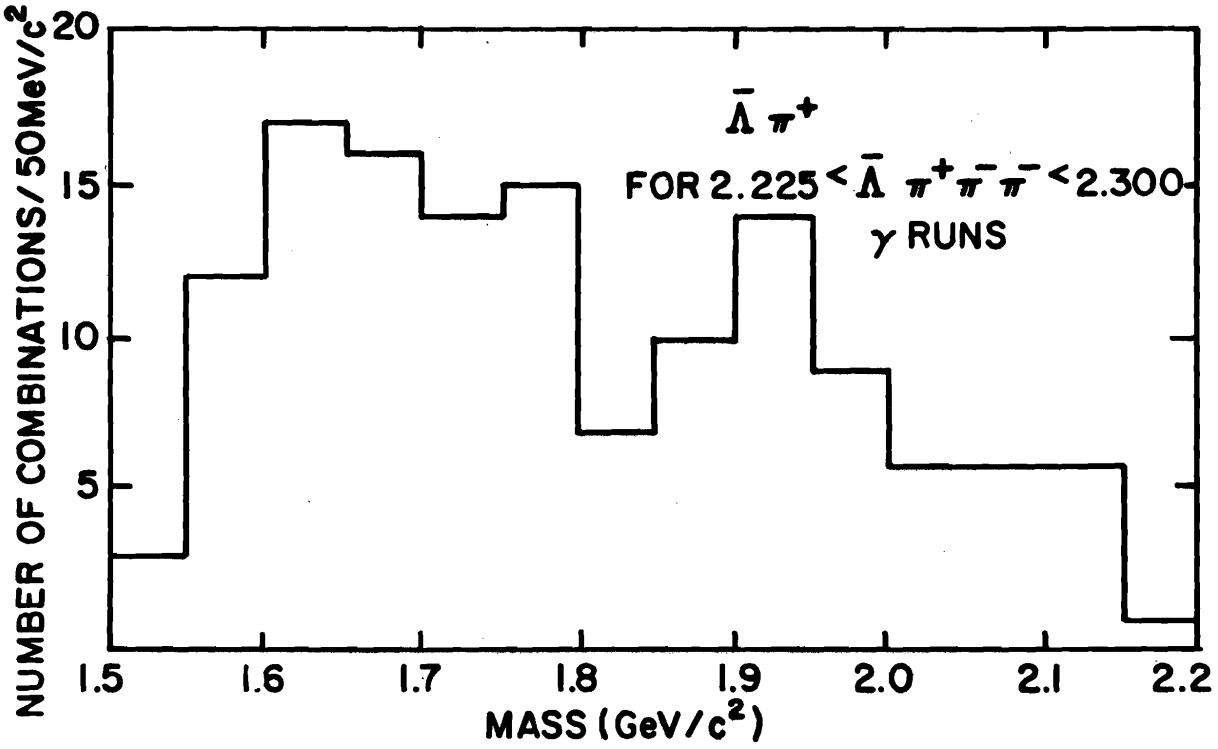
$\bar{\Lambda}\pi^+$
FOR $2.225 < \bar{\Lambda}\pi^+\pi^-\pi^- < 2.300$
γ RUNS
NUMBER OF COMBINATIONS/50MeV/c^2
20
15
10
5
1.5
1.6
1.7
1.8
1.9
2.0
2.1
2.2
MASS (GeV/c^2)

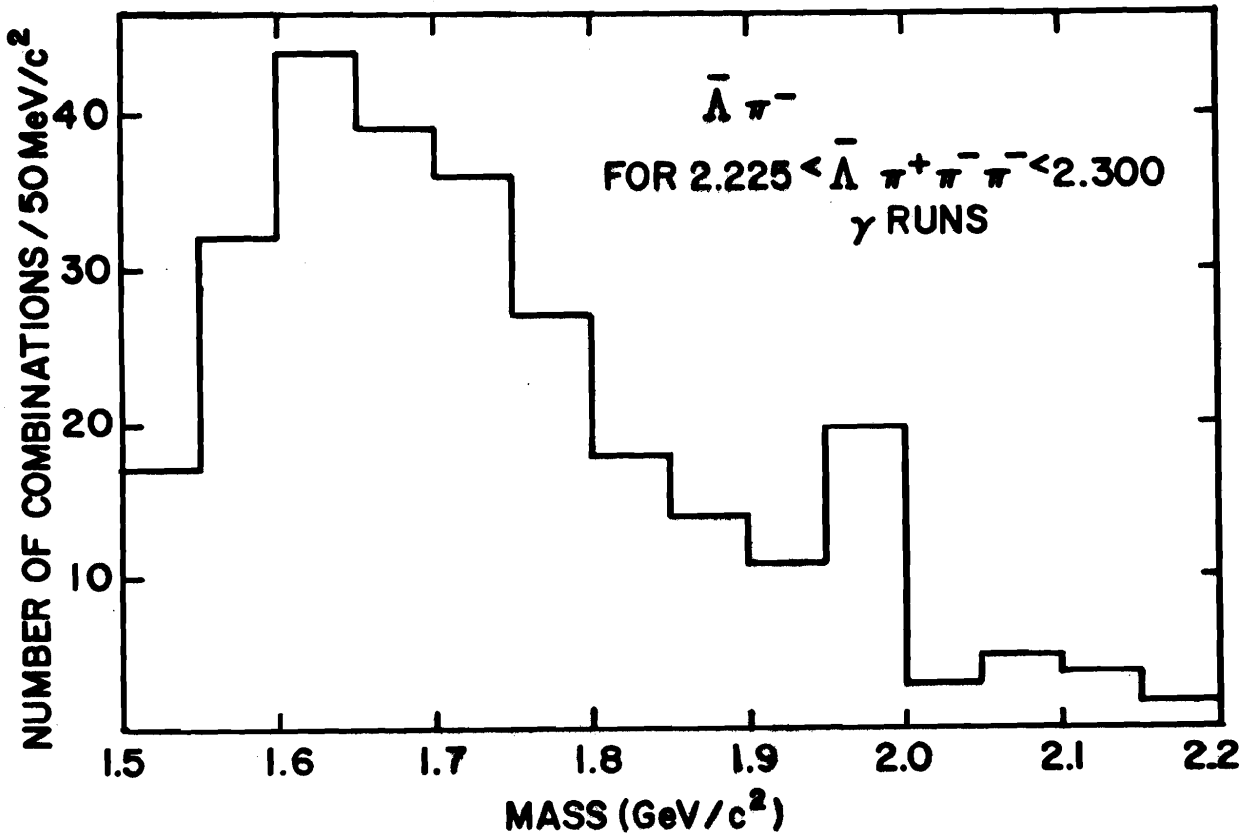
$\bar{\Lambda}\pi^-$
FOR $2.225 < \bar{\Lambda}\pi^+\pi^-\pi^- < 2.300$
γ RUNS
NUMBER OF COMBINATIONS/50MeV/c^2
40
30
20
10
1.5
1.6
1.7
1.8
1.9
2.0
2.1
2.2
MASS (GeV/c^2)

FIG. 32 a,b

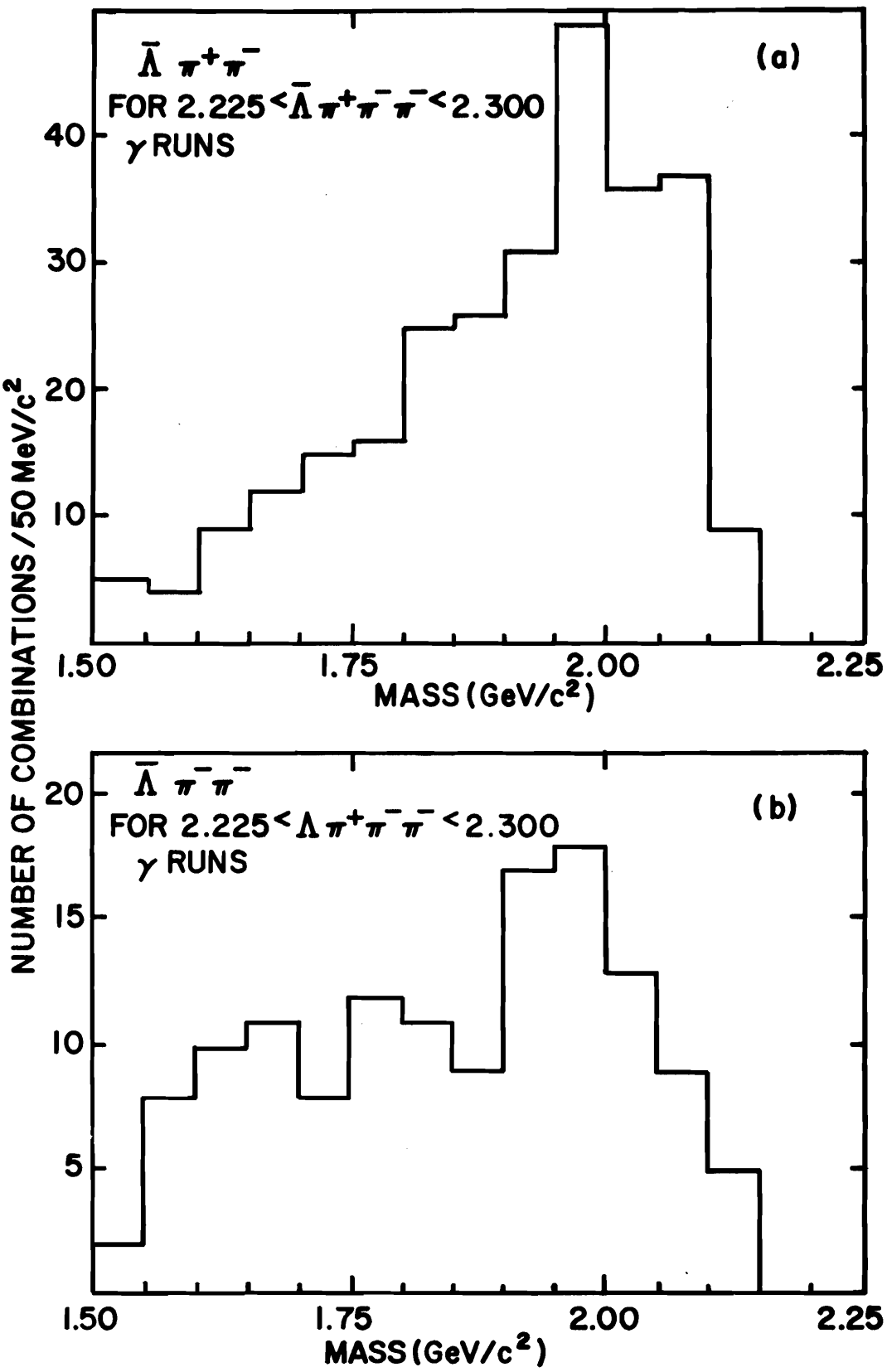
$\bar{\Lambda}\ \pi^+\pi^-$
FOR $2.225 < \bar{\Lambda}\pi^+\pi^-\pi^- < 2.300$
γ RUNS
(a)
40
30
20
10
1.50
1.75
2.00
2.25
MASS (GeV/c²)
NUMBER OF COMBINATIONS / 50 MeV/c²
$\bar{\Lambda}\ \pi^-\pi^-$
FOR $2.225 < \Lambda\pi^+\pi^-\pi^- < 2.300$
γ RUNS
(b)
20
15
10
5
1.50
1.75
2.00
2.25
MASS (GeV/c²)

FIG. 32 c,d

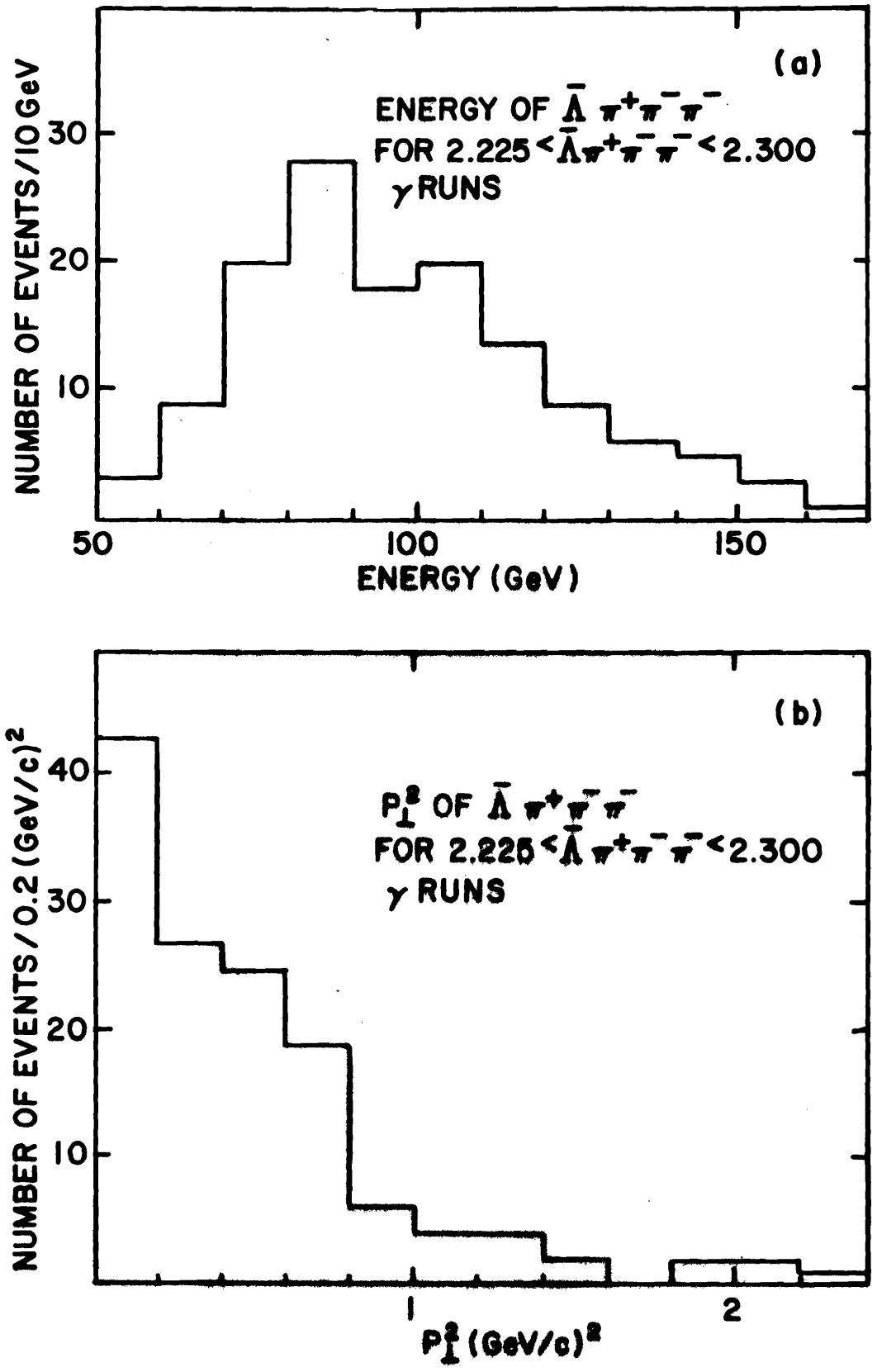
(a)
ENERGY OF $\bar{\Lambda}\pi^+\pi^-\pi^-$
FOR $2.225 < \bar{\Lambda}\pi^+\pi^-\pi^- < 2.300$
γ RUNS
NUMBER OF EVENTS/10 GeV
30
20
10
50
100
150
ENERGY (GeV)
(b)
$P_\perp^2$ OF $\bar{\Lambda}\pi^+\pi^-\pi^-$
FOR $2.225 < \bar{\Lambda}\pi^+\pi^-\pi^- < 2.300$
γ RUNS
NUMBER OF EVENTS/0.2 (GeV/c)^2
40
30
20
10
1
2
$P_\perp^2$ (GeV/c)^2

FIG. 33

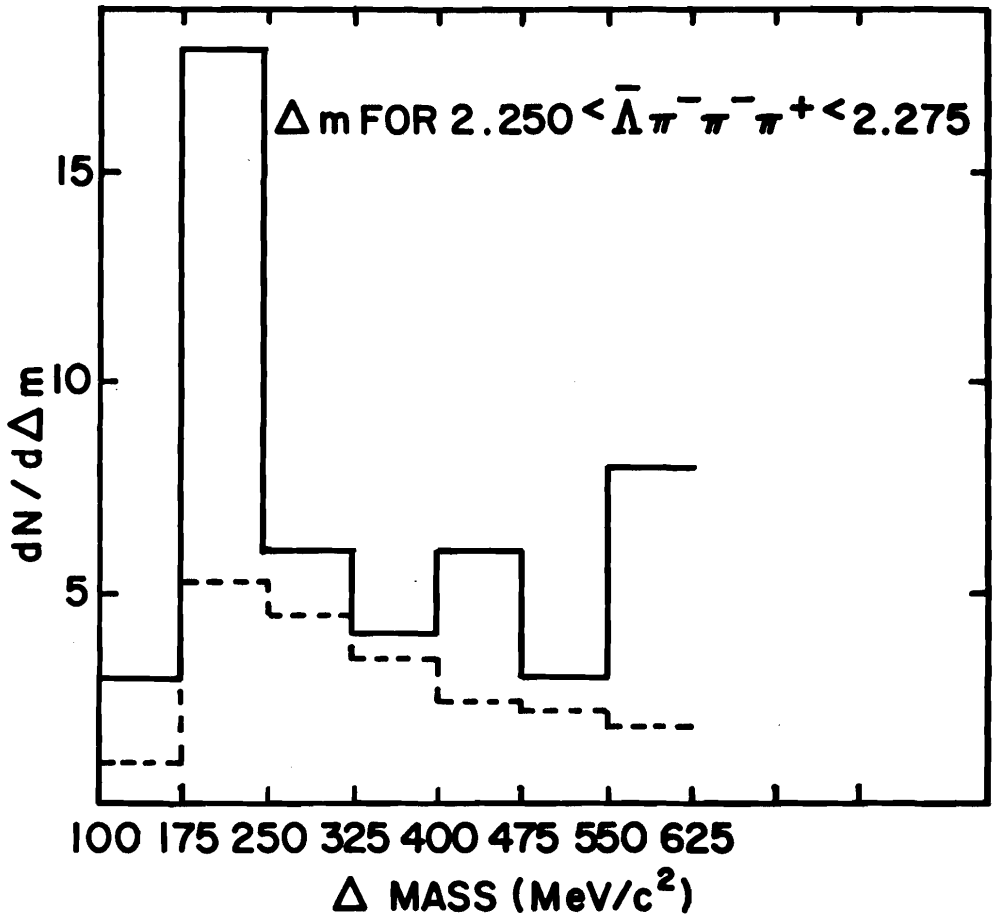
Δm FOR 2.250 < $\bar{\Lambda}\pi^-\pi^-\pi^+$ < 2.275
15
10
5
dN / dΔm
100 175 250 325 400 475 550 625
Δ MASS (MeV/c²)

FIG. 34

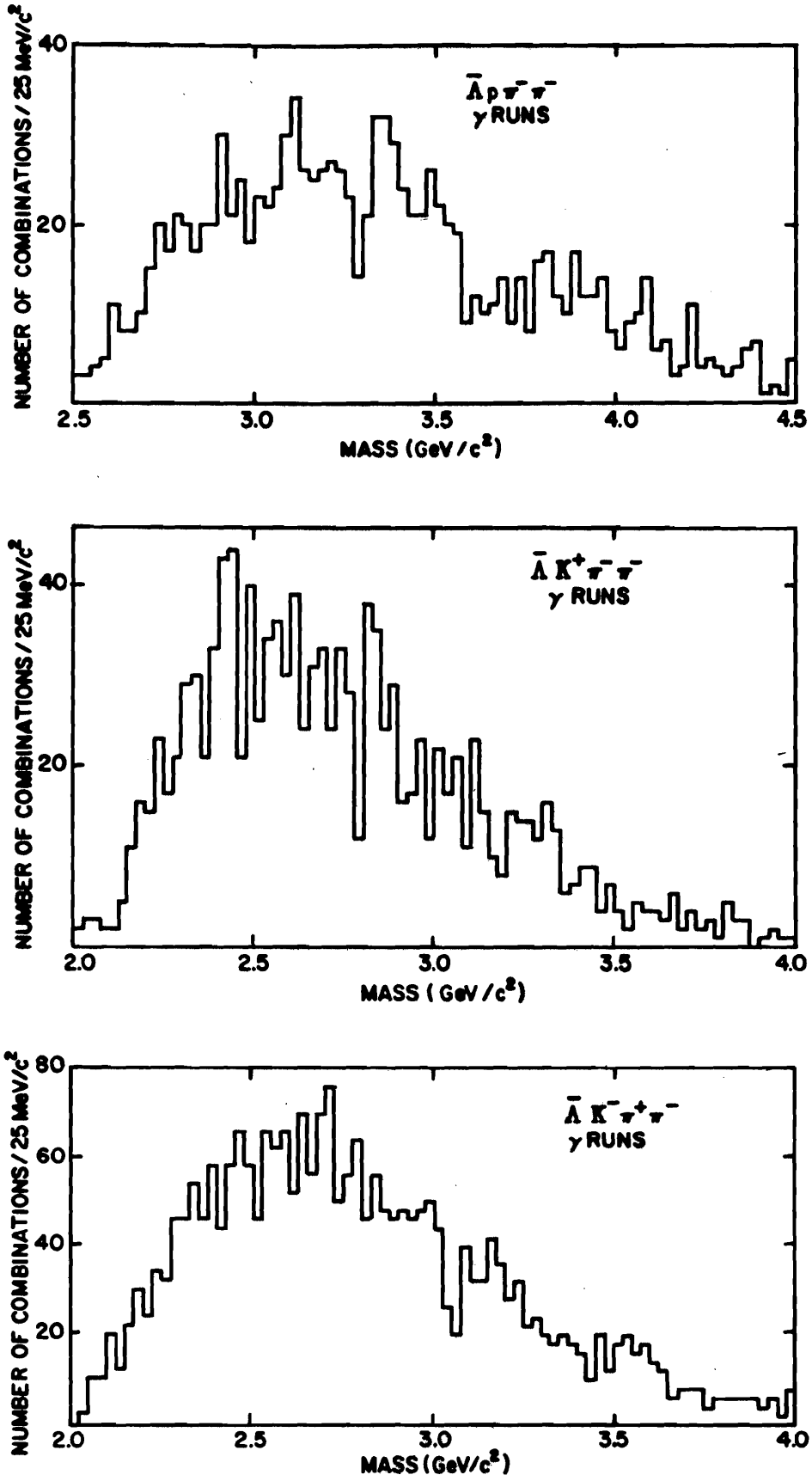
NUMBER OF COMBINATIONS / 25 MeV/c²
40
20
$\bar{\Lambda} p \pi^- \pi^-$
γ RUNS
2.5
3.0
3.5
4.0
4.5
MASS (GeV/c²)
NUMBER OF COMBINATIONS / 25 MeV/c²
40
20
$\bar{\Lambda} K^+ \pi^- \pi^-$
γ RUNS
2.0
2.5
3.0
3.5
4.0
MASS (GeV/c²)
NUMBER OF COMBINATIONS / 25 MeV/c²
80
60
40
20
$\bar{\Lambda} K^- \pi^+ \pi^-$
γ RUNS
2.0
2.5
3.0
3.5
4.0
MASS (GeV/c²)

FIG. 35

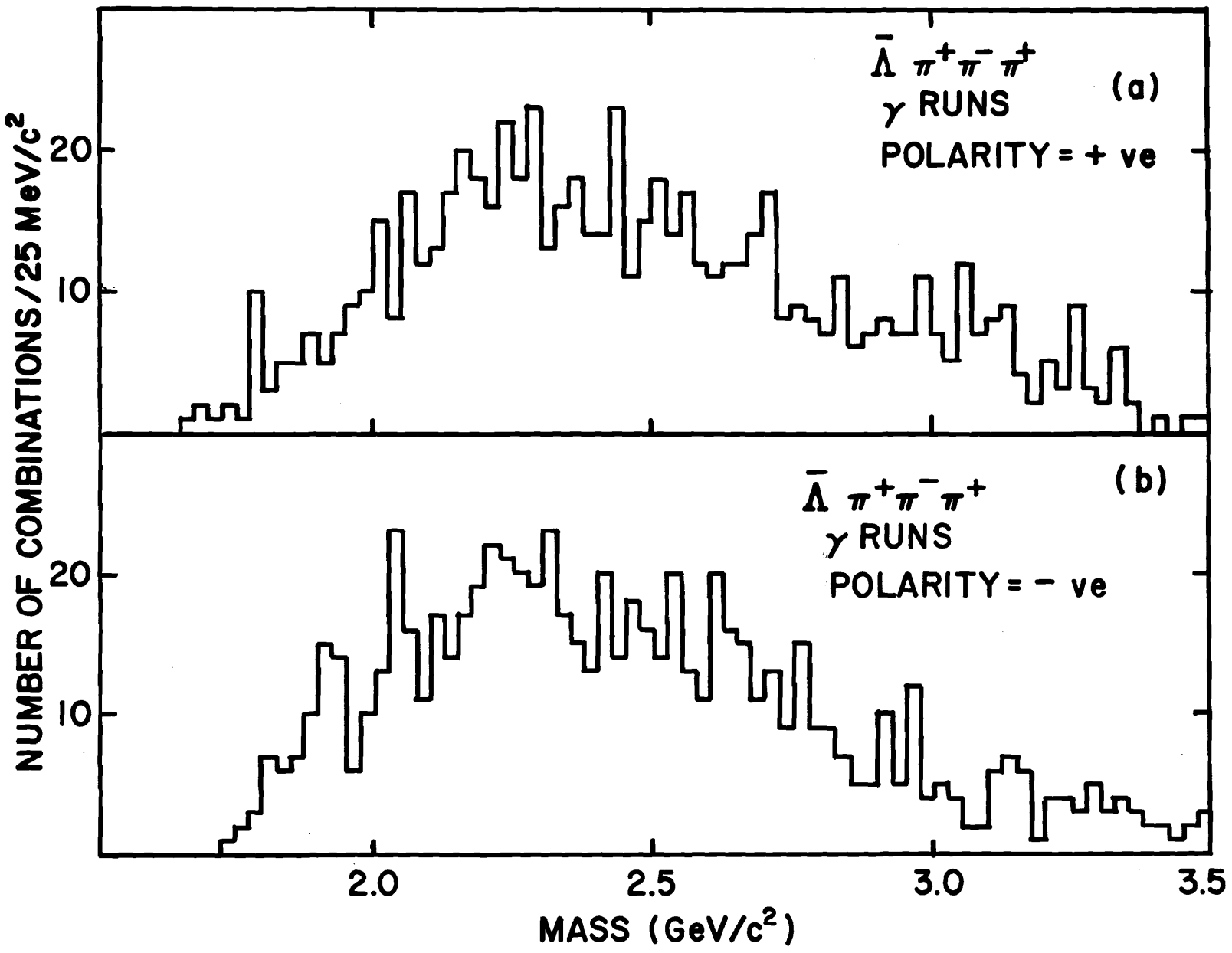
$\bar{\Lambda}\ \pi^+\pi^-\pi^+$
γ RUNS
POLARITY = + ve
(a)
$\bar{\Lambda}\ \pi^+\pi^-\pi^+$
γ RUNS
POLARITY = − ve
(b)
NUMBER OF COMBINATIONS/25 MeV/c^2
10
20
10
20
2.0
2.5
3.0
3.5
MASS (GeV/c^2)

FIG. 36

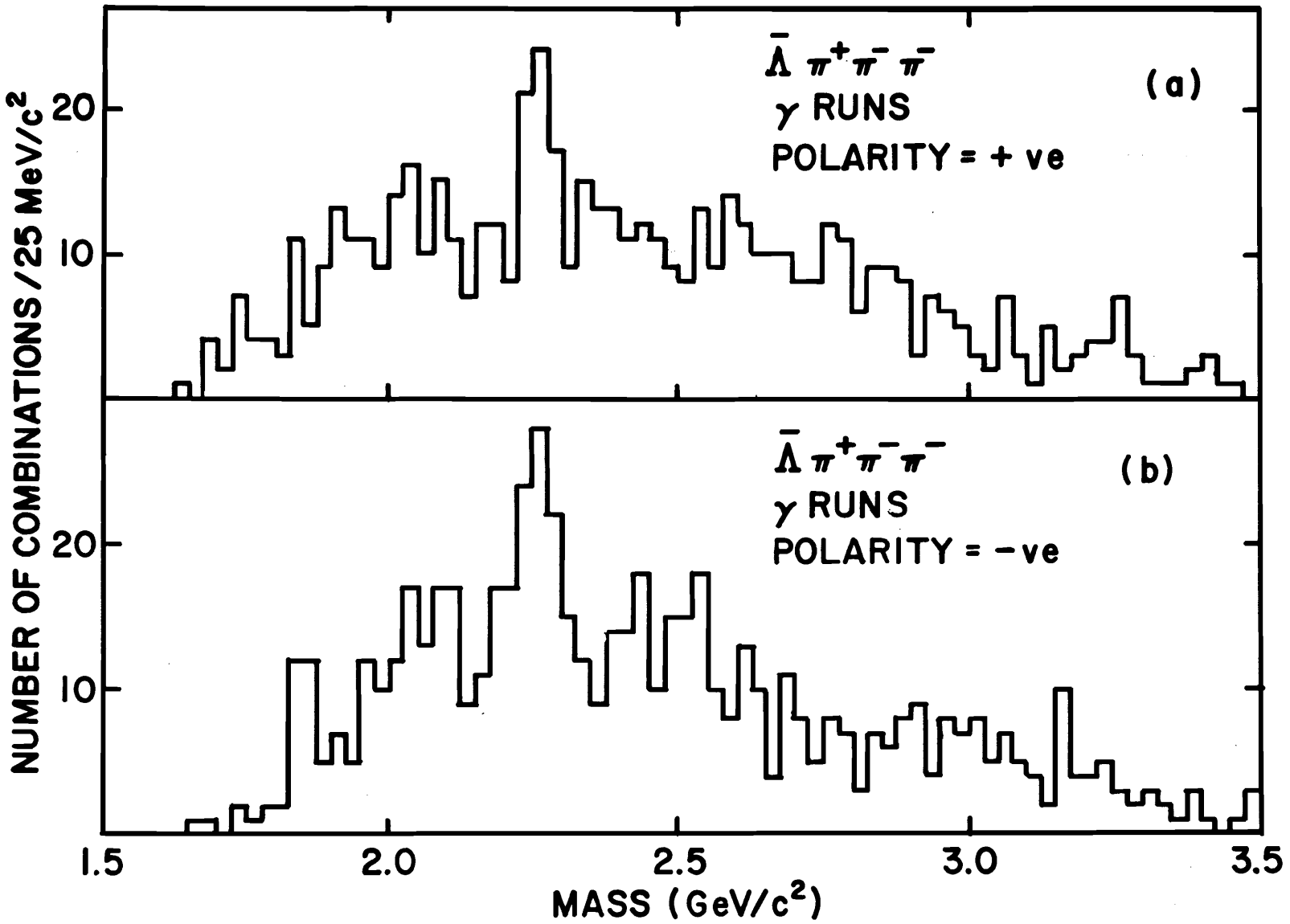
$\bar{\Lambda}\,\pi^+\pi^-\pi^-$
γ RUNS
POLARITY = + ve
(a)
$\bar{\Lambda}\,\pi^+\pi^-\pi^-$
γ RUNS
POLARITY = −ve
(b)
NUMBER OF COMBINATIONS / 25 MeV/c^2
20
10
20
10
1.5
2.0
2.5
3.0
3.5
MASS (GeV/c^2)

FIG. 37

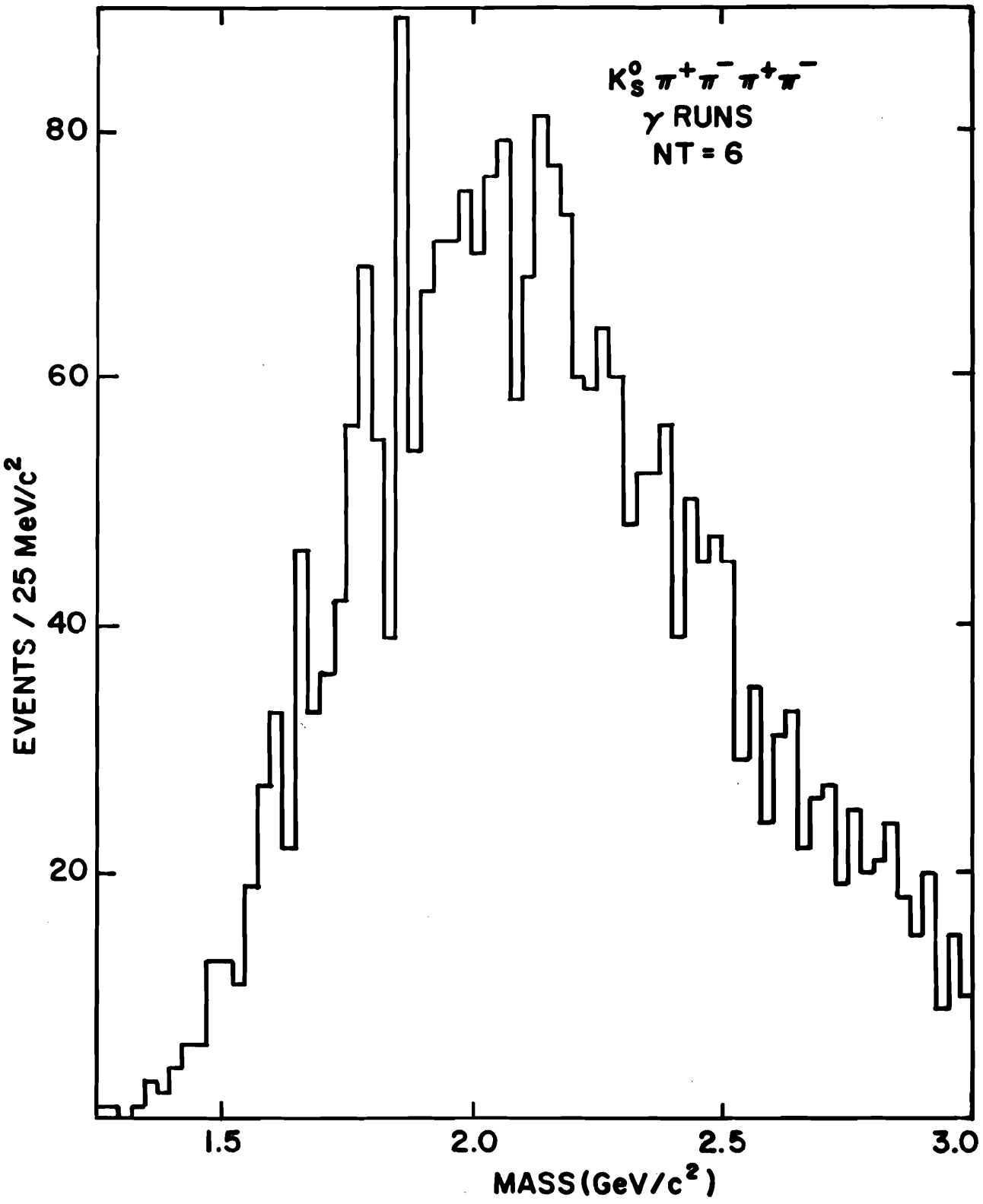
$K_S^0 \pi^+\pi^-\pi^+\pi^-$
γ RUNS
NT = 6
80
60
40
20
EVENTS / 25 MeV/c^2
1.5
2.0
2.5
3.0
MASS (GeV/c^2)

FIG. 38a

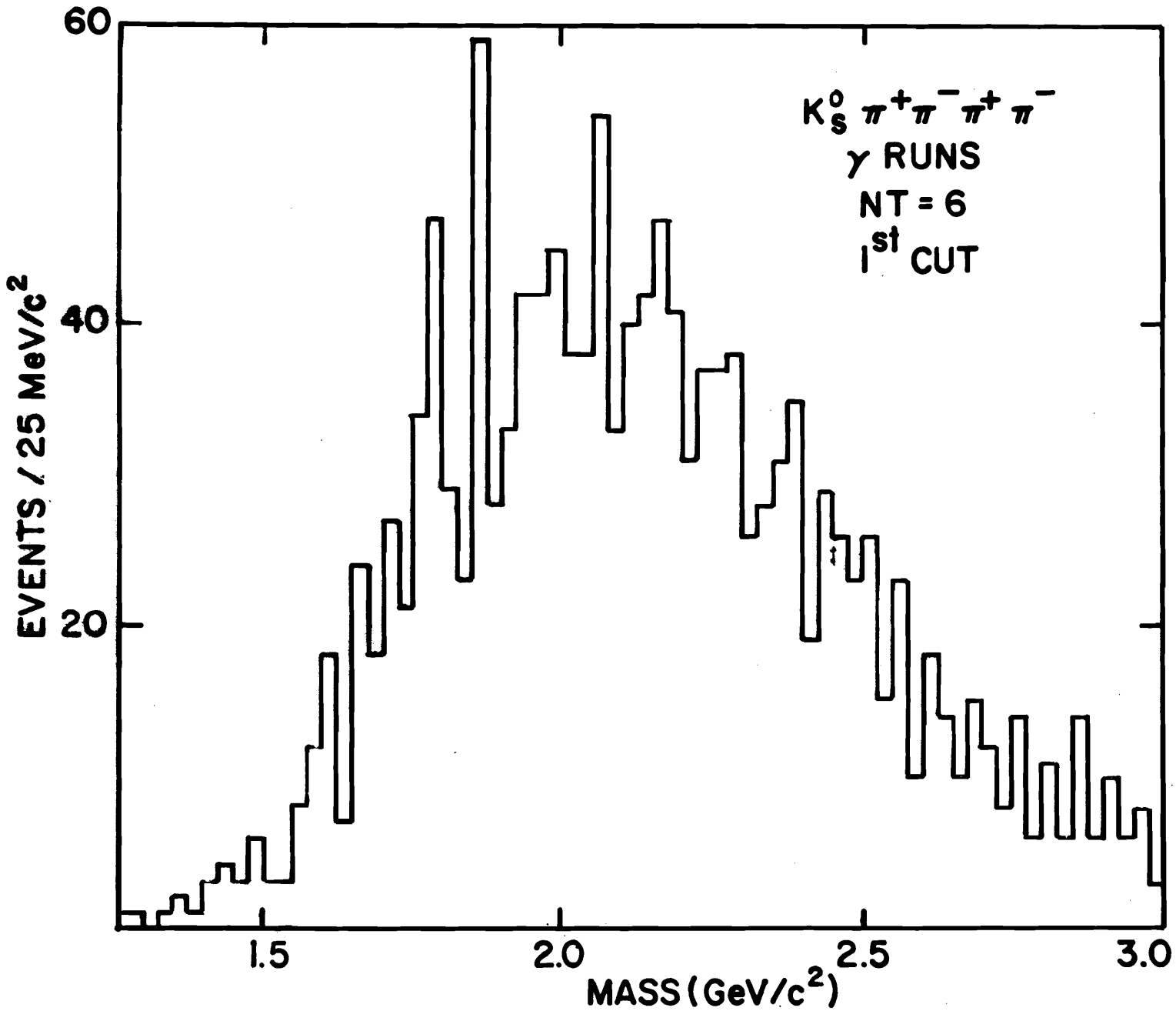
$K_S^0\ \pi^+\pi^-\pi^+\pi^-$
γ RUNS
NT = 6
1st CUT
EVENTS / 25 MeV/c^2
60
40
20
1.5
2.0
2.5
3.0
MASS (GeV/c^2)

FIG. 38b

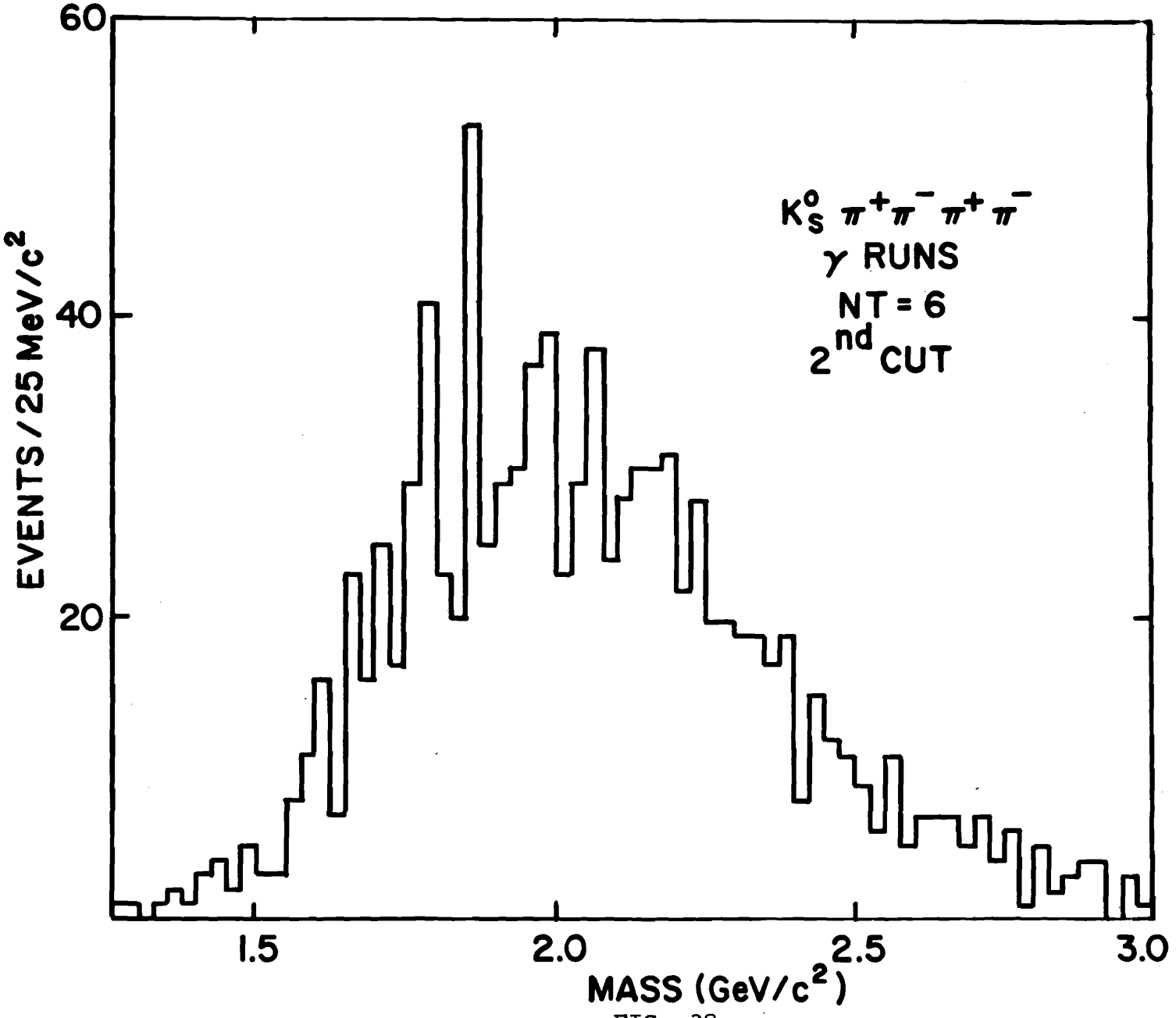
60
40
20
EVENTS / 25 MeV/c²
1.5
2.0
2.5
3.0
MASS (GeV/c²)
K⁰S π⁺π⁻ π⁺π⁻
γ RUNS
NT = 6
2nd CUT

FIG. 38c

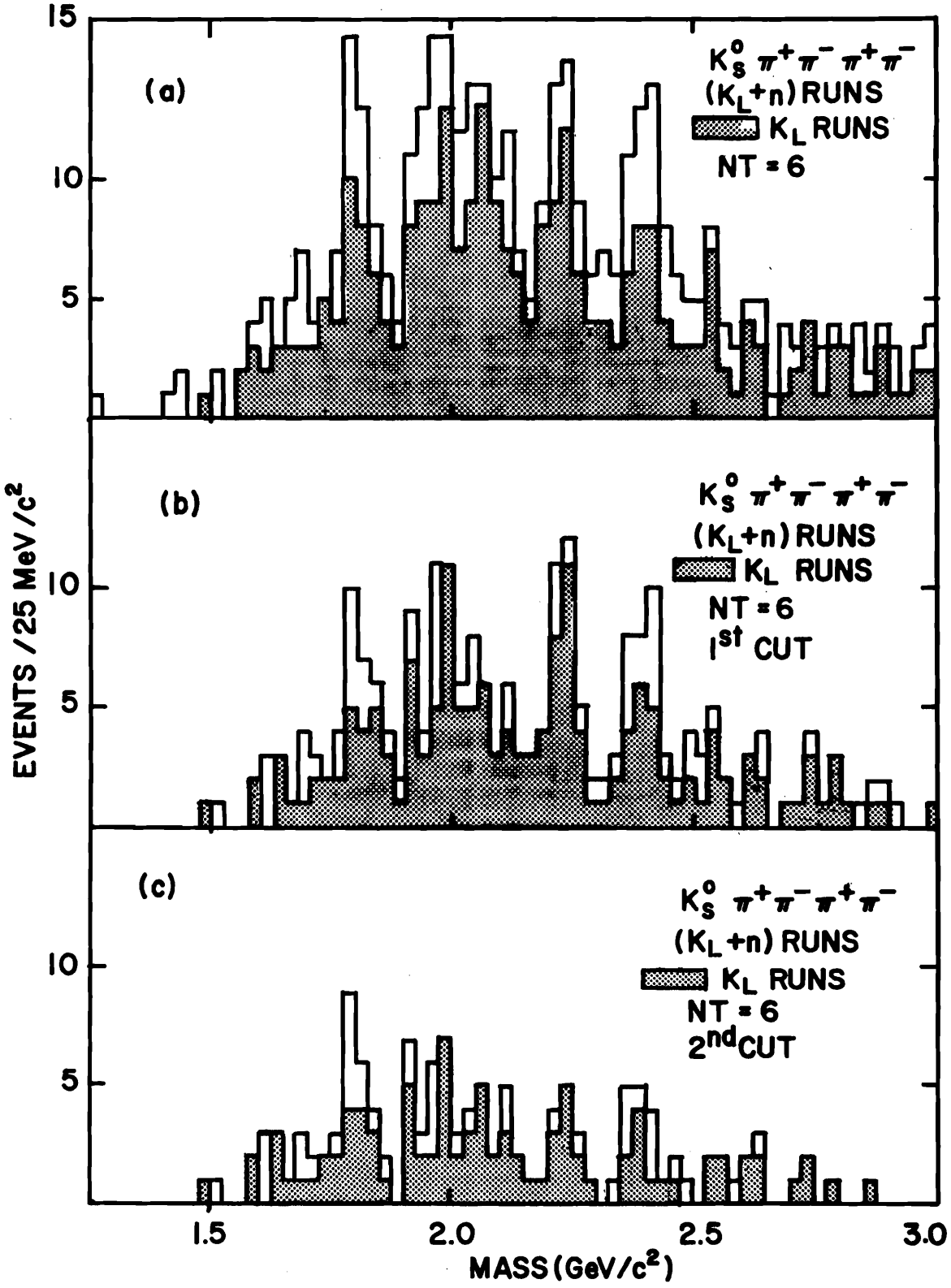
(a)
$K_S^0\ \pi^+\pi^-\pi^+\pi^-$
(K_L+n) RUNS
K_L RUNS
NT = 6
(b)
$K_S^0\ \pi^+\pi^-\pi^+\pi^-$
(K_L+n) RUNS
K_L RUNS
NT = 6
1st CUT
(c)
$K_S^0\ \pi^+\pi^-\pi^+\pi^-$
(K_L+n) RUNS
K_L RUNS
NT = 6
2nd CUT
EVENTS /25 MeV/c^2
MASS (GeV/c^2)
15
10
5
1.5
2.0
2.5
3.0

FIG. 39

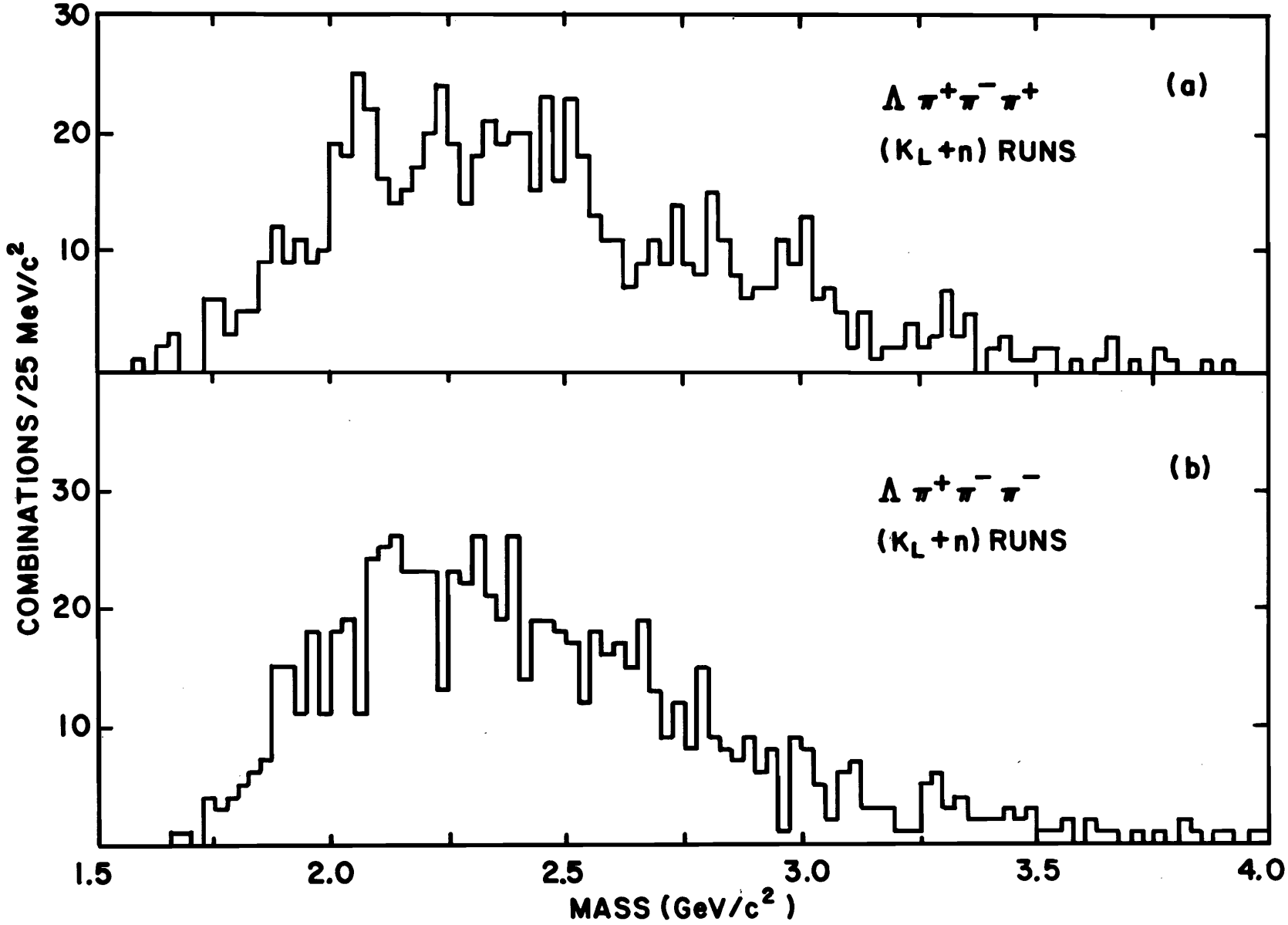
30
20
10
COMBINATIONS/25 MeV/c²
Λ π⁺π⁻π⁺
(K_L+n) RUNS
(a)
Λ π⁺π⁻π⁻
(K_L+n) RUNS
(b)
1.5
2.0
2.5
3.0
3.5
4.0
MASS (GeV/c²)

FIG. 40

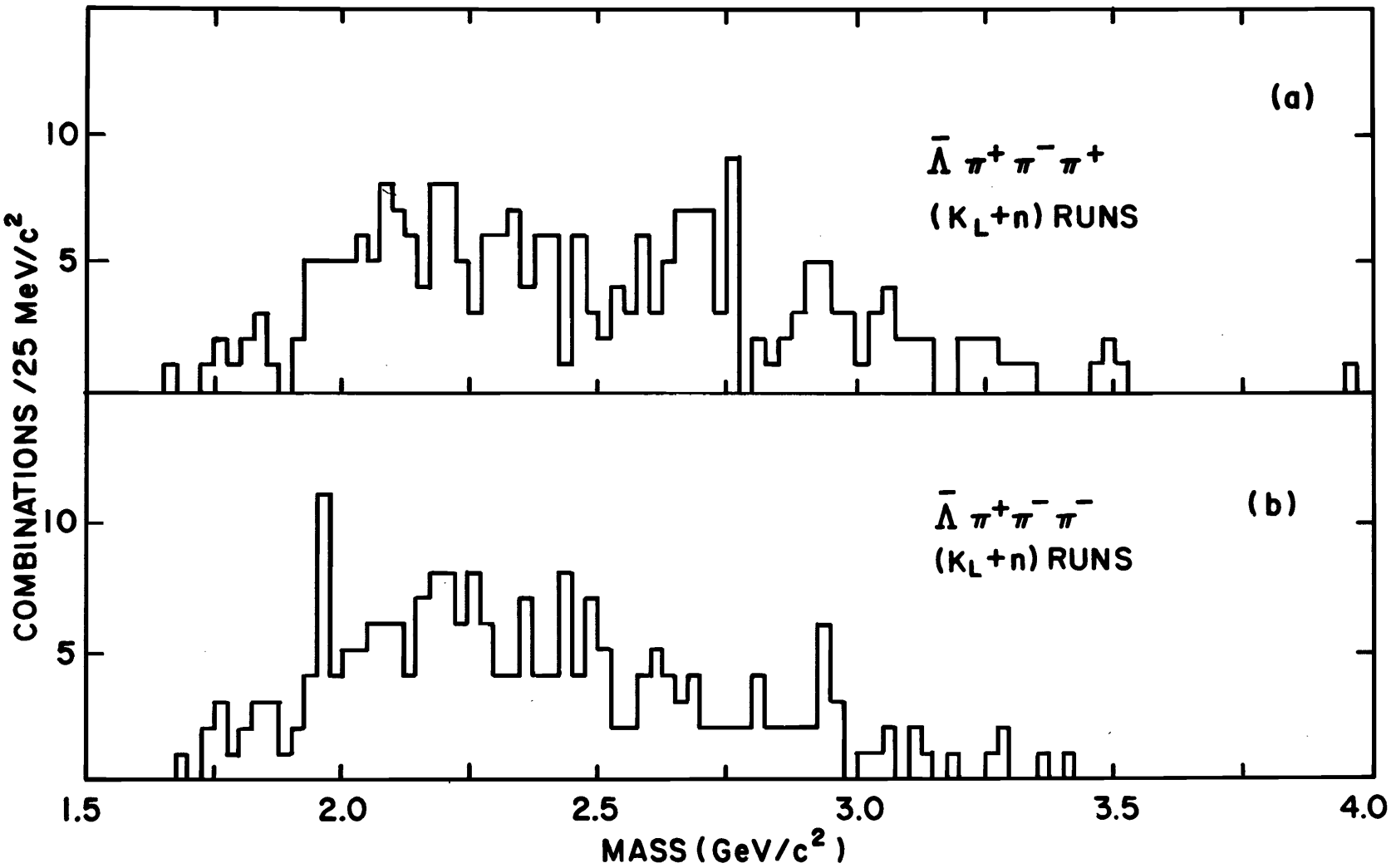
(a)
$\bar{\Lambda}\,\pi^+\pi^-\pi^+$
(K_L+n) RUNS
(b)
$\bar{\Lambda}\,\pi^+\pi^-\pi^-$
(K_L+n) RUNS
COMBINATIONS /25 MeV/c^2
10
5
10
5
1.5
2.0
2.5
3.0
3.5
4.0
MASS (GeV/c^2)

FIG. 41

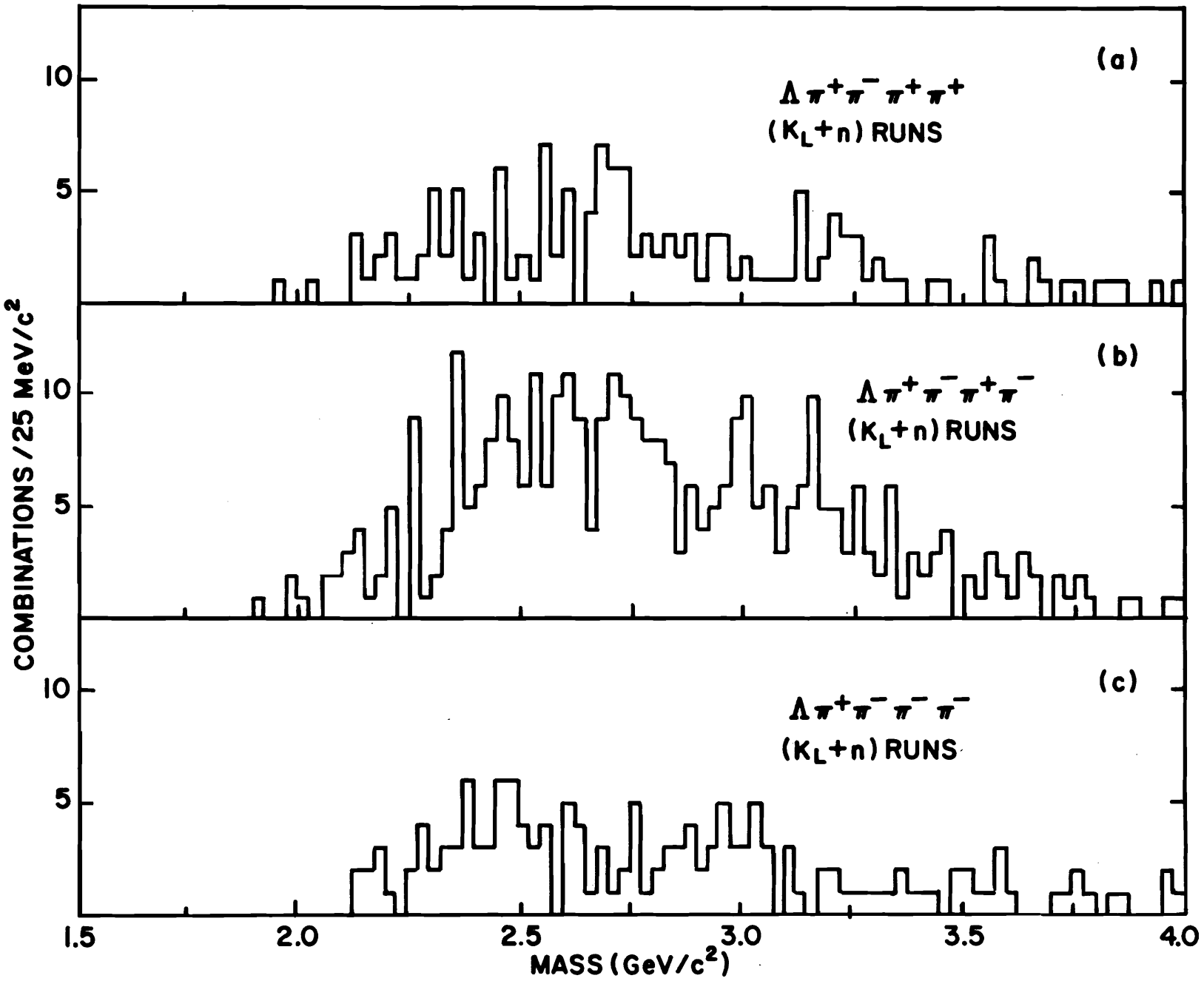
(a)
$\Lambda\pi^+\pi^-\pi^+\pi^+$
(K_L+n) RUNS
(b)
$\Lambda\pi^+\pi^-\pi^+\pi^-$
(K_L+n) RUNS
(c)
$\Lambda\pi^+\pi^-\pi^-\pi^-$
(K_L+n) RUNS
COMBINATIONS / 25 MeV/c^2
10
5
1.5
2.0
2.5
3.0
3.5
4.0
MASS (GeV/c^2)

FIG. 42

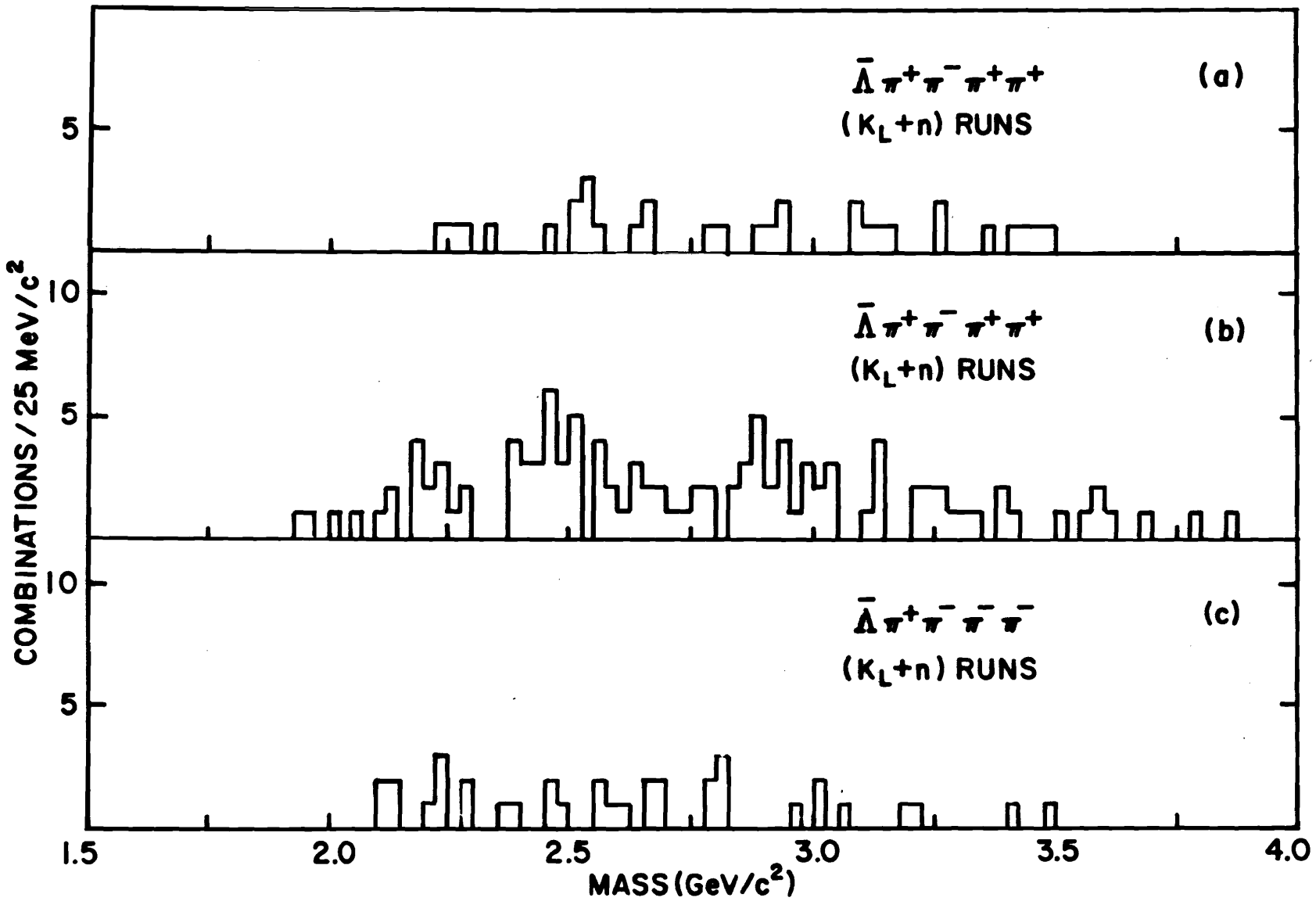
$\bar{\Lambda}\pi^+\pi^-\pi^+\pi^+$
(a)
(K_L+n) RUNS
$\bar{\Lambda}\pi^+\pi^-\pi^+\pi^+$
(b)
(K_L+n) RUNS
$\bar{\Lambda}\pi^+\pi^-\pi^-\pi^-$
(c)
(K_L+n) RUNS
COMBINATIONS / 25 MeV/c^2
5
10
5
10
5
1.5
2.0
2.5
3.0
3.5
4.0
MASS (GeV/c^2)

FIG. 43